Identification of Protein-Protein Interactors of the Corneal Dystrophy-Causing Protein, SLC4A11

by

Nada A. Alshumaimeri

A thesis submitted in partial fulfillment of the requirements for the degree of

Doctor of Philosophy

Department of Biochemistry

University of Alberta

Abstract

Endothelial corneal dystrophies are eye diseases characterized by dysfunction of the innermost layer of the cornea, resulting in disruption of the regulation and homeostasis of corneal deturgescence and, ultimately, impaired visual acuity. Gene mutations are responsible for many corneal endothelial dystrophies, suggesting that further insight into the roles of these genes and how their coded proteins interact with others may provide us with a better understanding of the causes behind these disorders. Mutations of the solute carrier family 4-member 11 (*SLC4A11*), a member of the SLC4 family of bicarbonate transporters, cause congenital hereditary endothelial dystrophy (CHED) and some cases of Fuchs endothelial corneal dystrophy (FECD). SLC4A11 is not, however, a bicarbonate transporter. Rather SLC4A11 is a H^+/ OH^-, H_2O, and NH_3 transporter. *SLC4A11* mutations compromise the trans-endothelial water flux of the cornea. This arises from misfolding of SLC4A11 protein, causing its retention in the endoplasmic reticulum (ER), or affecting the function of SLC4A11. SLC4A11 also plays a role in corneal endothelial cell (CEC) adhesion to the underlying Descemet's membrane as well, suggesting that defective CEC adhesion may contribute to the pathophysiology of endothelial dystrophies. This thesis investigates the role of SLC4A11 in endothelial corneal dystrophies by identification of protein-protein interactors of SLC4A11, using the membrane yeast two hybrid system (MYTH). Six unique, full-length proteins were detected as protein interactors with SLC4A11, and one of them, Ovarian Cancer Immunoreactive Antigen Domain Containing-1 (OCIAD1), was studied in greater detail using a variety of cell and tissue models due to its role in both the mitochondria and cell adhesion processes. Here, we show clear colocalization of SLC4A11 with OCIAD1 in bovine corneas, and that co-expression of the two proteins increases cell adhesion to the cornea Descemet's membrane

and protein migration to the cell surface in HEK293 cells. This thesis describes the identification of protein-protein interaction between OCIAD1 and SLC4A11.

Preface

The work in this thesis describes a portion of the international research collaboration led by my supervisor, Dr. Joseph Casey. All work mentioned in this text was done in Dr. Casey's laboratory at the University of Alberta, except for the generation of the cDNA library used to prepare and conduct the MYTH screen, which was ordered from and synthesized by the Bio S & T Company. We received the bovine corneas from Kastelen Sausage and Fine Meats (Ardrossan, AB, Canada). The thesis is my original work with the experiments performed in Canada, and they were designed by Dr. Casey and me. Cloning of the pCMBV-SLC4A11 (Chapter 2) was conducted by Chris Lukowski. All experiments described in Chapter 4 along with their figures were generated by. Dr. Bernardo Alvarez.

At the time of writing this, none of the experiments or work reported in this thesis have been published, although the results in Chapter 3 have been shared and discussed on a poster at the Association for Research in Vision and Ophthalmology (ARVO) conference (1).

Acknowledgements

I am very grateful for various people who supported me during my journey for my PhD degree. First, I would like to express my gratitude to my PhD supervisor Dr. Joseph Casey for his support, guidance, and many lessons that he has taught me. I learned from him many skills that helped me and will help me in the future. Those skills were patience, professionalism, time management, multitasking, presenting skills, and training junior scientists.

Special thanks to Dr. Bernardo Alvarez who contributed his time and effort to make my thesis complete. I would like to thank my committee members, Dr. Michael Walter, and Dr. Nicolas Touret for their professional guidance and valuable support. I am thankful to Dr. Elaine Leslie and Dr. Jutta Engel for agreeing to be my internal examiner and external examiner.

I am also thankful to the former Lab members Dr. Alka Kumari for the great time we spent sharing ideas and jokes in the lab. Dr. Bernardo Alvarez for his effort and hard work, Dr. Darpan Malhotra for his innovative experimental ideas, Dr. Katherine Badior for her delicious bakery, Dr. Sampath Loganathan for his help, Chris Lukowski for his organization of the lab, Kamala Lamsal for her big heart and help all the time and Ali Qadri for being a helpful summer student. Many thanks to the department of biochemistry, graduate students at the university and all the members of Membrane Protein Research Disease Group (MPDRG) for the informative scientific discussions. I acknowledge the privilege of getting the King Abdullah scholarship program.

I am particularly grateful to my best friend Nouf Bin Saleh who supported me continuously and for her great advice every time we talk. You have been there for me during my happy and hard times. Thank for encouraging me during my rough times even when we were many miles away.

I would like to express my great appreciation to my mother Dr. Wafa Almobaireek and my father Dr. Ahmed Alshumaimeri for their love, prayers and sacrifices to educate me and help to

build up my future. Thank you, my two sisters Nouf, and Noura and my two brothers Abdulrahman and Wael. Thank you for all days and nights spent with love with my daughter Jood and your support all the time.

Many thanks to my caring husband Dr. Abdullah Alshememry for the endless support and for all the late nights waiting for me finish my experiments in the lab. Thank you for believing in me and all the good times. Thank you for all the sacrifices you had to go through to support me endlessly. Finally, my dearest daughter, thank you for your love and smile even when I had to spend less time with you. I cannot be grateful enough to have such a blessing like you in my life.

Table of Contents

List of Figures

List of Tables

List of Abbreviations

Abbreviation	Word
A	
ABGL1	ATP/GTP binding protein like 1
Ade	Adenine
AE	Anion Exchanger
APOBEC	Apolipoprotein B messenger RNA-editing enzyme catalytic
AQP	Aquaporin
ARVO	Association for Research in Vision and Ophthalmology
ATPB1	Na^+/K^+ ATPase
B	
BCA	Bicinchoninic acid
BLAST	Basic local alignment search tool
BPA	Bisphenol A
BSA	Bovine serum albumin
BTR1	Bicarbonate transporter-related protein 1
C	
CaCC	Calcium activated Chloride Channel
CAM	Cell adhesion molecule
CD	Cytoplasmic domain
cDNA	Complementary deoxyribonucleic acid
CEC	Corneal endothelial cell
CFTR	Cystic fibrosis transmembrane conductance regulator
CHED	Congenital hereditary endothelial dystrophy
CMP	Cytidine-5'-monophosphate
CMP-SAT	CMP sialic acid transporter
Co-IP	Co-immunoprecipitation
COL17A1	Collagen 17A1
COL4A3	Collagen type IV alpha 3
COL8A2	Collagen Type VIII Alpha 2 Chain gene
COXIV	Cytochrome c oxidase subunit 4
CRYAA	Crystallin-Alpha-A
CS	Calf serum
C_{ub}	C-terminal moiety of ubiquitin
CXL	Collagen cross-linking
D	
DAPI	4′,6-diamidino-2-phenylindole
DM	Descemet's membrane
DMEM	Dulbecco's modified Eagle medium
DMSO	Dimethyl sulfoxide
DNA	Deoxyribonucleic acid

DUB	Deubiquitinating enzyme
E	
ECD	Endothelial corneal dystrophies
ECM	Extracellular matrix
EDTA	Ethylenediaminetetraacetic acid
EL3	Extracellular loop number 3
ER	Endoplasmic reticulum
ERAD	ER-associated protein degradation
ETC	Electron transport chain
F	
FA-CoA	Fatty acyl-CoA
FAK	Focal adhesion kinase
FBS	Fetal bovine serum
FECD	Fuchs endothelial corneal dystrophy
G	
GBP5	Guanylate Binding Protein 5
GFP	Green fluorescence protein
GH	Growth hormone
GRHL2	Grainyhead-like transcription factor 2
GST	Glutathione-S-transferase
H	
HA	Hemagglutinin
HCV	Hepatitis C virus
HEK293 cells	Human embryonic kidney 293 cells
HEPES	4-(2-hydroxyethyl)-1-piperazineethanesulfonic acid
HEY	Human ovarian carcinoma cell line
HGF	Hepatocyte growth factor
His	Histidine
HRP	Horseradish peroxidase
HS	Harboyan syndrome
I	
IC3D	The International Committee for Classification of Corneal Dystrophies
IPB	Immunoprecipitation buffer
J	
JAK	Janus kinases
K	
KANK4	KN motif and ankyrin repeat domain containing protein 4
KGF	Keratinocyte growth factor
L	
LacZ	β -galactosidase
LAMC1	Laminin gamma-1 protein
LB	Luria broth
LCB	Long-chain bases
LEPROTL1	Leptin receptor overlapping transcript-like 1

Leu	Leucine
LINC00707	Long intergenic non-protein coding RNA 707
LOXHD1	Lipoxygenase homology domain containing 1 protein
LPA	Lysophosphatidic acid
M	
MCT	Monocarboxylate Transporter
MD	Membrane domain
MPDZ	Multi-PDZ domain protein
MRPL55	Mitochondrial ribosomal protein L55
Myc	Myc epitope tag
MYTH	Membrane yeast two-hybrid
N	
NBCe1	Sodium bicarbonate cotransporter electrogenic
NCBI	National center for biotechnology information
NHE1	Na^+/H^+ exchanger
NKCC1	$Na^+/K^+/2Cl^-$ cotransporter
NS3-4A	Non-structural protein 3-4A
NSAID	Nonsteroidal anti-inflammatory drug
N_{ub}G	N-terminal moiety of ubiquitin (Ile13Gly)
N_{ub}I	N-terminal moiety of ubiquitin (wildtype)
O	
OCIAD1	Ovarian carcinoma immunoreactive antigen domain-containing protein 1
ORM	Orosomucoid
ORMDL2	ORM1-like protein 2
OVOL2	Ovo-like 2 gene
P	
PBS	Phosphate buffered saline
PCD	Posterior endothelial corneal dystrophies
PCR	Polymerase chain reaction
PEG	Polyethylene glycol
PIPES	Piperazine-N, N′-bis (2-ethanesulfonic acid)
PLA	Proximity ligation assay
PM	Plasma membrane
PMSF	Phenylmethylsulfonyl fluoride
PNGase F	Peptide N-glycosidase F
PPCD	Posterior polymorphous corneal dystrophy
PSG	Penicillin-streptomycin-glutamine
PVDF	Polyvinylidene difluoride
R	
RNA	Ribonucleic acid
ROS	Reactive oxidative species
RPE	Retinal pigment epithelium
rpm	Revolutions per minute
RRS1	Ribosome biogenesis regulator 1 homolog

S	
SD	Yeast synthetic dropout media
SDS	Sodium dodecyl sulfate
SDS-PAGE	SDS polyacrylamide gel electrophoresis
SiRNA	Small interfering RNA
SKOV3	Human ovarian cancer cell line
SLC	Solute carrier
SLC4A11	SLC family 4-member 11
SNSB	Sulpho-NHS-SS-biotin
SOB	Super optimal broth
SOC	Super optimal catabolite
SPOTS	Serine palmitoyl transferase, ORM1/2, Tsc3, and Sac1
SPT	Serine palmitoyl transferase
STAT3	Signal transducer and activator of transcription 3
T	
T	Total
TCF	Transcription factor
TF	Transcription factor
TMEM 128	Transmembrane 128
TMEM 254	Transmembrane 254
TMHMM	Transmembrane helices based on a hidden Markov model
TOM6	Translocase of the outer mitochondrial membrane6
Trp	Tryptophan
U	
U	Unbound
UPN251	Human ovarian carcinoma cell line
UV	Ultraviolet
V	
VPS55	Vacuolar protein sorting 55
W	
WT	Wild type
X	
X-Gal	5-bromo-4-chloro-3-indolyl-β-D-galactopyranoside
XECD	X-linked endothelial corneal dystrophy
Y	
YPAD	Yeast peptone adenine dextrose
Z	
ZEB1	Zinc finger E-box binding homeobox 1 gene

List of agar plates

Name of selective agar plate	Type of selection
LB plates	Luria broth agar plates with Kanamycin or Ampicillin antibiotics
YPAD	Yeast peptone adenine dextrose agar plates
Transformation	Synthetic dropout agar plate without leucine and tryptophan (SD-Leu-Trp)
Interaction plates	Synthetic dropout medium without leucine, tryptophan, histidine, adenine (SD-Leu-Trp-His -Ade)
Interaction plates + X-Gal	Synthetic dropout medium without leucine, tryptophan, histidine, adenine (SD-Leu-Trp-His -Ade), plus 5-bromo-4-chloro-3-indolyl-β-D-galactopyranoside (X-Gal)

Chapter 1: Introduction

1.1 Overview

This chapter provides an overview of the structure and function of the human eye, along with associated pathophysiologies and their molecular basis. The chapter will follow with a detailed background and the available evidence for the role of SLC4A11 in endothelial corneal disorders (ECD). The chapter concludes with a description of the research aims and objectives, scope and the rationale, hypotheses, and an outline of the thesis structure.

1.2 Introduction

1.2.1 Anatomy and physiology of the human eye

The human eye is a complex organ with many functional intricacies that capture the world in colour around us, converting signals to the brain which are then translated into high resolution images. The structure of the eye consists of an outer fibrous, middle vascular, and inner neural (or retina) layer (Figure 1.1). The sclera, also known as the "white of the eye" extends from the transparent cornea, which transmits light to the lens and retina, constitute the fibrous external layer and function to protect the eye from external stimuli (2, 3). The middle vascular layer consists of three highly functional components. First, the ciliary body is attached to the lens through zonule ligaments and together with the vascularized choroid structure allow the lens to focus light that reaches the retina at the back of the eye. The ciliary body is also responsible for continuous production of the aqueous humor, while the choroid provides the outer retina with necessary nutrients. The iris is a muscular structure with pigmented cells and overlays the ciliary body, and functions primarily to control the pupil aperture in response to varying levels of light. The

third layer of the human eye, the retina, converts light to sensory signals for image perception by the brain (4).

Neural retina is composed of two main types of retinal cells: photoreceptors and retinal pigment epithelium (RPE). The rod and cone photoreceptors are activated at low and high light conditions, respectively. While activation of rods leads to black and white vision, activated cones produce sharp and colored vision. On the other hand, the retinal pigment epithelium consists of a monolayer of cells with complex and varying functional roles, ensuring photoreceptor health such as capturing light (reflected and scattered), buffering ions, nutrient transport, protection against oxidative damage, and recycling of retinoids to maintain the visual cycle. RPE also plays an important role in growth factor secretion and forms a protective barrier for immune privilege of the eye (5, 6).

The human eye is further divided into an inner part, consisting of anterior and posterior chambers, and the outer vitreous chamber. The inner eye is filled with aqueous humor, a clear fluid that contains nutrients and neurotransmitters. Lastly, the outer vitreous chamber allows light to be transmitted to the retina through a gel-like fluid that fills the space between the lens and retina (7, 8).

1.2.2 Cornea Layers

The aspherical convex shaped transparent cornea forms the outer layer of the eye and allows for refracted light to enter the lens through the pupil. Furthermore, the avascular cornea also functions as a structural and protective barrier against infections (9). The cornea contributes roughly 70% of the total light refraction in the eye, and has an average

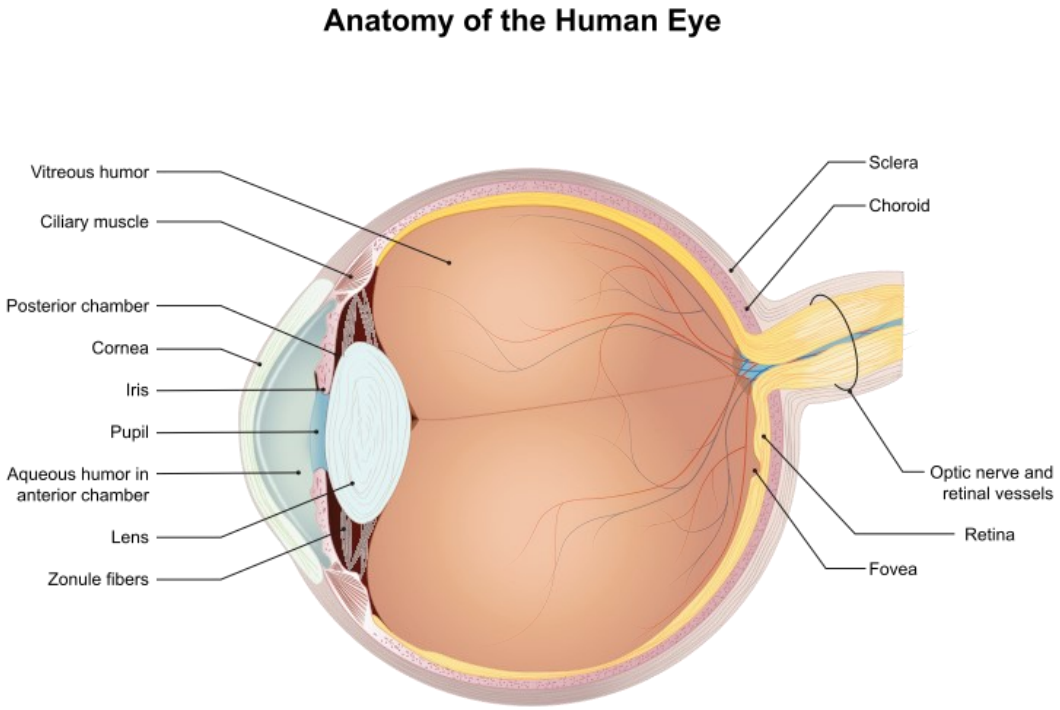

Figure 1.1: Structure of the human eye

Schematic diagram of eye components. The outer most layer is the cornea connected to the sclera. The middle part consists of the lens, ciliary muscle, zonule fibers, the retina, and the choroid. The inner part of the eye consists of the posterior and anterior chambers. Adapted and modified from (10).

diameter of 11.7± 0.4 mm (11), with a central thickness of 550 μm and peripheral thickness of 700 μm in healthy human eyes (12). Moreover, the cornea is composed of both cellular and acellular layers, while collagen and glycosaminoglycans constitute the acellular layer. The structure of the cornea is organized into five distinct layers: the outer epithelium, Bowman's layer, the stroma, Descemet's membrane, and the endothelial layer (Figure 1.2). Each layer of the cornea is explained as following:

1.2.2.1 Epithelium

The epithelium serves mainly as a protective barrier against microorganisms and toxic materials and contributes to corneal refractive power. In addition to containing microvilli on the surfaces of superficial cells, which function to increase the surface area in contact with tear film, these cells preserve junctional complexes between neighboring cells to prevent the diffusion of tear fluid through the inter-cellular space (13). Epithelial cells adhere together through desmosomes located on the lateral membrane borders. The corneal epithelium also contains a basement membrane, which contains basal membrane cells positioned between basal epithelial cells and the stroma (14). Basal membrane cells have specialized extracellular matrix functionality and are primarily composed of collagens, laminins, heparan sulfate, proteoglycans, and nidogens for anchoring (14). These components ensure adhesion of the basal membrane cells to the stroma and basement membrane. Damage to the basement membrane can result in elevation of fibronectin, a high-molecular weight glycoprotein involved in extracellular matrix formation (15), hindering the healing process (16).

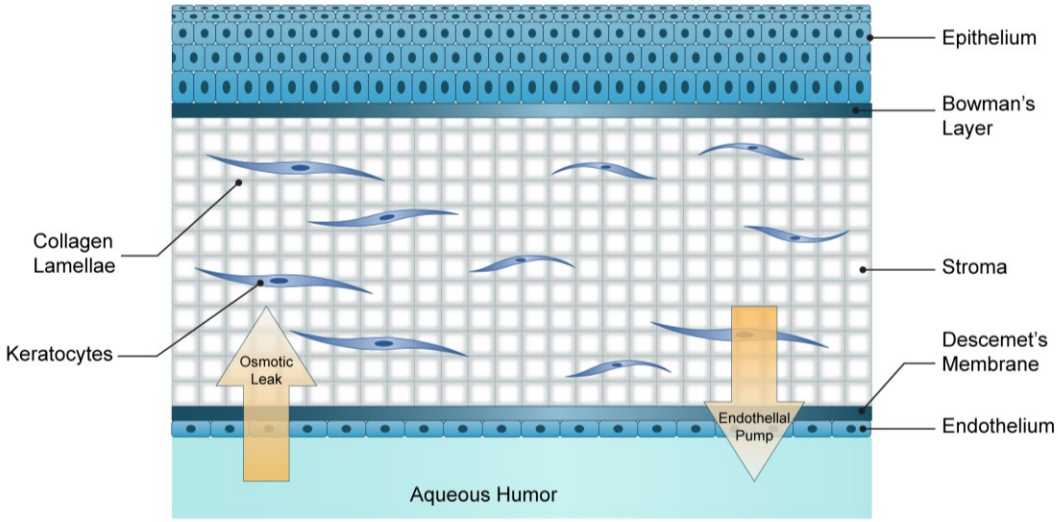

Figure1.2: Corneal layers

The cornea consists of five distinct layers. The outermost, the epithelium, is the layer exposed to light, followed by Bowman's membrane. Below this membrane are the stroma, Descemet's membrane, and the endothelial layer. The stroma is the thickest layer in the cornea containing a high concentration of dissolved proteoglycans, which leads to an osmotic leak in the stroma. Stromal hydration is maintained by the endothelial pump and regulated by transporters in endothelial layers. Adapted and modified from (17).

1.2.2.2 Bowman's membrane

Bowman's membrane lies immediately posterior to the epithelial basement membrane between the corneal epithelium and stroma, and consists of a random array of collagen fibrils (types I and V) and proteoglycans (Figure 1.2) (18). Due to its acellular structure, Bowman's membrane is unable to regenerate following injury, which may result in corneal scarring and eventual damage to vision (16).

1.2.2.3 Stroma

The corneal thickness is primarily composed of stroma (>90%), a connective tissue with a uniquely ordered extracellular matrix composed mainly of type I collagen fibrils interspersed with keratocytes; these, together with glycosaminoglycans, form important cellular components involved in the maintenance of corneal transparency (13). The collagen fibrils are further arranged into bundles of regular lamellae where type I collagen maintains highly organized structure through association with type V collagen and other components (Figure 1.2) (19). Other stroma components include mesenchymal cells (keratocytes), corneal fibroblasts, and nerve fibers. Corneal stroma is also highly abundant in glycosaminoglycan keratan sulfate, chondroitin, and dermatan sulfates, each of which are involved in maintaining corneal hydration (20). Moreover, the stroma also acts as a shield to protect the rest of the eye from harmful particles and bacteria. Previous studies have also identified the stroma acts as a reservoir for growth factors and cytokines, suggesting it may be a necessary component not only for development and homeostasis within the cornea, but also in wound healing (21). More specifically, investigations on the stroma have observed increased expression of hepatocyte growth factor (HGF) and

keratinocyte growth factor (KGF) in stromal keratocytes following wounding, indicating this functionality. This wound healing function has also been further shown in stromal keratocytes *in vitro*, where KGF accelerated epithelial coverage and wound healing (22).

1.2.2.4 Descemet's membrane

Descemet's membrane (DM) lies above the endothelium monolayer and is a basement membrane connective tissue for the corneal endothelium composed mainly of collagen (types IV and VIII), laminin, and perlecans (23). In humans, DM thickness increases with age and is accompanied by alterations in the arrangement of its collagen components (23). Descemet's membrane supports the function of endothelium by the porous structure allowing the passage of nutrients in the cornea (24). Descemet's membrane also attaches the endothelium to the cornea and maintains the transparency of the cornea (24).

1.2.2.5 Endothelium

The endothelial layer of the cornea rests on the DM and consists of a monolayer of specialized confluent cells (4 μm thick) arranged in a hexagonal mosaic pattern that functions to minimize light scattering and maintain corneal hydration and homeostasis. This monolayer of specialized cells lines the posterior corneal surface and does not replicate or undergo cell division under normal circumstances, as the cells are commonly arrested in the G1 phase of the cell cycle (25). The reason for this lack of cell progression in unknown, but some have indicated it be due to contact inhibition with neighboring cells (26). The corneal endothelium also secretes the components of DM which eventually forms the basement membrane, which was discussed previously. Secretion of the DM by the

endothelial cells continues throughout life (25). Likewise, endothelial cells also serve as a marker of stress, damage, or disease, as they may secrete banded DM in response to these stimuli to form posterior banded, or collagenous layers for protection (27).

1.2.3 Corneal endothelial fluid transport pump

The corneal endothelium maintains the nutrition of the corneal cells and regulating stromal hydration through an intricate process known as the 'Pump-Leak' mechanism (28). The stroma has a high composition of collagen and proteoglycans which causes an osmotic force that draws in fluid (25). The leak is a passive process through CEC and tight junctions from aqueous humor to the stroma (29). The tight junction's role is to maintain the boundaries of apical and basolateral surfaces and form a barrier against the diffusion of solutes through paracellular space (29). However the formed barrier is partially leaky to allow glucose and essential nutrients to reach into the stroma (25).

The Pump mechanism is associated with numerous ion channels, exchangers, and ATPases strategically positioned at the apical and basolateral membranes, and counterbalances stromal swelling pressures (30, 31). Endothelium has large number of mitochondria that are needed to produce energy for the activity of transporters (32). The pump mechanism is driven by both primary and secondary active transport and ionic gradients developed by the well-known, sodium/potassium pump (Na^+/K^+-ATPase) located in the endothelium's basolateral membrane (33). This pump is paramount to stromal hydration control, as inhibition of Na^+/K^+-ATPases using inhibitors, such as the cardiac glycoside ouabain, immediately results in stromal swelling and over-hydration (30, 34). The endothelial Pump-Leak mechanism also requires other ion movement across the

basolateral membrane specifically through a Na^+-HCO_3 cotransporter and Cl^- and HCO_3^- ions, and this process facilitates fluid secretion into the anterior chamber, likely through local osmotic gradients (33). More specifically, these sodium bicarbonate transporters are located on the stromal side of the endothelium and regulate basolateral bicarbonate uptake. Likewise, HCO_3^- is secreted across the apical membrane (into the anterior chamber) via anion channels or transporters, and together with bicarbonate transport generates a small trans-endothelial voltage to drive Na^+ across tight junctions. Numerous other anion transport mechanisms have been identified and characterized in the endothelium, including the basolateral $Na^+/2HCO_3^-$ cotransporter, $Na^+/K^+/2Cl^-$ cotransport, and Cl^-/HCO_3^- (AE2), highlighting the transport capabilities of the endothelium that are in place to correct hydration levels in response to swelling (33). Furthermore, SLC4A11, which localizes at the basolateral surface of the corneal endothelial cells facing the stroma, facilitates direct water movement into the endothelial cells (35). Water is further moved into the aqueous humor via the AQP1 water channel at the apical surface of corneal endothelial cells (Figure 1.3) (36). In conclusion, the corneal endothelial transport pump is important for the maintenance of stromal hydration (29). The consequence of a failed pump mechanism is corneal edema which impacts on corneal clarity and cause poor vision and lead to endothelial corneal dystrophies (37).

1.2.4 Posterior endothelial corneal dystrophies

The previous section discussed the importance of corneal layers, particularly the stroma and endothelium monolayer, and their involvement in the regulation and homeostasis of corneal deturgescence and the preservation of optical clarity. While the epithelium is able

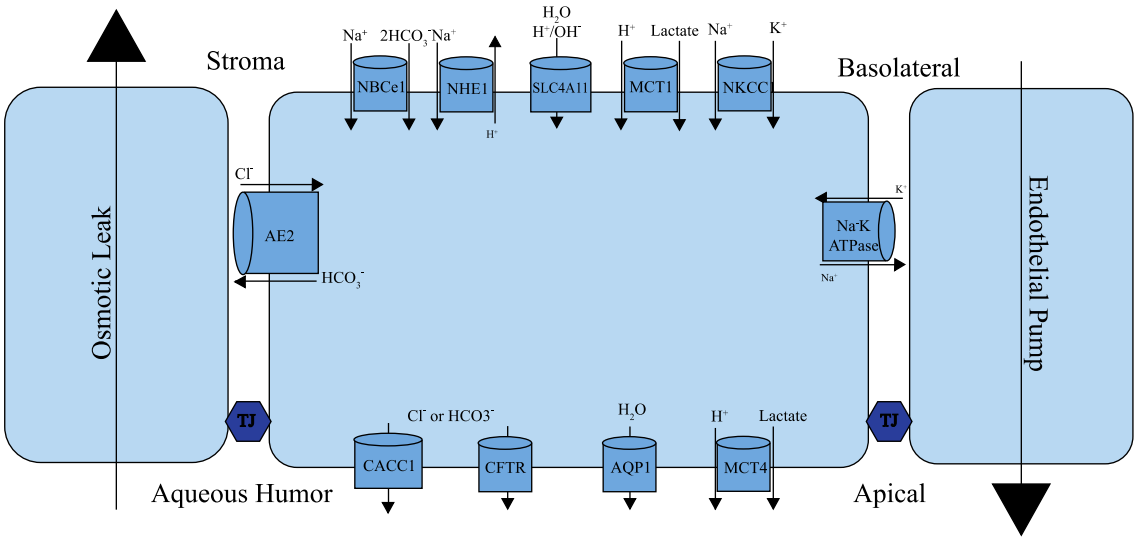

Figure 1.3: Endothelial corneal transport mechanism in regulation of stromal deturgescence

Corneal endothelial cells with NBCe1, NHE1, SLC4A11, MCT1, NKCC1, AE2 and Na^+/K ATPase at the basolateral surface. At the apical surface CACC1, CFTR, AQP1, and MCT4 are expressed. The proteins at the apical and basolateral surface contribute to form the endothelial pump mechanism. Adapted from (36).

to regenerate, the endothelium does not have the capacity to self-renew (38). Hence, CEC death prompts remaining CECs to compensate for the reduced function to maintain corneal transparency that commonly results in blurred vision (39). Despite symptomatic treatments such as collagen cross-linking (CXL) or topical Rho-associated kinase inhibitors, which aim to mitigate discomfort and pain caused by corneal edema (39), corneal transplantation, also known as keratoplasty, is the cornerstone therapy for definitive management of endothelial dysfunction. However, due to the lack of available cornea donors world-wide, other avenues, such as *in vitro* cultured human endothelial cells, for direct transplantation have been developed (39, 40).

Diseases of the corneal endothelial layer and DM are collectively referred to as posterior endothelial corneal dystrophies (ECD) and occur as inherited conditions that share common histopathological features, such as variable disease onset and overlapping genetic characteristics (41). The commonly described ECD-related conditions include Fuchs endothelial corneal dystrophy (FECD), CHED, Harboyan syndrome, posterior polymorphous corneal dystrophy (PPCD), and X-linked endothelial corneal dystrophy (XECD), which will be discussed below. The main features of posterior ECD conditions are summarized in Figure 1.4.

1.2.5 Fuchs endothelial corneal dystrophy

FECD is a common corneal endothelial degeneration disorder with a prevalence ranging from 3.8% to 11% and primarily affecting older individuals (>40 years) (39). It accounts for almost a quarter of all corneal transplants in the United States (42) and United Kingdom (43). The main histological characteristics of FECD include change in shape, size, and

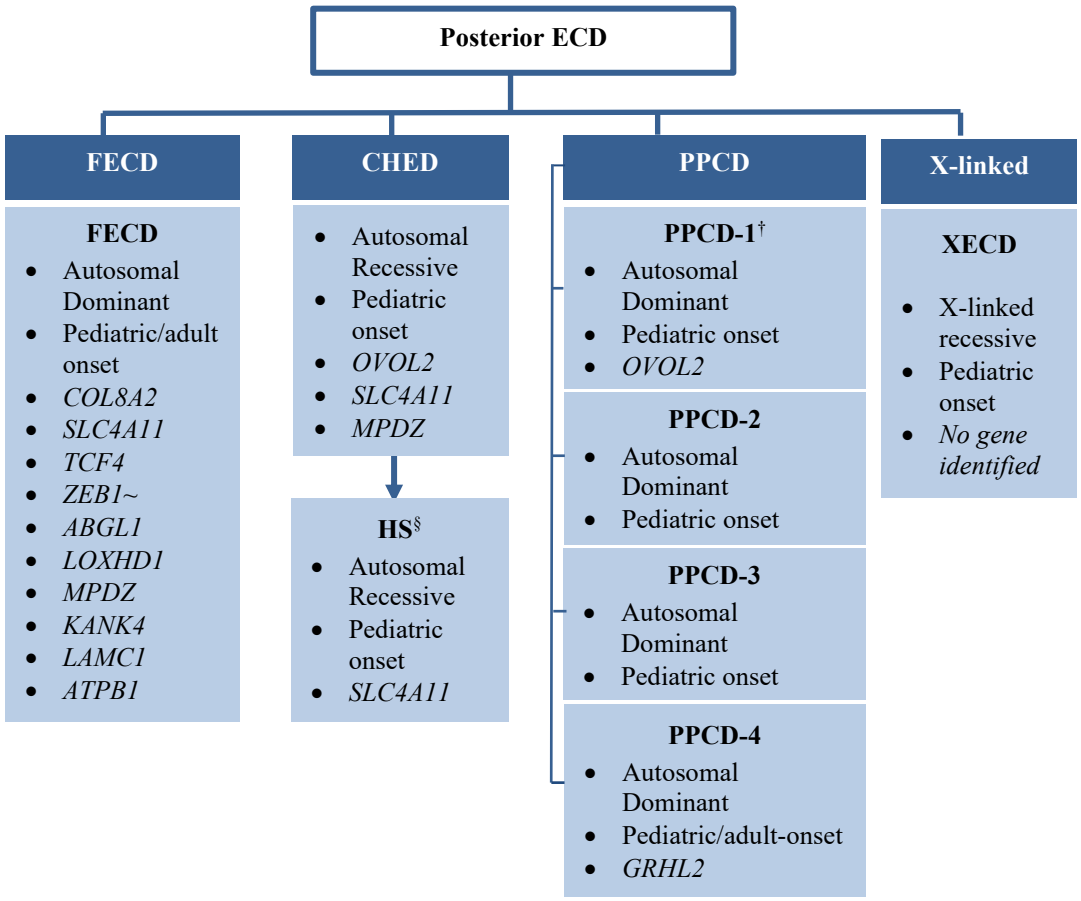

Figure 1.4 Posterior endothelial corneal dystrophies

Corneal dystrophies that affect the innermost layers of the cornea (DM and EC). † Map to the same region on chromosome 12q21.33. § Identified as manifestation of CHED with hearing defects. ~ Two-handed zinc-finger homeodomain (*ZEB1*) is also referred to as *TCF8.* ECD: endothelial corneal dystrophies; FECD: Fuchs' endothelial corneal dystrophy; CHED: Congenital hereditary endothelial dystrophy; HS: Harboyan syndrome; PPCD: posterior polymorphous corneal dystrophy; XECD: X-linked endothelial dystrophy; *COL8A2*: collagen type 8 alpha 2; *TCF4*: transcription factor 8; *ABGL1*: ATP/GTP binding protein like 1; *LOXHD1*: lipoxygenase homology domain containing 1 protein; *MPDZ*: multi-PDZ domain protein; *KANK4*: KN motif and ankyrin repeat domain containing protein 4; *LAMC1*: laminin gamma-1 protein; *ATPB1*: Na^+/K^+ ATPase; COL17A1: collagen 17A1; *GRHL2:* grainyhead-like transcription factor 2; *OVOL2*: ovo-like Zinc finger 2; *TCF8*: transcription factor 8 (32, 41).

number of residual endothelial cells together with guttae formation, which are collagenous excrescences of the Descemet's membrane (44). There are four stages of FECD progression: in the first stage there are no clinical symptoms; stage 2 is characterized by a reduction of endothelial cells and the gradual coalesce of guttae within the cornea; stage 3 marks the presence of stromal edema and stage 4 is when such edema results in progressive scarring and lowered visual acuity (39, 45).

The pathogenesis of FECD involves both genetic and environmental factors and occurs either as early-onset or late-onset. The early-onset type occurs as an autosomal-dominant disorder with well-established clinical and genetic characteristics (46). In contrast, late-onset FECD is the more common type and occurs in patients over 40 years of age, eventually resulting in visual impairment. Genetically, early-onset FECD has been associated with one locus (Chromosome 1p) and mutations in the Collagen Type VIII Alpha 2 Chain gene (*COL8A2*) (47). However, in late or adult-onset FECD multiple loci have been identified, including FCD1 (chromosome 13), FCD2 (chromosome 18), FCD3 (chromosome 5), and the recently discovered FCD4, which maps to chromosome 9 and segregates with *ZEB1* disease-causing mutations (39). In addition, solute carrier family 4-member 11 gene (*SLC4A11*) mutations have been identified in adult-onset FECD patients from various populations (48-50).

1.2.6 Congenital hereditary endothelial dystrophy

Congenital hereditary endothelial dystrophy (CHED) develops at birth, during infancy, or throughout the first few years of life as an autosomal-recessive inherited disorder with

characteristic corneal opacity (51). While CHED was originally distinguished by two distinct types, CHED1 and CHED2 (51), more recent genetic studies have indicated CHED1 is now an allelic condition of posterior polymorphous corneal dystrophy (PPCD) and maps to the same locus as PPCD1 on chromosome 20 (41, 52). As a result, the 2015-updated International Committee for Classification of Corneal Dystrophies (IC3D) classification categorized CHED1 as the severe phenotype of PPCD1 (53). CHED is mainly characterized by Descemet's membrane thickening, stromal edema, and altered endothelial cell morphology (Figure 1.5) (39). Most patients with CHED harbor mutations in the *SLC4A11* gene, which is a member of the SLC4 family of bicarbonate transporters (54).

1.2.7 Harboyan syndrome

The hallmark characteristic of Harboyan syndrome is CHED associated with progressive perceptive deafness in teen years. Mutations in the *SLC4A11* gene have been linked to both CHED and Harboyan syndrome phenotypes with preclinical evidence for the role of *SLC4A11* gene in the audio-vestibular system (55), but there is lack of evidence to support the phenotypic differences at the genetic level (56). However, recent clinical evidence suggests CHED progresses to sensorineural loss of hearing in some patients and, in fact, Harboyan syndrome is similar to CHED at a different developmental stage, with an increased risk for late-onset FECD (57).

1.3 SLC4A11

Section 1.2 highlighted the structure and physiology of the human eye, along with defects in the endothelial cornea leading to posterior endothelial corneal dystrophies. It is known that mutations of the membrane transporter SLC4A11 cause endothelial corneal dystrophies (32). SLC4A11 is a member of the SLC4 family characterized by their bicarbonate transporter functionality, but unlike other members, there is no evidence for its role in bicarbonate transport (Figure 1.5) (36). Phylogenetic analysis (Figure 1.5) reveals that SLC4A11 clusters separately from both the Cl^-/HCO_3^- exchanger and the Na^+-coupled bicarbonate transporters in the SLC4 family as well, suggesting a separate function. The role of impaired SLC4A11 in the pathogenesis of genetic endothelial corneal dystrophies, CHED and FECD, is well established (58, 59). In recent years, insights into the functions of SLC4A11 have clarified our understanding of normal corneal physiology and in turn the pathophysiological mechanism of endothelial corneal dystrophies (32). Specifically, SLC4A11 mediates trans-endothelial water flux in a hypoosmotic extracellular environment similar to aquaporin water channels (36), transports NH_3/H^+ during glutamine metabolism (60), or directly transports NH_3 (35). While some *SLC4A11* mutations result in impaired transport function (37, 61), the majority of SLC4A11 disease alleles cause protein misfolding or retention defects in the endoplasmic reticulum (54).

Furthermore, a recent study revealed that SLC4All contributes to CEC adhesion to DM, which may contribute to the progressive loss of CECs in affected patients due to defective endothelial cell adhesion (62). SLC4A11 promotes adhesion to the basement membrane layer that binds CECs (the Descemet's membrane) to form a cell adhesion molecule (CAM). Interestingly, recent work suggests that defects in this cell adhesion contribute to the pathophysiology of FECD and CHED (62).

1.3.1 SLC411 structure and expression

The main structural elements of SLC4A11 are highlighted in a topology model based on 26% sequence homology to SLC4A1 (AE1) whose crystal structure has been determined (Figure 1.6) (63, 64). The homology shows SLC4A11 assembled as a dimer and SLC4A11 has been biochemically shown to be dimeric (65). Each monomer is composed of a cytoplasmic domain (41-kDa) and an integral membrane domain (57-kDa) arranged in 14 transmembrane helices (36), and contains a third extracellular loop (EL3) with two N-linked glycosylation sites (63).

Three N-terminal splicing variants of human SLC4A11 have been identified v1, v2, and v3 (66). These variants are also called SLC4A11-A, -B, and -C, respectively (61). One variant differs from another variant by a difference of 20-60 amino acids in its N-terminus (65). Alternative splicing of the transcript gives rise to three transcripts differing at their 5' end (encoding the protein's N-terminus). The SLC4A11 variant 2 (v2) is the most expressed variant in human corneal endothelium (66) and variant 1 (v1) is not expressed in the human cornea. SLC4A11 variant 3 (v3) is approximately four times less expressed compared to v2 (66).

The cytoplasmic domain of SLC4A11 is essential for membrane transport function and required for stability of the integral membrane domain (35, 67). The topology model of SLC4A11-v2 has been validated based on the AE1 crystal structure homology model (64), predicting a core and gate sub-domains in the membrane domain where a substrate translocation pathway is formed by the cleft between the sub-domains (63). Using this AE1 structure, a homology model was predicted using a computer model and by analysis of the mutants based on the model. Moreover, specific mutations are predicted to impair

SLC4A11 transport functionally, including p.Glu675GIn, p.His724AIa, and p.His724Arg. P.Ala724Ala is located in a proposed region of the translocation pore and results in failure of the protein's migration to the cell surface. P.Gly509Lys, placed in the open region at the core/gate interface, experienced wild-type level of transport activity (54).

In humans, SLC4A11 has been detected in the corneal epithelium with high abundance in the endothelial layer. SLC4A11 is highly expressed in the basolateral membrane of the corneal endothelial monolayer, anterior to the stroma (36, 68). SLC4A11 is also expressed in several other tissues including kidney, inner ear (cochlea), brain, gastrointestinal tract, lungs, ovaries, and pancreas (69).

1.3.2 Mouse models of Slc4a11

In animal models, *slc4a11* expression is detected in corneal endothelial cells specifically in the basolateral membrane and less expression in epithelial cells (36, 61). Expression has also been observed in the inner ear (vestibular labyrinth) and is required for endocochlear potential, as *slc4a11*$^{-/-}$ mice exhibit abnormal auditory brain responses and progressive hearing loss (55, 70). All *slc4a11* mouse knockout models generated using the retroviral gene trap vector method showed corneal edema along with thickening of the basement membrane in aged mice, without any disturbances in the hexagonal array of the endothelial layer (55). Moreover, a knockout mouse model has revealed morphological corneal disturbances in all layers (70) together with both the progressive loss of CEC morphology and density with age similar to corneal phenotypes in patients with CHED (71). A summary of these knockout models is presented in the table below (Table 1.1).

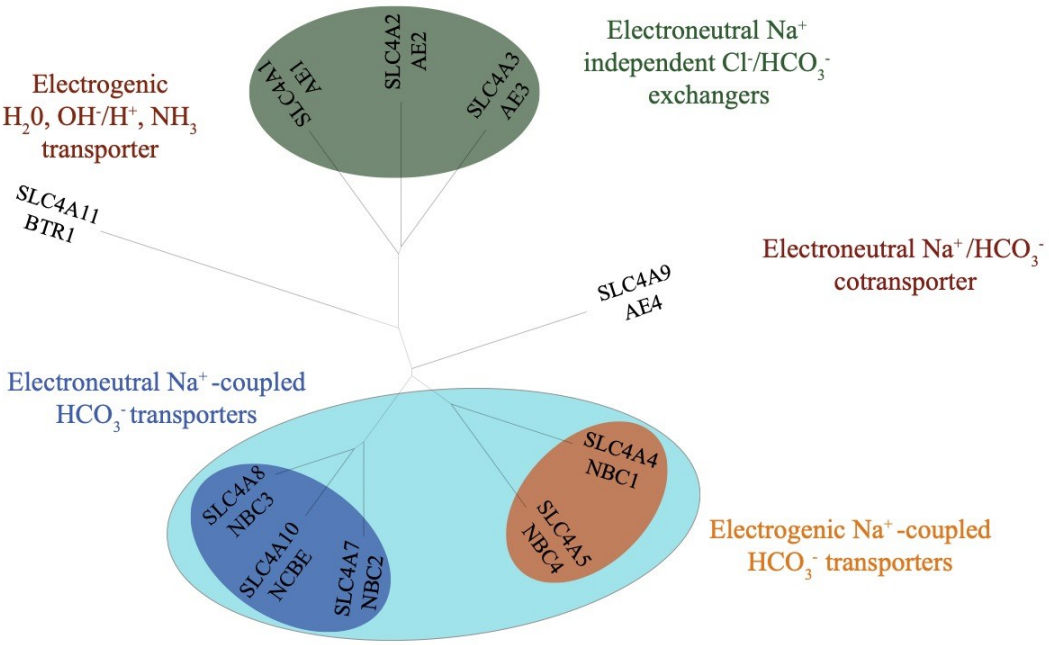

Figure 1.5: Phylogenetic tree of SLC4 family

All amino acids sequences of the SLC4 family members SLC4A1 (NP_000333.1), SLC4A2 (NP_003031.3), SLC4A3 (NP_005061.2), SLC4A4 (AAC51645.1), SLC4A5 (AAK97072.1), SLC4A7 (ACH61961.1), SLC4A8 (AAY79176.1), SLC4A9 (NM_031467.3), SLC4A10 (NP_071341.2), SLC4A11 (NP_114423.1) from NCBI database (https://www.ncbi.nlm.nih.gov). Sequences were aligned using the online Clustal Omega software (https://www.ebi.ac.uk/Tools/msa/clustalo/). The unrooted phylogenetic tree was generated by the online iTOL software (https://itol.embl.de).

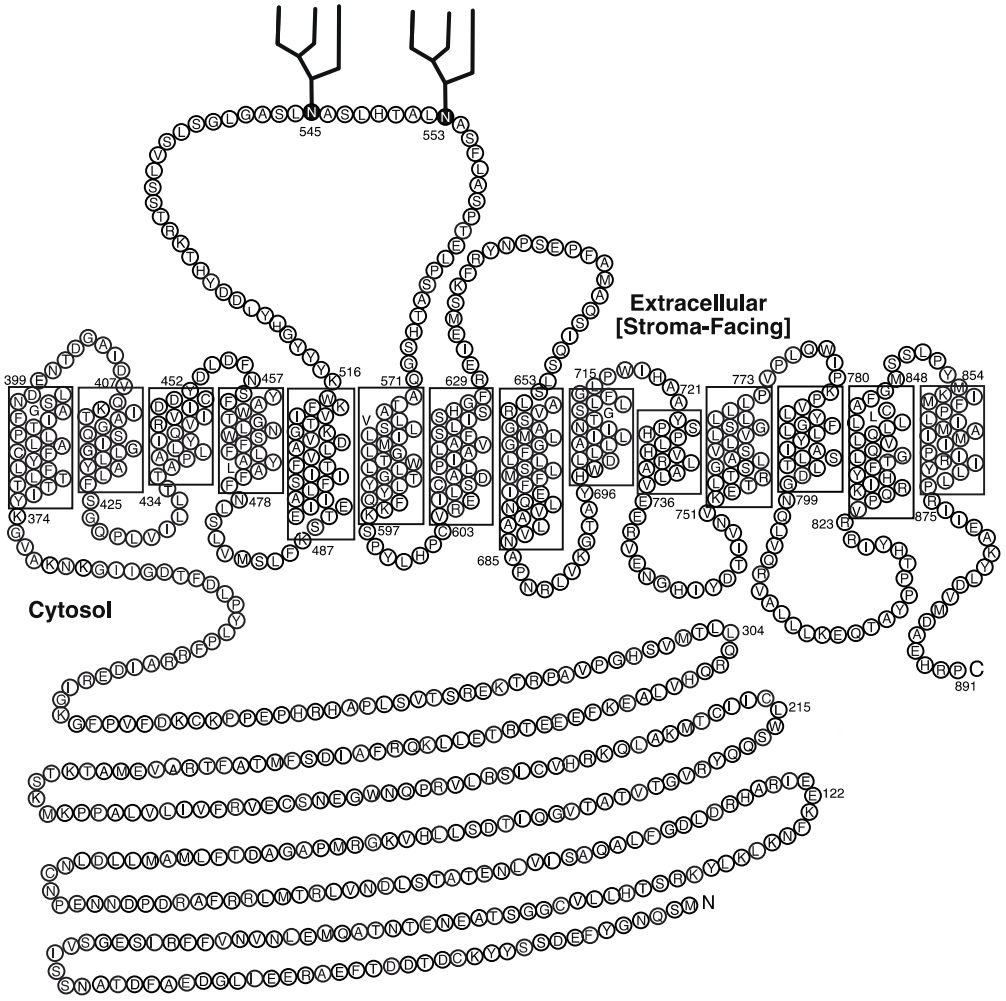

Figure 1.6: Topology model of SLC4A11

Topology model was established based on sequence alignments between human SLC4A1 (AE1) and human SLC411 variant 2, and then applied to a topology model for SLC4A11 (38). The branched structures (located at amino acids 545 and 553) are N-linked glycosylation sites (31).

Table 1.1: *Slc4a11* knockout mouse models

Slc4a11 knockout mouse models showing results of mutation, corneal phenotypic changes, and other associated phenotypes.

Knockout model	Result of mutation	Age of mice	Corneal phenotype	Other phenotypes	Proposed mechanisms	Reference
Retroviral gene trap vector	No protein (Disrupted gene expression)	3-10 months	Mild abnormal epithelial & stromal layer but no endothelial phenotype	Sensorineural deafness	None	(55)
β-galactosidase coding sequence in frame into the tenth exon of *Slc4a11*	Truncated protein	12 months	Morphological changes in all corneal layers	Deafness	Endocochlear function ion homeostasis Na^+-mediated fluid transport	(70)
Targeted deletion (Exon 9-13)	Truncated protein	3-22 months	Progressive stromal oedema & thickness of DM, disrupted collagen fibrils change in CEC size & density	Renal abnormalities	Fluid transport independently of aquaporin	(71)
Inducible knockout	Truncated protein		Increased corneal thickness, corneal edema, altered endothelial morphology, elevated nitrotyrosine staining	Not stated	None	(72)

1.3.3 Pathogenesis of endothelial corneal dystrophies associated with SLC4A11 dysfunction

1.3.3.1 SLC4A11 mutations

Over SLC4A11 90 mutations have been reported in CHED, adult-onset FECD, and Harboyan syndrome, and overlap of these mutations (missense, splice-site, non-sense) exists between the various corneal pathologies. The hallmark feature of these three disorders is corneal stromal edema associated with blurred vision. To date, 54-point mutations have been identified in SLC4A11, with approximately one third of these are present in the cytoplasmic domain and the remainder in the integral membrane domain (67, 73).

1.3.3.2 Molecular mechanism of SLC4A11 disease-causing mutations

Evidence from preclinical models indicates two mechanisms by which SLC4A11 disease phenotypes occur: 1) membrane trafficking disruptions where the mutated protein fails to migrate to the cell surface and is instead retained in the endoplasmic reticulum (ER), likely due to misfolding (73-75), and 2) functional defects where the mutated protein trafficking is not affected, but ECD results from compromised transporter function or defective cell adhesion (36, 61, 62, 76).

Most of the identified point-mutations lead to SLC4A11 misfolding with partial or complete retention of the protein in the ER, resulting in failure to reach surface of the cell (77). Characterization of 54 disease-causing SLC4A11 point mutations revealed that 57% of these mutations, which reside in the integral membrane domain of SLC4A11, result in SLC4A11 ER retention, while nearly half of all point-mutations induce trafficking defects

in CHED and HS (73). Proteins encoded by several *SLC4A11* missense mutations was found to be rescued by cell incubation at low temperature. Thus, some misfolded proteins are likely candidates for folding correction therapy in corneal dystrophy patients. The low temperature affects protein folding energetics, allowing mildly misfolded proteins to be processed to the cell surface to increase trafficking (73). Nine of the ER-retained *SLC4A11* mutants were in the SLC4A11 membrane domain most of which were located in a densely packed region (63), while five of the rescued mutants were located in the cytoplasmic domain. In a study to determine the water flux activity of SLC411 variants, HEK293 cells representing CHED, FECD, or unaffected individuals showed 60%, 5% or 25% activity, respectively (77).

When cells were treated with glafenine, a nonsteroidal anti-inflammatory drug (NSAID), trafficking defects due to *SLC4A11* mutations were restored, resulting in increased in SLC4A11-mediated water flux (78). Furthermore, *in vitro* screening of ophthalmic NSAIDs revealed that treatment with other NSAIDs, specifically diclofenac, restored SLC4A11 transport function by increasing trafficking in 20 of the 30 SLC4A11 mutants characterized by ER-retention phenotype. This suggests that application of these drugs may have therapeutic potential in the treatment of a subset of corneal dystrophy patients affected with *SLC4A11* mis-trafficked mutations (75).

1.4 Possible roles of SLC4A11 in the human cornea

1.4.1 Mitochondrial function and oxidative stress

Consistent with the hallmark characteristics of CHED, *slc4a11*$^{-/-}$ mice exhibit significant corneal endothelial edema, decrease in cell density and oxidative stress (71). In addition to

glucose, CECs need to generate energy from glutamine as a fuel source to sustain continuous corneal hydration. Recent evidence indicates SLC4A11 has an important role in mitochondrial protection (79, 80) by facilitating glutamine metabolism in endothelial cells and acting as an ammonia-activated mitochondrial uncoupler (79). In particular, loss of SLC4A11 activity increased glutamine-induced hyperpolarization and production of mitochondrial superoxide, leading to greater endothelial cell death (79).

1.4.2 Corneal endothelial cell adhesion

Together with the active fluid and ion transport mechanism, the corneal endothelium attachment to the basement membrane is essential to maintain barrier integrity for stromal deturgescence and is therefore essential for corneal transparency. This barrier function involves a complex interplay of cell tight junctions with five integral membrane protein families referred to as cell adhesion molecules (CAMs), including endothelial cadherins, integrins, the immunoglobulin CAM superfamily, proteoglycans, and endothelial selectins. In humans, corneal DM is 10–12 μm thick and composed of collagen VIII, and is distinct from other basement membranes which are typically composed of collagen IV, laminin, fibronectin, and ECM proteins such as proteoglycans (81). Integrins expressed by CECs consist of α and β chains that function as heterodimers mediating interaction between the DM and extracellular matrix (ECM) proteins secreted by the endothelial layer (82).

Apart from a role in mitochondrial protection and its transport function, several lines of evidence from *in vitro* studies demonstrate that SLCA4A11 plays a critical role in CEC adhesion as well (62). The basolateral membrane of human CECs is rich in SLC4A11

protein which has a large third extracellular loop that is not involved in water flux function (78).

Together with mass spectroscopy analysis, glutathione-S-transferase (GST) pull-down assays have further identified SLC4A11 as interacting with the primary DM protein COL8A2 and COL8A1 in the DM of endothelial cells (62). Given that SLC4A11 expression is downregulated in isolated cultures (68, 83), when human CECs were incubated in the presence of DM for two weeks, SLC4A11 expression (along with concurrent upregulation of COL8A2) resulted in elevated DM-CEC adhesion, highlighting the critical role of DM signaling in the regulation of this complex interaction for the maintenance of cellular adhesion (62). Collectively, these findings suggest that for some FECD- causing mutations, reduced cell adhesion may provide one underlying pathogenic mechanism behind SLC4A11 dysfunction, as interaction of DM with the endothelial cells is required for normal function. This mechanism may also offer insights towards novel therapeutic strategies for endothelial dystrophies as well.

1.4.3 Relation to cancer

Several previous studies have linked SLC4A11 to cancer pathways. Analysis of the xenoestrogen, Bisphenol A (BPA), a component of numerous consumer products, revealed its involvement in dysregulation of various signalling pathways. Ninety-four genes dysregulated in the presence of ovarian cancer cell lines were identified as potential biomarkers. *In silico* analysis of these proposed biomarkers revealed the upregulation of the *SLC4A11* gene, alongside Guanylate Binding Protein 5 (*GBP5*), Long intergenic non-protein coding RNA 707 (*LINC00707*), Ribosome biogenesis regulator 1 homolog (*RRS1*),

and Mitochondrial ribosomal protein L55 (*MRPL55*), indicating that they are biomarkers of ovarian cancer. SLC4A11 up-regulation is associated with a poor prognosis in ovarian carcinoma. Moreover, expression of SLC4A11 is observed in high-grade serous carcinoma, low-grade serous carcinoma, mucinous adenocarcinoma, and metastatic serous carcinoma (84, 85). SLC4A11 gene amplification and hypomethylation are mechanisms involved in the upregulation of SLC4A11 expression seen in ovarian cancer (86).

1.5 Ovarian Cancer Immunoreactive Antigen Domain Containing 1 (OCIAD1)

One of the most interesting proteins that will be studied in this thesis is OCIAD1 (Chapter 4), a low-molecular weight protein (29 kDa) originally identified from immune-screening of an ovarian cancer cDNA library, and has also been discovered via proteomics analysis, where elevated expression of the protein was observed in metastatic tumors compared to primary tumors (87, 88). Interestingly, increased OCIAD1 expression causes resistance to chemotherapy treatment by increasing lysophosphatidic acid (LPA)-induced cell adhesion to extracellular matrix proteins collagen I and laminin 10/11 (89). This resistance is significant considering LPA, a lipid signaling molecule which actively promotes cancer cell adhesion to extracellular matrices, migration of ovarian metastasis to the extracellular matrix, and overall cancer cell survival (90), is a molecule highly targeted in ovarian cancer treatment strategies (91, 92). Due to this OCIAD1-LPA relationship in ovarian cancer, it appears that OCIAD1 has an important role in metastatic tumor growth and survival through mediation of cell adhesion. Transfection of OCIAD1-specific siRNA completely inhibited LPA-induced cell adhesion on collagen I but not vitronectin in two ovarian cancer

cell lines, HEY and UPN251 (89). Moreover, OCIAD1 siRNA-treated UPN251 cells displayed reduced basal level cell adhesion to collagen I, while over-expression of the protein in HEY cells dramatically increased LPA-induced cellular adhesion to both collagen I and laminin 10/11 (89).

These data suggest that OCIAD1 interacts with LPA-induced signaling pathways such as G-protein coupled receptors; however, further analysis on this interaction discovered that OCIAD1 does not use this pathway to increase ovarian metastasis cellular adhesion. Instead, it appears that the protein may act as an intermediary molecule, activating integrins to bind collagen I and increase cellular adhesion and, thus, cell survival (88, 89). OCIAD1 also facilitates the signal transducer and activator of transcription 3 (STAT3) activation of the Janus kinases JAK/STAT signaling pathway, a significant interaction considering that STAT3 activation is important in regulating cell adhesion and cytoskeletal modulation through phosphorylation of the focal adhesion kinase (FAK), along with its induction in response to intercellular adhesion (93-95).

1.5.1 Association with OCIAD2

Similar to OCIAD1, the expression of immunoreactive antigen domain containing 2 (OCIAD2) is induced in certain cancers as well, namely, early invasive lung adenocarcinomas (96). This association is perhaps unsurprising as OCIAD2 has high sequence identity with OCIAD1. The OCIAD gene family includes only OCIAD1 and OCIAD2, and patients with certain tumors develop auto antibodies against these proteins (87). Likewise, it has been concluded that both OCIAD1 and OCIAD2 are highly

immunoreactive proteins in ovarian tumors and may be a particularly useful marker to evaluate the progression and malignancy of ovarian mucinous tumors (96).

1.5.2 Interaction with Beta-Actin

Co-precipitation and proteomic analyses found that OCIAD1 is physically attached to α-actinin 4 (a modulator of integrins and regulator of β-actin architecture). In addition OCIAD1 interacts with β-actin (88). This interaction may regulate OCIAD1's involvement and control over integrin function, and the authors have hypothesized that α-actinin 4 may be the intermediary between OCIAD1 and integrins. This hypothesis makes sense, as α-actin 4 is an adapter molecule that alters integrin function and maintain the structure and architecture of β-actin, which is important for cellular attachment to the extracellular matrix, cell survival, and chemoresistance (97). Under the influence of LPA, cell adhesion increases in cells expressing OCIAD1 to α1, α5, and αv actins (88).

1.5.3 OCIAD1 Mitochondrial Expression and regulation of the ETC Complex I activity

A second distinct function for OCIAD1 has been proposed as a major regulator of electron transport chain (ETC) Complex I activity. If so, the protein may be more than just an immunoreactive agent in tumorigenesis, and this appears to hold true considering its expression in mitochondria (98). Early experiments in rodents on the discovery of OCIAD1 found that it is primarily expressed in the early embryonic mesoderm and cardiovascular lineages; however, as development progresses the protein eventually localizes to endosomal compartments and mitochondria (99), where it regulates multiple signaling pathways (JAK/STAT, Notch, PI3K/AKT) as to influence cell proliferation or

differentiation (100). Using a highly technical mass spectrometry approach, researchers determined that OCIAD1 interacted with several proteins of the inner mitochondrial membrane, many of which were associated with different complexes of the ETC (98).

1.5.4 OCIAD1 post-translational modifications: phosphorylation/cleavage

18:1 LPA rapidly stimulates phosphorylation of OCIAD1 at serine residues, S108, S123, and S191, resulting in increased OCIAD1 activity and, thus, increased regulation of cell attachment through the subsequent control of integrin function (88). More specifically, serine phosphorylation of OCIAD1 induced by LPA increases cellular adhesion to β1 integrin, and this effect is completely dysregulated in *OCIAD1*-null or *OCIAD1*-inhibited HEY cells (88).

Interestingly, OCIAD1 was recently identified as a novel cellular substrate of the hepatitis C virus (HCV) non-structural protein 3-4A (NS3-4A) protease, which is a key enzyme involved in the viral replication complex, and a primary target of protease inhibitors in clinical settings (101). Using quantitative proteomics, the authors found that the HCV NS3-4A protease cleaved OCIAD1 at Cys 38, which is a residue close to a transmembrane segment of the protein, but the protease had no enzymatic activity on OCIAD2. Moreover, this cleavage was observed in liver biopsies from patients with chronic hepatitis C. These data suggest OCIAD1 may be involved in the pathogenesis of hepatitis C *in vivo*, however, more work needs to be done to fully understand its involvement.

1.6 Membrane yeast two hybrid system (MYTH)

Determination of protein interactions is an important step in the identification of a protein's biological function. In the past, the hydrophobic nature of membrane proteins presented a technical challenge thereby preventing the study of their interactions. Membrane proteins play a key role in disease processes and serve as pharmaceutical targets. Therefore, mapping of protein interactions is crucial. Fortunately, a method known as the membrane yeast two-hybrid (MYTH) assay was developed to enable the study of membrane protein interactions. MYTH uses the principle of ubiquitin splitting to detect protein-protein interactions *in vivo*, facilitating the large-scale screening of protein interactions in a wide range of organisms using *Saccharomyces cerevisiae* as the host organism. This technology relies on the interaction between a 'bait' and 'prey' proteins. The membrane bound bait protein is fused to the C-terminus of ubiquitin (denoted C_{ub}) and to the LexA-VP16 transcription factor, while the prey protein is fused to the N-terminal portion of ubiquitin (Nub). Wild-type N_{ub} and C_{ub} fragments will spontaneously re-associate with one another, but modified NubG will prevent this re-association unless the fragments are in proximity or interact. Once the Nub and Cub fragments re-associate, the full-length ubiquitin is recognized by the endogenous yeast machinery and cleaved by deubiquitinating enzymes (DUB). This cleavage releases the LexA-VP16 TF, which then binds to a transgenic, synthetic promoter to generate a product that can be selected by the growth of yeast on different media (Figure 1.7) (102).

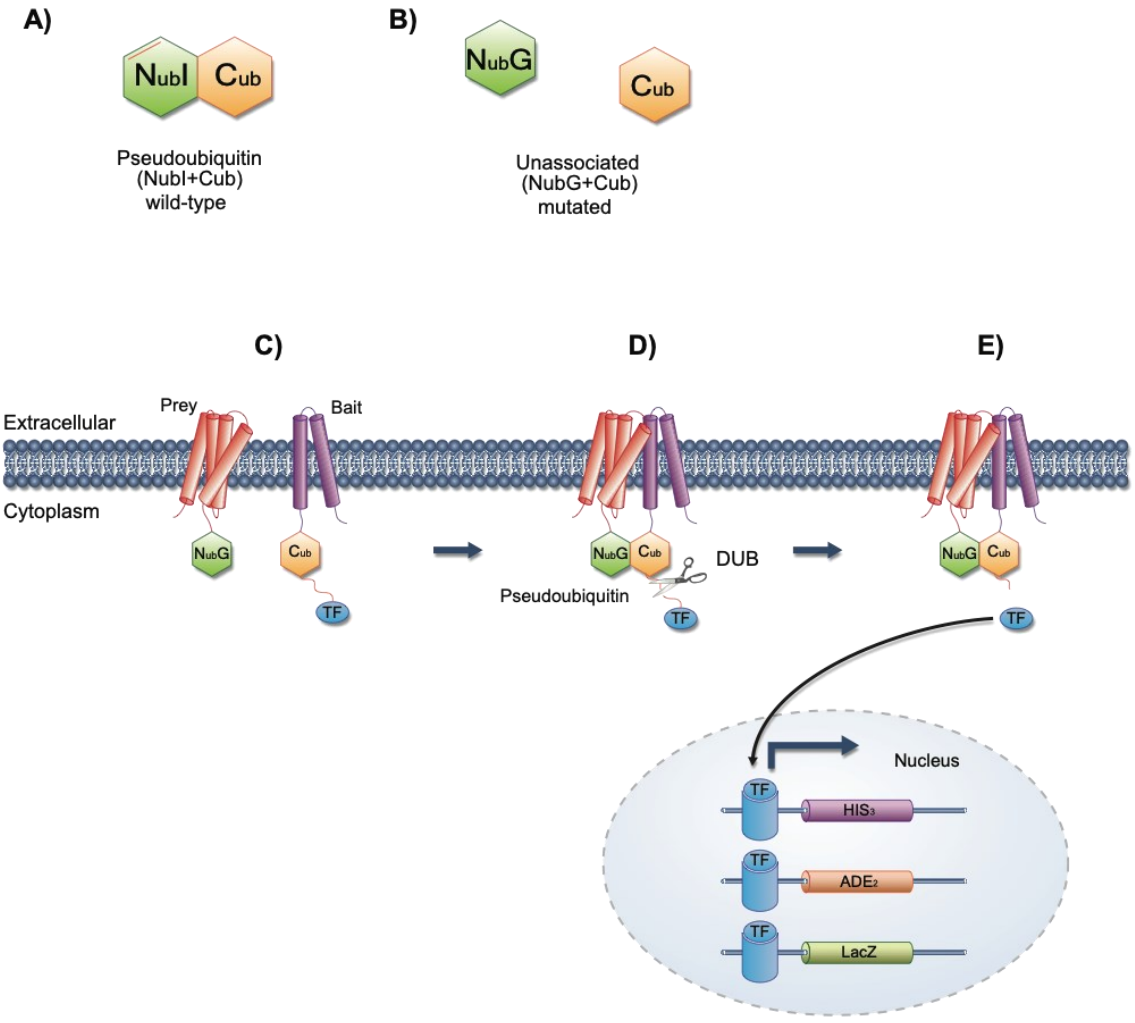

Figure 1.7: Membrane yeast two hybrid system (MYTH)

(A) MYTH screening relies on split ubiquitin: ubiquitin can be expressed as two half proteins, C- and N- terminal moieties (C_{ub} and $N_{ub}I$), which can reassociate to form pseudoubiquitin. C_{ub} and $N_{ub}I$ can be tagged onto bait and prey proteins to detect protein-protein interactions. **(B)** $N_{ub}I$ is mutated to the $N_{ub}G$ to prevent the spontaneous reassociation of pseudoubiquitin for the use in MYTH. **(C)** The bait protein is shown in purple while the prey protein is shown in red. The bait protein is tagged with C_{ub}-LexA/VP16 transcription factor denoted as 'TF' while the prey protein is tagged with the

$N_{ub}G$. **(D)** The interaction between the bait protein and the prey protein results in the formation of pseudoubiquitin molecule which is detected by the cytosolic deubiquitinating enzymes (DUB). **(E)** The transcription factor (TF) is released when DUB cleaves after the C-terminus of the C_{ub} tag. Then the transcription factor (LexA/VP16) may enter the nucleus and induce expression of the reporter genes *HIS3, ADE2,* and *lacZ.* This allows growth on selective plates lacking adenine and histidine. Induction of *lacZ* leads to expression of β-galactosidase which produces blue colonies on plates containing X-Gal. Adapted and modified from (102).

1.7 Hypotheses

This thesis addresses the hypothesis that SLC4A11 interacts with proteins important for the pathogenesis of endothelial corneal dystrophies. Specifically, some of these protein interactors have important functions related to cell adhesion and possibly mitochondrial dysfunction as well.

Recent studies demonstrated that *SLC4A11* mutation, which encodes a plasma membrane protein involved in endothelial corneal dystrophies, may negatively impact trans-endothelial water flux in the cornea due to protein misfolding or retention of the protein in the ER. Additional studies have described corneal endothelial SLC4A11 to be highly involved in cell adhesion as well, indicating that loss-of-function mutations in the gene may perturb cell adhesion processes. To investigate the association of SLC4A11 with cell adhesion and corneal water transport, the MYTH screening method was used to identify SLC4A11-specific protein interactors. Overall, six full-length proteins were identified, and Chapter 3 of this thesis describe each of these proteins and how/why they may be involved with SLC4A11 and endothelial corneal dystrophy. One of these protein interactors was OCIAD1, a protein expressed in the mitochondria that also regulates cell adhesion. Interestingly, extracellular loop 3 of SLC4A11 interacts with COL8A2, a major component of the DM, and abnormalities in cell adhesion likely mediate some of the loss of corneal endothelial cells in FECD and CHED. Due to this finding, we decided to further examine the interaction between OCIAD1 and SLC4A11, specifically concerning cell adhesion. Thus, Chapter 4 and the latter end of this thesis address the hypothesis that the interaction between SLC4A11 and OCIAD1 is important for cell adhesion using a variety of cell types and cornea tissue.

1.8 Thesis objectives and overview

There are two primary objectives of this thesis:

1. To generate a list of proteins that interact with SLC4A11, using the Split-Ubiquitin Based Membrane Yeast Two-Hybrid (MYTH) screening system. This list will allow us to identify or determine significant SLC4A11 protein interactors in the context of endothelial corneal dystrophies.
2. To characterize and better understand the role of SLC4A11 and one of the identified interactors (OCIAD1) in corneal endothelial cells and endothelial corneal dystrophies.

Chapter 2 provides a detailed explanation of the materials and methods used in the experiments, including generation of the cDNA library used in the MYTH screen, cell types and tissues used, etc.

Chapter 3 describes the MYTH screen results and the function of each of the six identified protein interactors.

Chapter 4 explores the significance of the interaction between OCIAD1 and SLC4A11, specifically concerning cell adhesion in an ovarian cancer cell line (SKOV3 cells), HEK293 cells, and bovine cornea tissues. This chapter also demonstrates the importance of the interaction of OCIAD1 and SLC4A11 and provides a better understanding as to why mutations of the SLC4A11 gene may promote endothelial corneal dystrophy due to dysregulation of cell adhesion.

Chapter 5 summarizes the major findings and potential future directions to further our understanding of the pathology behind corneal endothelial dystrophies, specifically involving mutations in SLC4A11 and dysregulation of the corneal water flux system or cell adhesion.

Chapter 2: Materials and Methods

Materials

Table 2.1: List of materials

Materials Used	Source
DNA Constructs and Cloning	
Restriction Enzymes	New England BioLabs (Ipswich, USA), Thermo Fisher Scientific (Ottawa, ON, Canada)
Phusion high fidelity DNA polymerase	New England BioLabs (Ipswich, USA)
Plasmid Midiprep kit	Qiagen (Germantown, MD, USA)
Oligonucleotides	Integrated DNA Technologies (Coralville, IA, USA)
Gel extraction kit and Mini plasmid extraction kit	FroggaBio (Ontario, Canada)
polynucleotides (dNTP), DNase I, and T4 DNA ligase	Thermo Fisher Scientific (Ottawa, ON, Canada)
Yeast and Bacterial Cultures and Transformation	
THY.AP4 yeast strain	Kindly provided by Dr. Igor Stagljar, University of Toronto
Tris (2,3-dibromopropyl) phosphate, ethylenediaminetetraacetic acid (EDTA), Yeast Extract, Peptone, Glucose, NaCl, 5-bromo-4-chloro-3-indolyl-β-D-galactopyranoside (X-Gal), phenylmethylsulfonyl fluoride (PMSF), Dimethyl sulfoxide (DMSO), and electroporation cuvettes, 1 mm gap	Thermo Fisher Scientific (Ottawa, ON, Canada)
Adenine hemi sulfate, Poly-L-lysine, yeast synthetic dropout medium (SD-leucine, SD-tryptophan, SD-leucine-tryptophan, SD-leucine-tryptophan-adenine-histidine), Salmon sperm DNA, and Polyethylene glycol (PEG)	Sigma Aldrich (Oakville, ON, Canada)
Lithium Acetate	Acros Organics (New Jersey, USA)
Glass beads (0.5 mm)	BioSpec (Ottawa, ON, Canada)
100 mm Petri dishes and 150 mm Petri dishes	Sarstedt (Montreal, QC, Canada)
Mammalian Cell Culture and Transfection	
Dulbecco's Modified Eagle's medium (DMEM), fetal bovine serum (FBS), calf serum (CS), and penicillin-streptomycin-glutamine (PSG)	Life Technologies (Carlsbad, CA, USA)

Trypsin EDTA (0.25%)	Gibco (Co Dublin, Ireland, UK)
T75, 100 mm and 6 well cell culture dishes	Sarstedt (Montreal, QC, Canada)
Biochemical Assays	
Bovine eyes	Kastelen Sausage and Fine Meats (Ardrossan, AB, Canada)
EDTA-free Complete Protease Inhibitor tablets	Roche Applied Science (Indianapolis, IN, USA)
Immobilon-P Polyvinylidene difluoride (PVDF) membranes and Luminata TM Crescendo Western horseradish peroxidase (HRP) Substrate chemiluminescence reagent	Millipore (Billerica, MA, USA)
BCA Protein Assay Kit	Pierce (Rockford, IL, USA)
HA tag monoclonal antibody (clone 16B12)	BioLegend Inc. (San Diego, CA, USA)
Protein A-Sepharose conjugated	Invitrogen (Rockford. IL, USA)
Anti-human OCIAD1 antibody (H00054940-B01P), mouse	Abnova (Walnut, CA, USA)
Fluorometric-format CytoSelect 48-well cell adhesion assay (Collagen I-coated) and CytoSelect 48-well cell adhesion assay (Fibronectin-coated) kits	Cell Biolabs (San Diego, CA, USA)
Anti-Myc tag antibody (05274), mouse	Millipore (Billerica, MA, USA)
Custom antibodies: rabbit or mouse anti-human SLC4A11 (M36) antibody, anti-bovine OCIAD1, anti-bovine TMEM 254, and anti-bovine ORMDL2	Primm biotech (Cambridge, MA, USA)
HRP-conjugated sheep anti-mouse antibody	GE Healthcare Bio-Sciences Corp. (Piscataway, NJ, USA)
Goat anti-rabbit antibody Anti-Myc tag antibody, rabbit (SC789) HA-tag antibody (SC805), rabbit Anti-Na^+/K^+ ATPase (SC28800), rabbit Anti-Na^+/K^+ ATPase (SC48345), mouse Anti-GAPDH (SC47724), mouse	Santa Cruz Biotechnology (Santa Cruz, CA, USA)
iQ-SYBR green super mix	Bio-Rad Laboratories (Hercules, CA, USA)
Phenyl methane sulfonyl fluoride (PMSF)	Thermo Fisher Scientific (Ottawa, ON, Canada)

Methods

2.1 Cloning

2.1.1 DNA constructs

The plasmids for MYTH screening (pPR3N, pCMBV, Ost- $N_{ub}G$, Ost- $N_{ub}I$, Fur4-$N_{ub}G$ and Fur4-$N_{ub}I$) were a generous gift from Dr. Igor Stagljar, University of Toronto (102).

2.1.1.1 Bait cloning (SLC4A11-PCMBV)

SLC4A11 was amplified from the plasmid pAMC1 (66) into pJET cloning vector (Thermo Fisher Scientific, ON, Canada) using the phosphorylated forward and reverse primers with Sfi1 restriction site (5'-AGCATACAATCAACTCCAAGCTGGCCGCTCTAGACGGCCAAAAAATGTCCCAGAACGGTTACTTCGAG-3'), and (5'-ATCGAATTCCTGCAGATATACCCATGGAGGCCTTTGGCTGGTCTGTGCTCAGCGTCCATAAC-3'), respectively. pAMC1 plasmid construction was described previously (78). Then used the pJET clone as a template for more PCR with primers including Stu1 restriction site to clone the insert into pCMBV vector. The forward and reverse primers used to clone into pCMBV are (5'- ACTGATCTCGGCCAAAGGAAAAATGTCCCAG -3') and (5'-CTAGCTCCCATGGAGGCCTGGTCTGT -3'), respectively. PCR products and vectors were digested with the proper restriction enzymes then purified by gel extraction kit and ligated using T4 DNA ligase. Ligated product was purified using PCR clean-up kit then electroporated into DH5α electro competent cells and amplified as explained at Section 2.4. Plasmid was extracted using Midiprep kit and stored at -20 °C. Clone integrity was confirmed by sequencing at Institute

for Biomolecular Design (IBD), Department of Biochemistry, University of Alberta or The Molecular Biology Service Unit, Department of Biological Sciences, University of Alberta.

2.1.1.2 Potential interactors cloning

Cloning of interacting proteins (cDNA of bovine or Human ortholog) into pcDNA 3.1 (+) for protein expression in cell culture. Cloning was performed by PCR amplification of identified interactors with an addition of the restriction sites Nhe1 and Xho1 and either a MYC or HA epitope tag in the primers as listed in detail (Table 2.2 and 2.3). cDNA for the human orthologs of the identified protein interactors OCIAD1, ORMDL1, CMP-SAT, LEPROTL1, clone ID HsCD00444701, HsCD00440927, HsCD00439242, HsCD00440680, respectively were from DNASU DNA Repository (AZ, USA). TMEM 254 cDNA (SC108384) was from OriGene (Rockville, MD, USA). PCR products were digested, separated on agarose gel then purified using a gel extraction kit, ligated then purified and electroporated into DH5α cells as explained below and extracted using a Midiprep kit. Clone integrity was confirmed by sequencing at Institute for Biomolecular Design (IBD), Department of Biochemistry, University of Alberta or The Molecular Biology Service Unit, Department of Biological Sciences, University of Alberta.

2.1.1.3 Cloning of bovine Slc4a11

Cloning of bovine *Slc4a11* into pcDNA 3.1 (+) for protein expression in cell culture, the plasmid was named (pNDA35). Cloning was performed by PCR amplification of bovine *Slc4a11* with an addition of the restriction sites Nhe1 and HindIII and an HA epitope tag. The primers used for amplification were, forward primer

Table 2.2: Oligonucleotides used to clone bovine potential interactors into pcDNA 3.1 + vector.

Construct (plasmid name, vector, protein encoded)	Forward Primer	Reverse Primer
pNDA8 (pcDNA-Myc-bovine Ociad1)	5'-GCTAGCGCCACCATGGAACAAAAACTCATCTCAGAAGAGGATCTGATGAATGGGAGGGCT-3'	5'-CCGCCGCTCGAGTCACTCATCCCAAGTATCTC-3'
pNDA12 (pcDNA-Myc-bovine Tmem 254)	5'-TACGCTAGCGCCACCATGGAACAAAAACTCATCTCAGAAGAGGATCTGCGGAAGGCAAGAGGAGATG-3'	5'-CCGCCGCTCGAGTTAAGTTTGTTTTTGGTGTTTTGGT-3'
pNDA15 (pcDNA-Myc-bovine Tmem 128)	5'-TACGCTAGCGCCACCATGGAACAAAAACTCATCTCAGAAGAGGATCTGGATGTTCTACGGGCTCGG-3'	5'-CCGCCGCTCGAGTCATCCAAGGAGTGAGGTCA-3'
pNDA20 (pcDNA-Myc-bovine Ormdl2)	5'-TACGCTAGCGCCACCATGGAACAAAAACTCATCTCAGAAGAGGATCTGAATGTGGGGGTGGCAC-3'	5'-CCGCCGCTCGAGTCAGTATTTGTTGATGCCAAAG-3'

Table 2.3: Oligonucleotides used for cloning human orthologs of potential interactors into pcDNA 3.1 + vector.

Construct (plasmid name, vector, protein encoded)	Forward Primer	Reverse Primer
pNDA22 (pcDNA-Myc-human-OCIAD1)	5'-GGAGCTAGCGCCACCATGGAACAAAAACTCATCTCAGAAGAGGATCTGAATGGGAGGGCTGATTTTC-3'	5'-GGACCTCGAGTCACTCATCCCAAGTATCTCCATAC-3'
pNDA23 (pcDNA-Myc-human-TMEM 254)	5'-GGAGCTAGCGCCACCATGGAACAAAAACTCATCTCAGAAGAGGATCTGGCTACGGCAGCCGGC-3'	5'-GGACCTCGAGTCAAGTTTGTTTTTGGCGCTT-3'
pNDA24 (pcDNA-Myc-human-ORMDL2)	5'-GGAGCTAGCGCCACCATGGAACAAAAACTCATCTCAGAAGAGGATCTGAACGTTGGAGTTGCCCAC-3'	5'-GGACCTCGAGTCAATACTTATTAATTCCAAAGATCCG-3'
pNDA25 (pcDNA-Myc-human-CMP -SAT)	5'-GGAGCTAGCGCCACCATGGAACAAAAACTCATCTCAGAAGAGGATCTGGCTGCCCCGAGAGACA-3'	5'-GGACCTCGAGCTACACACCAATAACTCTCTCCTTTG-3'
pNDA30 (pcDNA-HA-human-OCIAD1)	5'-GGAGCTAGCGCCACCATGTATCCGTATGATGTGCCGGATTATGCGAATGGGAGGGCTGATTTTC-3'	5'-GGACCTCGAGTCACTCATCCCAAGTATCTCCATAC-3'

(5'-CTGGCTAGCGCCACCATGTATCCGTATGATGTGCCGGATTATGCGTCGCAGAATGGATACTTTGAG-3') and reverse primer (5'-CTGAAAGCTTTCAGTGTTCAGCATCCATG-3') cDNA for the bovine Slc4a11 was amplified from the plasmid (CML.B. SLC4A11). PCR products were digested, separated on agarose gel then purified using a gel extraction kit, ligated then purified and electroporated into DH5α cells as explained below in section 2.4 and extracted using a Midiprep kit. Clone integrity was confirmed by sequencing at Institute for Biomolecular Design (IBD), Department of Biochemistry, University of Alberta or The Molecular Biology Service Unit, Department of Biological Sciences, University of Alberta.

2.2 Preparation of Chemically competent cells

DH5 alpha cells were grown in 1 L super optimal broth (SOB) media (2% (w/v) Bacto tryptone, 0.5% (w/v) yeast extract, 10 mM NaCl, 2.5 mM KCl, 10 mM $MgCl_2$, 10 mM $MgSO_4$, pH 7) to A_{600} of 0.5 at 18 °C. Cells were cooled at 4 °C for 10 min then centrifuged at 3000 g for 10 min at 4 °C. Cells were washed twice with ice cold transformation buffer (TB) (15 mM $CaCl_2$, 250 mM KCl, 55 mM $MnCl_2$, 10 mM piperazine-N,N′-bis(2-ethanesulfonic acid) (PIPES), pH 6.7) with gentle swirling. DMSO was added dropwise with gentle swirling to a 7% concentration and incubated at 4 °C for 1 min. Cells were aliquoted (250 µl) in sterile 1.5 ml centrifuge tubes and snap frozen in liquid nitrogen and stored at -80 °C (103). The resulting transformation efficiency of the cells was $7x10^5$ colonies/µg DNA.

2.3 Bacterial Chemical Transformation

Chemically competent DH5α cells were thawed at 4 °C for 30 min. Purified plasmid (100 pg DNA) was added to the cells and incubated for 30 min at 4 °C. Cells were then incubated at 42 °C for 30 s followed by incubation on ice for 2 min. LB medium was added to the cells and incubated for 90 s at 37 °C, with shaking at 250 rpm. Cells were then centrifuged at 5000 g for 5 min, the supernatant was discarded, and the cells were resuspended in LB medium and plated on the appropriate selective plates containing antibiotics for 16 h at 37 °C (104).

2.4 Bacterial Transformation by Electroporation

DH5α electro-competent cells were prepared (105) with minimum transformation efficiency of 1 X 10^9 Colony Forming Units (CFU)/µg of the transformed cDNA constructs. Frozen cells were thawed on ice for 10 min. Purified plasmid (10 pg DNA) was added to the cells and transferred to pre-chilled 1 mm gap electroporation cuvettes (Thermo Fisher Scientific, ON, Canada) and incubated for 1 min at 4 °C. Cells were electroporated with the Eppendorf Electroporator 251 at 1800 V with a time constant close to 5 ms. The electroporated cells were revived by adding super (450 µl) optimal catabolite (SOC) medium (2% (w/v) tryptone, 0.5% (w/v) yeast extract, 10 mM NaCl, 2.5 mM KCl, 10 mM $MgSO_4$, 10 mM $MgCl_2$, 20 mM glucose) and incubated at 37 °C with 250 rpm shaking for 1 h. Cells were then spread on plates containing the appropriate selection medium with antibiotics and incubated at 37 °C for 16 h (105).

2.5 Membrane Yeast Two Hybrid (MYTH) Screening

All steps for MYTH screening were performed as described (102) unless mentioned differently after each method. The cDNA library was synthesized from bovine corneas and cloned in the plasmid pPR3N (will be explained in detail in 2.5.1). Two different yeast strains THY.AP4 (MATa

leu2, ura3, trp1: (lexAop)-lacZ (lexAop)-HIS3 (lexAop)-ADE2) or L40 *(MATa HIS3 200 trp1-901 leu2-3, 112 ade2 LYS2: (lexAop)$_4$-HIS3 URA3:: (lexAop)$_8$-lacZ GAL4)* were transformed with the plasmids pAMBV, pCMBV, and pTMBV (cloned with human SLC4A11 cDNA) and tested for the best growth on selective transformation plates, synthetic dropout medium without leucine and tryptophan (SD-Leu-Trp). All yeast strains and plasmids were generously provided from Dr. Igor Stagljar. The strain THY.AP4 transformed with pCMBV-SLC4A11 was selected for screening. After validation, THY.AP4 yeast cells transformed with pCMBV-SLC4A11, were co-transformed with the cDNA library to screen for potential interactors and grown on selective transformation (SD-Leu-Trp) and interaction plates, synthetic dropout medium without leucine, tryptophan, histidine, adenine (SD-Leu-Trp-His -Ade). Positive colonies growing on selective plates from first and second screenings (section 2.5.6) were amplified and pPR3N plasmid was recovered from the colony. The colonies were then transformed and amplified in bacterial cultures by chemical transformation and electroporation (sections 2.3 and 2.4) and the plasmid was extracted. The purified plasmid was sequenced to determine the sequence of the potential interactor. The sequence was identified by alignment and data analysis on BLAST (basic local alignment search tool) from NCBI (national center for biotechnology information) https://blast.ncbi.nlm.nih.gov.

2.5.1 cDNA Library synthesis

Bovine cornea (one) was dissected from a cow no less than 6 hours after death and snap frozen in liquid nitrogen, then shipped to Bio S and T Company (Québec, Canada) at 4 °C in dry ice. Total RNA (3.9 µg) was purified from bovine corneas using Norgen's animal tissue RNA purification kit. Double stranded cDNA was synthesized from the extracted RNA using a modified smart

cDNA synthesis method, using oligo dT to prime reverse transcription. First strand cDNA was annealed to the primers (5'-CAGTGGTATCAACGCAGAGTGGCCATTACGGCCAAGTTACGGG-3') and (5'-AAAAAAAAAAAAAAAGGCCGCCTCGGCCACTCTGCGTTGATACCACTG-3') with the Sfi1 restriction site underlined to synthesize of double stranded cDNA. Amplified cDNAs were Sfi1 digested, and size fractioned on a 1% agarose gel. cDNA fragments greater than 1.2 kb were purified for cloning. The purified digested cDNA fragments were ligated in the vector pPR3N at the Sfi1 restriction site. The ligated products were transformed into DH10B-T1^{R} bacterial cells (Invitrogen Inc.). About 1x10^{5} clones were grown per large Petri dish (10 dishes). Transformed cells were pooled and stored in a 1% glycerol stock in ten separate tubes (contain about 1x10^{5} clones and 3 ml per tube) at -80 °C. Plasmids were extracted using a midiprep kit, stored at -20 °C, and used for transformation for MYTH screening.

2.5.2 Lithium Acetate Yeast transformation

The THY.AP4 *(MATa leu2, ura3, trp1:: (lexAop)-lacZ (lexAop)-HIS3 (lexAop)-ADE2)* reporter yeast strain containing the selectable markers (*ADE2, HIS3*, and *LacZ*) and activated under the control of promoters with LexA operator site was used for MYTH screening (102). Cells were grown in 50 ml 2X yeast peptone adenine dextrose (YPAD) medium (2% (w/v) Bacto yeast extract, 4% (w/v) Bacto peptone, 4% (w/v) glucose, 0.2 M glucose, 0.1 mM adenine sulfate) with 200 rpm shaking at 30 °C and grown to A_{600} of 2. Cells were harvested by centrifugation at 3000 g for 5 min and washed twice with sterile distilled H_2O. Cells were transferred into 1.5 ml microcentrifuge tubes and centrifuged for 30 s at 13000 g. Cells were resuspended in 1 ml sterile water and aliquoted into 10^{8} cells in each tube. Cells were centrifuged at 13000 g for 30 s and the supernatant

was discarded. Cells were resuspended with a transformation mix containing (33% (w/v) PEG, 0.1 M LiAc, 50 µl of 2 mg/ml boiled salmon sperm single stranded carrier DNA, 1 µg purified plasmid), and were then vortexed and incubated for 90 min at 42 °C. Next, the cells were centrifuged at 13000 g for 30 s and resuspended in sterile distilled H_2O and plated on appropriate transformation selection plates (SD-Leu) or (SD-Trp) or YPAD and incubated at 30°C for 3-4 days (106). Colonies were picked and stored at -80 °C in glycerol stocks for each transformation.

2.5.3 Frozen Glycerol Yeast Stocks

Transformed yeast cultures grown in appropriate media (1 ml) were supplemented with glycerol to a final concentration of 30% in sterile cryovials tubes and mixed. Tubes were kept in liquid nitrogen to freeze the cells then stored at -80 °C.

2.5.4 Bait validation test

pCMBV-SLC4A11 was co-transformed with cDNA encoding Fur4 (pFur4- N_{ub}I or pFur4- N_{ub}G), an uracil permease localized at the plasma membrane, or transformed with Ost1, an oligosaccharyltransferase at the endoplasmic reticulum membrane (pOst1- N_{ub}I or pOst1- N_{ub}G). Validation of the non-activating bait of the MYTH screening was performed by co-transformation of pCMBV-SLC4A11 with Fur4-N_{ub}I as a positive control or with Fur4-N_{ub}G as a negative control. Similar tests were performed with Ost-N_{ub}I positive or Ost-N_{ub}G negative controls using the lithium acetate yeast transformation. Transformed yeast cells were grown on transformation plates (List of agar plates) . Colonies were picked and resuspended in 100 µl 0.9% (w/v) NaCl. Cells were serially diluted in 0.9% (w/v) NaCl to 1:10, 1;100, and 1:1000. Diluted cells (2.5 µl)

were spotted on both transformation selection plates (SD-Trp-Leu) and interaction selection plates (SD-Trp-Leu-Ade-His) + X-Gal. Plates were incubated at 30 °C for 4 days.

2.5.5 Large-scale transformation for library screening

THY.AP4 yeast cells transfected with pCMBV-SLC4A11 were grown in 200 ml of synthetic dropout medium without leucine (SD-Leu) to A_{600} of 0.8-1 at 30 °C with shaking at 200 rpm. Cells were divided into four 50 ml Falcon tubes and centrifuged at 700 g for 5 min at 4 °C. The cells were then washed with sterile distilled H_2O, then washed twice with 1 ml fresh lithium acetate (LiAc)/Tris- Ethylenediaminetetraacetic acid (EDTA) solution (100 mM LiAc, 100 mM Tris, 1 mM EDTA pH 7.5). Next, cells were washed with 2.5 ml polyethylene glycol (PEG)/ LiAc solution (100 mM LiAc, 40% (w/v) PEG, 1 mM EDTA, 10 mM Tris, pH 7.5), supplemented with 2.5 ml of 2 mg/ml boiled salmon sperm single stranded carrier DNA and 10 μg cDNA library. Cells were incubated in a 30 °C water bath for 45 min and vortexed briefly every 15 min. DMSO (160 µl) was added and the cells were incubated at 42 °C for 20 min. The supernatant was discarded, and the pellet was resuspended with 3 ml of 2X YPAD medium and pooled together in in a 50 ml falcon tube. Cells were then incubated at 30 °C with shaking at 200 rpm for 90 min. Then the cells were harvested at 700 g centrifugation for 5 min at 4 °C and resuspended in 4.9 ml 0.9% (w/v) NaCl. The resulting cell suspension (100 µl) was taken for serial dilutions in 0.9% (w/v) NaCl and spread on agar plates with transformation selection medium (SD-Leu-Trp) to determine the total number of transformants. In first selection, the remaining volume of resuspended cells was plated equally onto 150 mm diameter agar plates containing interaction selection medium (SD-Trp-Leu-Ade-His) for 4 days at 30°C.

In second selection, grown colonies were picked and resuspended in 100 µl 0.9% (w/v) NaCl. Then 2.5 µl of the resuspended colony was spotted on an interaction selection plate (SD-Trp-Leu-Ade-His) containing 0.2 mM 5-bromo-4-chloro-3-indolyl-β-D-galactopyranoside (X-Gal) dissolved in N, N-dimethyl formamide, 50 mM sodium phosphate dibasic, and 25 mM sodium phosphate monobasic) and incubated at 30 °C for 4 days. Addition of X-gal enabled positively interacting colonies to appear as blue colored colonies. Interacting colonies with this blue color were further analyzed (Section 2.5.6) (102).

2.5.6 Analysis of potential interacting colonies

Colonies where bait and prey proteins interacted (as indicated by their blue color) were grown in 5 ml SD-Trp medium for 16 h at 30 °C with shaking at 200 rpm. Plasmid was isolated using a commercial miniprep kit with one modification: after resuspension of the cells at the first step, a small volume of 0.5 mm glass beads was added to the cells and vortexed vigorously for 2 min. Further steps were followed as per the manufacturer's instructions. The isolated plasmid was then chemically transformed into DH5α chemically competent *E. coli* cells (Section 2.3) and amplified in LB medium, containing 100 µg/ml ampicillin for 16 h at 37 °C, with shaking at 250 rpm as explained above. Plasmid was isolated from *E. coli* using Qiagen miniprep kit, following the manufacturer's instructions, and cultures were stored at -20 °C. Plasmids that did not chemically transform were electroporated into DH5α cells as explained above (Section 2.4).

Isolated plasmids were then sent for sequencing using the $N_{ub}G$ forward internal sequencing primer (5'-CCGATACCATCGACAACGTTAAGTCG-3'). From the sequencing results, first was translated then the sequence after the cloned linker was aligned with BLAST protein database to identify the interacting protein (107). Potential interacting partners were

identified based on determination of the full-length proteins, oriented with their N- terminus in the cytosol. Exclusion criteria is explained in section 3.2.4.

2.6 Mammalian Cell Culture

Human Embryonic Kidney cells (HEK) 293 and SKOV3 ovarian cancer cells were grown and cultured in Dulbecco's Modified Eagles Media (DMEM) containing (5% (v/v) fetal bovine serum, 5% (v/v) calf serum, and 1% (v/v) penicillin-streptomycin-glutamine. Cells were cultured at 37 °C in a humidified 5% CO_2 atmosphere.

2.6.1 Poly-L-lysine coating of cell culture coverslips

All steps were performed in a cell culture hood using sterile solutions. Round 25 mm glass coverslips were placed in 100 mm tissue culture dishes and immersed in 5 M NaOH for 15 min and removed. Coverslips were rinsed with water for 5 min followed by 95% EtOH for 5 min and rinsed again with water for 5 min. Coverslips were washed twice with PBS for 5 min then incubated with 1 mg/ml poly-L-lysine dissolved in PBS for 15 min. Poly-L-lysine was removed and the coverslips were dried under ultraviolet light for 16 h. The coverslips were stored at 22 °C or rinsed with PBS before use (36).

2.6.2 Calcium phosphate transfection

HEK293 or SKOV3 cells were grown in DMEM containing 100 mm cell culture dishes at 25% confluency for 4 h at 37 °C in a humidified incubator with an atmosphere of 5% CO_2. Transfection solution was prepared by mixing 590 µl of 2X HEPES solution (140 mM NaCl, 1.5 mM Na_2HPO_4,

50 mM 4-(2-hydroxyethyl)-1-piperazineethanesulfonic acid (HEPES) pH 7) with 590 µl DNA mix (2 M $CaCl_2$, 0.2-5.6 µg DNA plasmid) and incubated for 15 min at 22 °C then added dropwise to the cells. Cells were incubated for 40-48 h at 37 °C in an incubator with 5% CO_2 (108).

siRNA against *OCIAD1* (5′-AAUUGGUCUUGGAACCUCUGCAUUC-3′) and 5′-GAAUGCAGAGGUUCCAAGACCAAUU-3′), and scrambled siRNA, *OCIAD1*-RNAi, and SC-RNAi, respectively, were transfected into SKOV3 cells using Lipofectamine 3000 Reagent (Invitrogen) according to the manufacturer's protocol.

2.6.3 Cell lysis

HEK293 transfected cells were harvested after 40-48 h incubation in a 37 °C incubator with 5% CO_2 balanced air. Cells were washed with 10 ml ice cold PBS (140 mM NaCl, 3 mM KCl, 6.5 mM Na_2HPO_4, 1.5 mM KH_2PO_4, pH 7.4). Then cells were de-attached from the plates using a cell scraper at 4°C and solubilized in 4 °C immunoprecipitation buffer (IPB) (1% (v/v) IGEPAL CA-630, 5 mM EDTA, 150 mM NaCl, 0.5% (w/v) sodium deoxycholate, 10 mM Tris, pH 7.5) containing fresh 1 mM PMSF from a 100 mM stock dissolved in ethanol and EDTA-free Complete Protease inhibitor Cocktail. Then cells were incubated at 4°C for 20 min. Lysates were centrifuged at 13,000 g for 10 min at 4 °C and the resulting supernatant was either suspended in equivalent volume of 2X SDS-PAGE sample buffer and resolved by SDS-PAGE or stored at -20 °C (77).

2.7 Preparation of custom antibodies

Antibodies were raised in rabbit or mouse against synthetic peptides, corresponding to the identified human SLC4A11-protein interactors, by PrimmBiotech (Cambridge, MA USA). Table

Table 2.4: List of custom antibodies.

The list includes the name of each antibody, the antigen sequence it binds to and the species that the antibody was raised in.

Antibody	Synthetic Peptide	Species
Anti- OCIAD1	NH_2-CRSSPPGHYYQKSKYDSS-COOH	Mouse
Anti- TMEM 254	NH_2-SQNGYFEDSSYYKC-COOH	Rabbit
Anti- ORMDL2	NH_2-CETPDQGKARLLTHWEQ-COOH	Mouse
Anti- bovine Slc4a11	NH2- SQNGYFEDAGYLKC- COOH	Rabbit

2.4 shows the name of custom antibodies used and the sequence of the synthetic peptide used for immunization of animals.

2.8 Immunoprecipitation

2.8.1 Immunoprecipitation of SLC4A11 and ORMDL

Immunoprecipitation was performed following the steps described previously (77). HEK293 cells were calcium phosphate-transfected with human HA-SLC4A11 (pAMC1) and human Myc-ORMDL2 cDNAs (pNDA24), or human SLC4A11 and human Myc-ORMDL2 cDNA. Post-transfection 40 h, cells were lysed in immunoprecipitation buffer (IPB: 1% (v/v) IGEPAL CA-630, 5 mM EDTA, 150 mM NaCl, 0.5% (w/v) sodium deoxycholate, 10 mM Tris, pH 7.5), containing a Complete Protease inhibitor Cocktail and incubated at 4 °C for 20 min. Sample lysates were centrifuged at 13,200 g for 20 min at 4 °C.

At the same time, 25 µl of Dynabeads Protein G magnetic resin for each sample was washed with 200 µl of IPB and incubated with 2 µg of rabbit anti-HA antibody (AB137838 Abcam, USA) at 4 °C for 30 min. 300 µg of lysates was incubated with the lysate and beads mixture overnight at 4 °C. Total protein (10 µg) was incubated at 4 °C was set aside. Samples (lysate and beads mixture) were washed three times with IPB, containing complete protease inhibitors, resuspended in 50 µl of 2x SDS sample buffer, heated at 65 °C for 5 min and resolved on SDS PAGE (Section 2.9).

2.8.2 Immunoprecipitation of SLC4A11 and OCIAD1 in bovine cornea lysates

Freshly isolated bovine eyes (Four) were preserved at 4 °C and kept on ice before dissections. Eyes were washed with 4 °C PBS and the dissected cornea was cut in small pieces and resuspended in IPB Buffer containing PMSF and protease inhibitors for 30 min at 4 °C. Lysate was prepared and 220 μg of total protein was immunoprecipitated with 2 μg of IgG mouse anti-OCIAD1 antibody, or immunoprecipitated with2 μg of IgG mouse anti-Na^+/K^+ ATPase antibody. Lysates were resolved on 7.5 % SDS-PAGE, blotted, and probed with the custom rabbit anti-bovine SLC4A11 antibody (PrimmBiotech, Inc. Cambridge, MA – USA). Samples of the lysate were probed to indicate the total amount of Slc4a11. Samples of the lysate were also resolved on 10% acrylamide SDS-PAGE gels, blotted, and probed to indicate the total amount of OCIAD1 in the sample.

2.8.3 Immunoprecipitation of SLC4A11 and OCIAD1 in HEK293 cells and SKOV3 cells

For the immunoprecipitation assays, lysates from HEK293 and SKOV3 cells, which were transiently transfected with empty vector (pcDNA), co-transfected with OCIAD1-Myc and a HA tag bovine SLC4A11 (bSlc4a11-HA), or co-transfected with OCIAD1-Myc and a HA tag human SLC4A11 (hSLC4A11-HA) were prepared. Cell lysates were prepared using IPB^+ buffer (containing 10 mM Tris-HCl, pH 7.5, 1% NP40, 5 mM EDTA, 0.15 M NaCl, 0.5% deoxycholate, and 2 mg/ml BSA) and then transferred to an Eppendorf tube. After this, the lysates were precleared by adding resin and Sepharose mixture (prepared by adding equal volumes of 25 % slurry of protein A Sepharose in IPB buffer complemented with 0.02% NaN_3 and 35% slurry of Sepharose CL-4B in IPB buffer containing 0.02% NaN_3) and incubated with end-to-end rotation for 1 h at 4°C. After incubation, the resin of each lysate was sedimented by centrifugation at 9000 rpm at 4°C for 5 min. Supernatants without resin were transferred to a fresh microcentrifuge tube,

and the antibody and Sepharose mixture were added and incubated with end-to-end rotation overnight at 4°C. Resins were then sedimented by centrifugation at 9000 rpm for 5 min at 4°C. Supernatants were discarded carefully to avoid removing the resin. Remaining resins were washed consecutively with 1X ice-cold buffer 1 (containing 10 mM Tris-HCl, pH 7.5, 0.1% NP40, 1 mM EDTA, 0.15 M NaCl), buffer 2 (containing 10 mM Tris-HCl, pH 7.5, 2 mM EDTA, 0.05% SDS) and buffer 3 (containing 10 mM Tris-HCl, pH 7.5, 2 mM EDTA). The pellets formed after these treatments, were treated with 2X Laemmle sample buffer containing β-mercaptoethanol (at a final concentration of 2%). Before loading the gel, the samples were heated for 2 – 4 min at 70°C, and the resins were sedimented in a microcentrifuge. Finally, the samples were resolved on SDS PAGE, blotted, and probed with a mouse anti-HA antibody.

2.9 Immunoblots

Cell lysates were suspended in an equivalent volume of 2X SDS-PAGE sample buffer containing 2% (w/v) SDS, 10% (v/v) glycerol, 0.5% (w/v) bromophenol blue, 75 mM Tris, pH 6.8 with 2% (v/v) 2-mercaptoethanol and incubated at 65 °C for 5 min. Samples were centrifuged to remove insoluble material at 16,000 g for 10 min then resolved on 7.5% or 12% (w/v) acrylamide gels. Proteins were electro-transferred to Immobilon-P Polyvinylidene difluoride (PVDF) membrane as described (109). Membranes containing transferred proteins were incubated for 16 h at 4°C with gentle rocking in TBS-TM buffer (5% (w/v) non-fat milk powder in TBS-T (0.15 M NaCl, 0.1% (v/v) Tween-20, 50 mM Tris-HCl, pH 7.5)) with either mouse anti-Myc Millipore (Billerica, MA, USA), mouse anti-HA BioLegend Inc. (San Diego, CA, USA), the custom antibodies from PrimmBiotech (Cambridge, MA, USA), mouse anti-OCIAD1 or rabbit anti-TMEM 254 or mouse anti-ORMDL2 antibodies at 1:1500 or 1:2000 or 1:1000 or 1:1000 or 1:1000 dilution, respectively.

Membranes were washed three times with TBS-T for 15 min at 20 °C with gentle rocking. Membranes were incubated with sheep anti-mouse or donkey anti-rabbit HRP conjugated secondary antibody 1:5000 dilution in TBS-TM with shaking at 22 °C for 1 h and further washed with TBS-T three times. Blots were incubated with Luminata TM Crescendo Western HRP Substrate chemiluminescence reagent for 1 min and visualized using a GE ImageQuant LAS4000 blot imager (110).

2.10 Preparation of bovine Descemet's membrane extract

Corneas were dissected from fresh bovine eyeballs from two fresh eyeballs (approximately 4-6 h after sacrifice) and rinsed in PBS. Protocol is a modified version of that previously described (62). Descemet's membrane (DM) was micro-dissected and immersed in 0.05% (w/v) sodium azide and incubated at 22 °C for 2 h with end-over-end rotation. Sodium azide was removed by centrifugation at 5000 g for 2 min. DM was resuspended in 0.05% (w/v) sodium azide and 3% (v/v) Triton-X100 for 3 h with rotation at 22 °C. Supernatant was removed by centrifugation at 5000 g for 2 min and rinsed three times with sterile distilled water. Then DM was digested with 20 U/µl DNase I at 37 °C for 1 h. DM was centrifuged at 5000 g for 2 min and rinsed three times with sterile distilled water then resuspended in 0.05% (w/v) sodium azide and 4% (w/v) sodium deoxycholate for 3 h at 22 °C with rotation. Supernatant was removed by centrifugation at 5000 g for 2 min then 25 mg of purified DM was aliquoted in sterile centrifuge tubes and digested in 250 µl of 0.05 mg/ml pepsin dissolved in 0.5 M acetic acid for 24 h at 37 °C with rotation. Undigested DM was pelleted by centrifugation at 10,000 g for 10 min. Pepstatin was added to the supernatant in 1:1 molar ratio (pepsin: pepstatin) for inhibition of pepsin activity. Digested DM extract was aliquoted equally in sterile centrifuge tubes and frozen at -80 °C for 1 h and lyophilized for 16 h

and stored at -20 °C. Before use for cell adhesion assay, DM extract was reconstituted in PBS and quantified by BCA assay kit following manufacturer's instructions (62).

2.11 Cell adhesion assay

2.11.1 HEK293 cells

Protocol is a modified version of that previously described (62). Black flat clear bottom 96 well dishes with lid (Corning) were coated with 0.5 µg DM extract per well for 16 h at 4 °C. The wells were blocked with 100 µl of 10 mg/ml bovine serum albumin (BSA) dissolved in PBS for 1 h at 37 °C. HEK293 cells were transiently co-transfected with: 1.6 µg GFP cDNA and 1.5 µg of pcDNA3.1 (empty vector) cDNA; or 1.6 µg GFP cDNA and 1.0 µg of pcDNA3.1 and 0.5 µg of OCIAD1, cDNAs; or 1.6 µg GFP cDNA and 0.5 µg of pcDNA3.1 and 1.0 µg of SLC4A11, cDNAs; or 1.6 µg GFP cDNA and 0.5 µg of OCIAD1 and 1.0 µg of SLC4A11, cDNAs. Transfected cells were detached from the plates with 0.25% Trypsin-EDTA and sedimented by centrifugation at 500 g for 5 min then resuspended in DMEM. Cells were counted using a Countess II Automated cell counter then diluted to 6 x 10^5 cells/ml in DMEM. BSA was removed and the wells were coated with 50 µl of transfected cells (3 x 10^4 cells), followed by incubation for 3 h at 37 °C in an incubator with 5 % CO_2 in an air environment. Samples were analysed in quadruplicate. GFP fluorescence was measured for each well at 485 nm excitation and 512 emission using SynergyMX Plate Reader (BioTek, Winooski, VT, USA). Plates were centrifuged inverted at 6.8 g for 15 s to release loosely or non-adherent cells. A paper towel between the plate and the lid was added to absorb the excess solution using an Eppendorf 5810R centrifuge with an A-4-62 MTP rotor with bucket microplate-F carrier. PBS (200 µl) was added to each well and GFP fluorescence was measured. The previous steps for washing the cells and measuring GFP fluorescence were

repeated six times. The percentage of adhered cells was calculated at wash 5 relative to initial GFP fluorescence before washing using the calculation (GFP fluorescence after disruption/ GFP fluorescence before disruption) X 100% (62).

2.11.2 SKOV3 cells

SKOV3 cells were transfected with OCIAD1-RNAi (5′ AAUUGGUCUUGGAACCUCUGCAUUC 3′ and 5′ GAAUGCAGAGGUUCCAAGACCAAUU 3′) or SC-RNAi (non-overlapping low GC content RNAi negative control duplex) (Invitrogen, CA), or cotransfected with OCIAD1-RNAi and SLC4A11 cDNA. Cell adhesion experiments were performed on Collagen I-coated or BSA-coated (control) 48-well plates. Cell suspensions of transfected SKOV3 cells at a density of 1.0 x 10^6 cells/ml were prepared in serum-free DMEM medium containing 0.5% BSA, 2 mM $CaCl_2$ and 2 mM $MgCl_2$. Cell suspensions (150 µl) were applied to coated wells and incubated for 60 minutes in a cell culture incubator. Medium was aspirated and wells washed 4x with 250 µl PBS. Cells were lysed by incubation with 200 µl of Cyquant GR dye/lysis buffer and 20 minutes shaking at room temperature. The mixture (150 µl) was transferred to a 96-well plate and the fluorescence measured at 480 nm/520 nm in a SynergyMX Plate Reader. Cell adhesion was quantified as fluorescent units (arbitrary units) of control or transfected cells adhering to the Collagen I matrix, normalized to control or transfected cells adhering to BSA.

2.12 Cell surface biotinylation

HEK293 cells in 100 mm culture dishes were transiently transfected with SLC4A11-HA cDNA (pAMC1 plasmid), or transiently co-transfected with WT SLC4A11 and OCIAD1 cDNAs. In other

experiments, SKOV3 cells which endogenously express high OCIAD1 protein levels were transiently transfected with SLC4A11-HA cDNA or transfected with AE1-HA cDNA. Forty hours post-transfection, plates with transfected cells were transferred and maintained on ice. Cells were rinsed with cold PBS followed by 4 °C Borate buffer (154 mM NaCl, 7.2 mM KCl, 1.8 mM $CaCl_2$, 10 mM boric acid, pH 9.0). After washing, cells were incubated with 0.5 mg/ml Sulpho-NHS-SS biotin (Thermo Scientific, Rockford, IL, USA) in Borate buffer for 30 min. Cells were incubated for 5 min in Quenching buffer (QB) (192 mM glycine, 25 mM Tris, pH 8.3) at 4 °C. Cells were then washed with 4 °C QB and incubated with 500 µl IPB Buffer containing 1 mM PMSF and EDTA-free Complete Protease inhibitor cocktail (Roche, Mannheim, Germany) for 20 min on ice. Lysate was detached from the plates using a cell scraper and collected into pre-chilled microfuge tubes. Lysates were centrifuged at 13,000 g for 10 min and the resulting supernatant was split equally into two fractions. First fraction (total protein, T) was stored at 4 °C for later SDS-PAGE analysis. The second fraction was incubated with 100 µl of high-capacity streptavidin agarose resin (50% suspension) for 18 h at 4 °C with end-over-end rotation. Following centrifugation at 9800 g for 2 min, the supernatant fraction was collected (unbound fraction, U). Equal volumes of T and U fractions were resolved on SDS-PAGE and immunoblots as described above in section 2.9. Quantitative densitometry analysis for each band was performed using ImageQuant TL 1D software, v8.1 (GE Healthcare Life Sciences, ON). The percentage of biotinylated protein was calculated using the formula ((T-U)/T) x 100% (62). Biotinylation of samples was normalized to GAPDH expression that was detected on immunoblots.

2.13 Immunostaining of bovine cornea

For immunofluorescence experiments, isolated corneas from bovine eyes were stored in 10% (v/v) formalin and subsequently frozen at -80°C in a Shandon Cryomatrix (Thermo Electron). Cryostat sections (20 μm thick) of corneas were then cut onto glass slides. Following washing (2 × 5 min with PBS), and blocking (10% chicken serum in PBS, 30 min), cornea sections were incubated with primary antibodies in PBS buffer containing 0.5% (vol/vol) Triton X-100 (overnight, in a humidified chamber, 25°C), washed (3 × 5 min in PBS), and incubated with secondary antibody (1 h, in a humidified chamber, 25°C). Primary rabbit anti-Slc4a11 and mouse anti-Ociad1 antibodies were used at 1∶100 dilution and 1∶250, dilutions, respectively. Secondary chicken anti-rabbit conjugated to Alexa Fluor 488 (green), or secondary goat anti-mouse conjugated to Alexa Fluor 594 (red) were used at 1:200 dilutions. Slides were washed three times in PBS and mounted and viewed using confocal microscopy.

2.14 Imaging and analysis by confocal microscopy

Protocol is a modified version of that previously described (65). Multiple corneal sections from bovine eyes were studied. Morphology of bovine cornea was investigated by hematoxylin and eosin staining on 20 μm thick cryostat-cut corneas (62). Whole corneas were fixed and incubated with rabbit anti-SLC4A11 and mouse anti-OCIAD1 primary antibodies at 1∶100 and 1∶250 dilutions, respectively. Immunofluorescence signals were visualized by Alexa fluor 488-conjugated anti rabbit antibody (green, 1:100 dilution), and Alexa fluor 594-conjugated anti-mouse IgG antibody (red, 1∶100 dilution). Sections were mounted in Prolong Anti-fade solution (1 drop per coverslip) containing DAPI for nuclei staining (Molecular Probes, Eugene, OR, USA) to identify nuclei, and images were collected with a Zeiss LSM 510 laser-scanning confocal microscope with a x20 oil immersion objective or visualized with a x60 oil immersion objective.

Filtering was used to integrate the signal collected over 20 frames to decrease noise (scan time = 7 s/frame). Merged images were collected and analyzed with the ImagePro Software.

2.15 Localization of SLC4A11 and OCIAD1 Proteins in SKOV3 Ovarian Cancer Cells

Protocol is a modified version of that previously described (65). Immunofluorescence analysis was conducted on SKOV3 or SKOV3 cells transiently transfected with SLC4A11-HA cDNA (pAMC1 plasmid) and expressing endogenous OCIAD1. Cells grown on 22 × 22 mm laminin (30 μg/ml)-coated coverslips were washed in PBS and fixed for 20 min in 4% (w/v) paraformaldehyde in PBS. After three washes with PBS, the cells were incubated for 2 min in PBS containing 0.1% (v/v) Triton X-100. Slides were blocked for 30 min with PBSG (0.2% (w/v) gelatin in PBS) and incubated with a 1:100 dilution of rabbit anti-SLC4A11 antibody or rabbit anti-HA antibody, and 1:200 dilution of mouse anti-OCIAD1 antibody for 1 h in a humidified chamber at room temperature. After three washes with PBSG, coverslips were incubated for 1 h in a dark humidified chamber using a 1:250 dilution of Alexa Fluor 594-conjugated chicken anti-mouse IgG, and with Alexa Fluor 488-conjugated chicken anti-rabbit IgG. Coverslips were mounted in Prolong Gold Antifade Solution containing DAPI (Molecular Probes) and fluorescent images were obtained with a Zeiss LSM 510 laser-scanning confocal microscope with a x20 oil immersion objective or visualized with a x60 oil immersion objective.

Chapter 3: MYTH Screen for SLC4A11-Protein Interactions

All experiments were performed by Nada Alshumaimeri except the cloning of pCMBV-SLC4A11, which was done by Chris Lukowski and the synthesis of the prey cDNA library, which was done by Bio S and T company.

3.1 Introduction

The cornea forms the outer layer of the eye and consists of five distinct layers: the outer epithelium, bowman's layer, the stroma, Descemet's membrane, and the endothelial layer. The largest layer of the cornea is the stroma, which contains a high concentration of proteoglycans and collagen to maintain corneal structure and transparency. The osmotic gradient is regulated by the ion transport system in the endothelium to maintain stroma hydration at 78% H_2O (111). A water conductive pathway is formed by SLC4A11 on the basolateral surface and aquaporin 1 on the apical surface of the endothelial cells to reabsorb fluid and maintain the balance of water in the cornea (36).

SLC4A11 was initially cloned as a homologue of the SLC4 family (a bicarbonate transporter gene family). SLC4A11 has distinct functions separate from other SLC4 family proteins and does not function as a bicarbonate transporter (112). Interestingly, an SLC4A11 plant ortholog functions as a borate transporter (113). However, the mammalian cell does not have a cell wall that requires stabilization by borate. Consistent with this, experiments have found that SLC4A11 is not a borate transporter (36). SLC4A11 functions as a facilitator of water transport, a direct transporter of NH_3, or indirect transporter of NH_3 when coupled with H^+, an OH^- (H^+) transporter, and as an anchor between the CEC and DM. In addition, mouse SLC4A11 is an Na^+-independent electrogenic H^+ (OH^-) transporter (36, 114-117).

Several *SLC4A11* mutations result in different phenotypes, including a truncated protein, a functionally inactive protein, or an endoplasmic reticulum (ER)-retained protein due to improper folding during biosynthesis (48, 118) *SLC4A11* mutations lead to three different PCD: some cases of late-onset FECD, CHED, and HS (54, 56, 119).

SLC4A11 is an 891 amino acid integral membrane protein divided into two domains: an N-terminal cytosolic domain and a 14 transmembrane segment domain with a short cytosolic tail.

SLC4A11 is widely expressed in human tissues, including the corneal endothelium, kidneys, ovaries, tongue, lungs, blood cells, colon, and pancreas, and brain (65). Two homology models for SLC4A11 were developed upon comparison to its most similar membrane protein, AE1 (SLC4A1) (63, 67). A three-dimensional homology model of the SLC4A11 membrane domain (MD) revealed the folding of SLC4A11 is divided into two sub-domains, core and gate (63). Moreover, the cytoplasmic (CD) homology model demonstrated that the protein folding forms a pathway along with the membrane domain enabling substrate transport. CD is essential to stabilize the folding of SLC4A11 and trafficking to the cell surface. The strong association of CD and MD suggests that CD has a role in covering the exposed hydrophobic areas of MD. Deletions of the CD when SLC4A11 is expressed, lead to protein misfolding and cause the degradation of SLC4A11 protein in the ER. Lastly, the CD is insoluble when expressed in bacterial cultures, indicating that *in vitro* investigations on SLC4A11 requires expression of the whole protein (67).

The MD of SLC4A11 forms the pathway for water transport. Defects in this water transport function mediated by SLC4A11 explain the connection to corneal edema caused in ECD, as it may be due to *SLC4A11* mutations (35). The extracellular loop 3 in SLC4A11 interacts with COL8A2, a major component of the DM, and abnormalities in cell adhesion likely mediate the loss of endothelial corneal cells in FECD and CHED (114). SLC4A11 CD is important for its function and stabilizing roles. Given that the expression of SLC4A11 requires expression of the whole protein, we established the membrane yeast two-hybrid system (MYTH) to identify SLC4A11–protein interactors.

The MYTH technique is a high-throughput, unbiased approach used to detect protein–protein interactions. The principle behind this technique is the use of ubiquitin as a sensor for the detection of protein interactions. Ubiquitin is split into two stable fragments, the C-terminal moiety

of ubiquitin (C_{ub}) and the N-terminal moiety of ubiquitin ($N_{ub}I$). The two fragments of ubiquitin are capable of spontaneous reassociation, forming a stable pseudoubiquitin. Introduction of the Ile13Gly mutation yields $N_{ub}G$, which prevents the spontaneous reassociation except when forced to be close to each other due to interactions of bait and prey proteins. Split ubiquitin is used as a tag for protein interactions where a bait (protein of interest) is tagged with C_{ub} fused to the transcription factor (TF). The TF reporter molecule consists of VP16 transcriptional activation domain from herpes simplex virus and the DNA binding domain from *E. coli,* LexA. Conversely, a prey protein constructed from a cDNA library is tagged with $N_{ub}G$. Interaction between the bait and prey proteins brings the N- and C-terminal moieties of ubiquitin to close proximity, allowing them to reassociate to form functional pseudoubiquitin. Deubiquitinating enzymes release the TF, which enables its migration into the nucleus, promoting transcription of the genes required for growth of auxotrophic yeast strain on appropriate selective plates for the first selection step (102). In addition, *LacZ* encodes β -galactosidase, an intracellular enzyme that digests the disaccharide lactose into galactose and glucose. In MYTH screening, 5-bromo-4-chloro-3-indolyl-β-D-galactopyranoside (X-Gal) is used as a substrate for β -galactosidase to convert X-Gal into galactose and 5-bromo-4-chloro-3-hydroxyindole, a reactant that spontaneously oxidizes into 5,5'-dibromo-4,4'-dichloro-indigo, which is a blue insoluble product (120). The second selection step of potential interactors is dependent on the growth of blue colonies on selective plates.

Identification of protein interactors in MYTH requires two screenings, the first screen is the selection of interactors that activate the reporter system (*HIS3* and *ADE2* genes), and the second screen is the selection of interactors that activate the reporter system (*HIS3, ADE2*, and *LacZ*) genes which allows for colonies expressing interacting proteins to grow blue. After screening for positive colonies from the second screen, the plasmids are purified, sequenced, and aligned with

the NCBI protein database to identify potential interacting proteins. From these identified interactors, spurious hits can be further eliminated from the list depending on data analysis (102).

The expression of SLC4A11 protein requires the presence of the cytoplasmic domain for its function and processing to the cell surface. The cytoplasmic domain is important for the dimerization and stabilization of SLC4A11, and the membrane domain and cytoplasmic domain cannot be expressed separately. Both domains of SLC4A11 are strongly associated together (67). This led us to utilize MYTH screening using full-length human SLC4A11 to identify SLC4A11-protein interactors.

3.2 Results

3.2.1 Bait generation

To begin with MYTH screening, human SLC4A11 cDNA was tagged at the 3' end with C_{ub}-TF by cloning into the MYTH bait vector, pCMBV (102). The C-terminal tagging position was chosen to prevent the interruption of interactions at the large N-terminal cytoplasmic domain of SLC4A11. TF is LexA-VP16 that is released into the nucleus to activate the reporter genes (*HIS3*, *ADE2* and *LacZ*) for the detection of interactions. pCMBV contains the auxotrophic marker, LEU2, to enable selection of yeast transformed with pCMBV. pCMBV also encodes ColE1 origin of replication and kanamycin resistance gene to allow propagation of plasmid in bacteria. The pCMBV plasmid contains the CYC1 promoter that activates the expression of SLC4A11-C_{ub}-TF.

3.2.2 Bait validation test

To validate SLC4A11- C_{ub} as a bait for MYTH screening, we used the N_{ub}GI (N_{ub}I or N_{ub}G) control test to ensure that the bait does not activate the reporter genes when expressed alone without

interacting with the prey protein. $N_{ub}G$ is the mutated form of $N_{ub}I$ that prevents the spontaneous formation of pseudoubiquitin unless the two moieties are in close proximity due to interaction of bait and prey proteins. For the $N_{ub}GI$ test, the bait-C_{ub} grows on an interaction selection medium that confirms the interaction when co-transformed with the positive control prey-$N_{ub}I$ and does not grow with the negative mutated control prey-$N_{ub}G$. The controls $N_{ub}I$ or $N_{ub}G$ controls are fused to a non-interacting prey protein consisting either of a protein that is localized at the plasma membrane, Fur4, or an endoplasmic reticulum membrane protein, Ost1. Since SLC4A11 is detected on immunoblots as both a mature band (complex glycosylated) at the PM and immature band (core glycosylated) at the ER (102, 118), we tested whether the identified interactions from MYTH will occur at the PM or ER by using both provided controls at the PM and ER in the bait validation test.

The plasmid SLC4A11-pCMBV, was transformed into the MYTH reporter yeast strain THY.AP4 *(MATa leu2, ura3, trp1:: (lexAop)-lacZ (lexAop)-HIS3 (lexAop)-ADE2)*. This strain has the selectable reporter genes (*ADE2, HIS3,* and *LacZ*) (102). Yeast THY.AP4 strain was co-transformed with pCMBV-SLC4A11 encoding SLC4A11- C_{ub} and cDNA encoding Fur4-$N_{ub}I$ as a positive control at the plasma membrane, that has WT $N_{ub}I$ which spontaneously activates the reporter system in yeast. In contrast, for the negative control the strain was co-transformed with pCMBV-SLC4A11 and the negative prey control, Fur4- $N_{ub}G$ which should not grow on selective plates because presumably Fur4 is a non-interacting protein and $N_{ub}G$ mutation prevents the activation of the screen due to the absence of spontaneous reassociation property. The other validation step was done by transforming the yeast strain with Ost1- $N_{ub}I$ that was considered as the positive control for the ER membrane. The strain was also co-transformed with pCMBV-

SLC4A11 and the negative control Ost1-N_{ub}G. Selection on plates lacking leucine and tryptophan (SD-Leu-Trp) was performed (Figure 3.1 top section).

The result shows the growth of all transformants, which confirms their transformation into yeast. Then, the same transformants were also spotted onto interaction selection plates, synthetic dropout agar plates lacking leucine, tryptophan, histidine, and adenine, with the addition of X-Gal (SD-Leu-Trp-His-Ade + X-Gal) (Figure 3.1, bottom). The results show that upon spotting the transformants on interaction selection plates, only the growth of the strain co-transformed with SLC4A11-pCMBV and Fur4-N_{ub}I the positive control for PM was observed as a blue colony. This validates that SLC4A11 does not self-activate the MYTH system unless there is an interacting protein, and the interaction is detected at the plasma membrane. The spots at bottom panel for the colonies transfected with Fur4- N_{ub}G, Ost1- N_{ub}I and Ost1-N_{ub}G show no growth and a faint spot which is the dried solution that was spotted on the plate.

3.2.3 Library screening

Selection of the prey cDNA library depends on the nature of the bait protein. SLC4A11 is highly expressed in endothelial corneal cells. Ideally, a cDNA library from human cornea would be the most optimal in this scenario; human corneas are difficult to obtain in adequate quantities. Bovine corneas are almost three times larger than human corneas and much easier to obtain. Thus, we examined the amino acid sequences of human and bovine SLC4A11 (Figure 3.2). High identity between human and bovine SLC4A11 amino acid sequences (82 %) led us to use bovine cornea for the synthesis of the cDNA library. A bovine cornea was dissected, snap frozen and sent to Bio

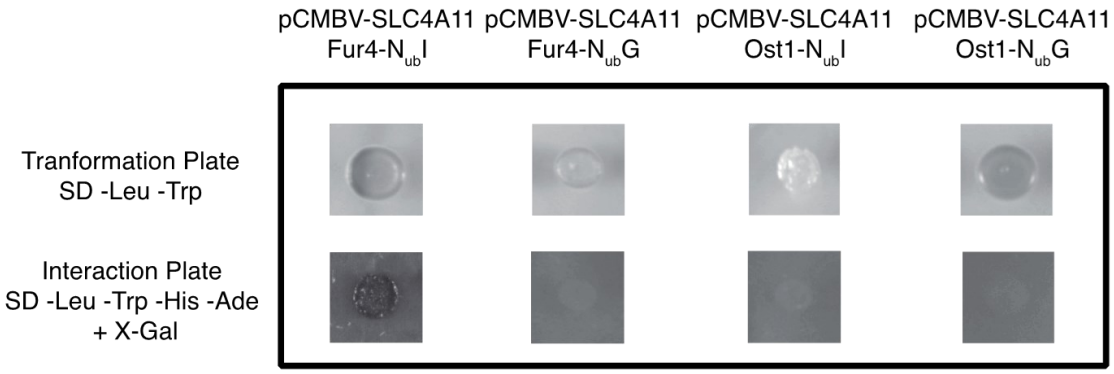

Figure 3.1: Bait validation test

N_{ub}GI control test to validate SLC4A11 as a bait for MYTH screening in the THY.AP4 strain. THY.AP4 yeast strain was co-transformed with the pCMBV-SLC4A11 vector and N_{ub}I-Fur4, N_{ub}G-Fur4, N_{ub}I-Ost1, or N_{ub}G-Ost1 and grown on yeast extract peptone dextrose agar plates (YPD). Colonies from the different transformants were picked up and dissolved in 100 µl 0.9% (w/v) NaCl then 2.5 µl of the resuspended colony was spotted onto transformation selection plates, synthetic dropout agar plates lacking leucine and tryptophan (SD-Leu-Trp) at top lane or interaction plates, (SD-Leu-Trp-His-Ade + X-Gal) at bottom lane.

S and T Company (Québec, Canada) for cDNA library synthesis. RNA was extracted from the cornea then double stranded-DNA was synthesized and amplified. The cDNA was cloned into the MYTH prey vector, pPR3N, by the company. pPR3N plasmid encodes for CYC1 promoter and NubG at the N-terminus (102). pPR3N contains Trp1 for auxotrophic selection in yeast under the activation of the CYC1 promoter. Also, it contains ColE1origin of replication and ampicillin resistance gene for selection in bacteria.

Following cloning of the cDNA into the prey vector, we co-transformed the prey cDNA library with the pCMBV-SLC4A11 bait vector thirty times (three times for each tube). We initially screened 6 x 10^7 transformants which was calculated from the selection of yeast growth on transformation plates (SD-Leu-Trp). Total number of transformation plates used was 270 plates. The number of transformants represents the coverage of the screen. The number of transformants was calculated using the following formula:

Total transformants = number of colonies x dilution factor x volume of suspended cells

Among these, 385 colonies grew on interaction selective plates (SD plates lacking Leu, Trp, His, and adenine) that screened for clones with bait-prey interaction. A second screen was performed to validate the interactions and test the strength of the interactions identified. This screen made use of the *LacZ* gene, encoding β-galactosidase, whose transcription is turned on by the LexA transcription factor released upon pseudoubiquitin reconstitution. β-galactosidase converts X-Gal to a blue compound that colours colonies blue. All 385 colonies were spotted onto interaction plates, containing X-Gal. So, yeast cells in which there is a high level of interaction between bait and prey proteins will lead to high levels of *LacZ* transcription and, thus dark blue colour, while less intense blue colonies indicate less interaction between the bait and prey. Could be the reason for the intensity of blue colonies due to the size of picked up colonies from first selection. The

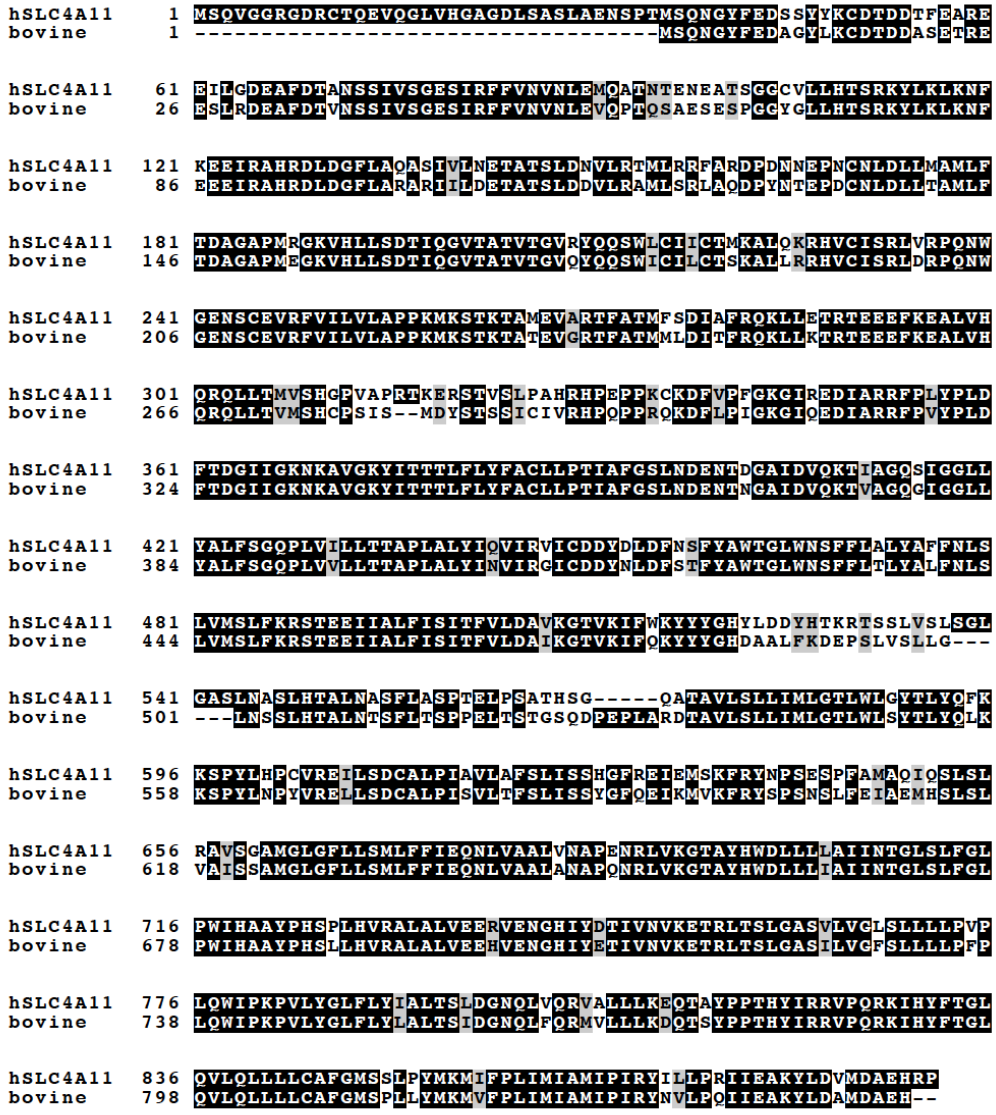

Figure 3.2: Alignment of human and bovine SLC4A11 amino acid sequences

Human (H) with the NCBI Reference Sequence: NP_114423.1 and bovine (B) NP_001178243.1 SLC4A11 amino acid sequences were obtained from NCBI database and aligned using Clustal Omega multiple sequence alignment tool https://www.ebi.ac.uk/Tools/msa/clustalo/. Amino acids were colored using the tool BOXSHADE tool https://embnet.vital-it.ch/software/BOX_form.html. Black shaded amino acids represent amino acid identity between sequences, whereas grey represents conservative amino acids. Sequence identity is 82%.

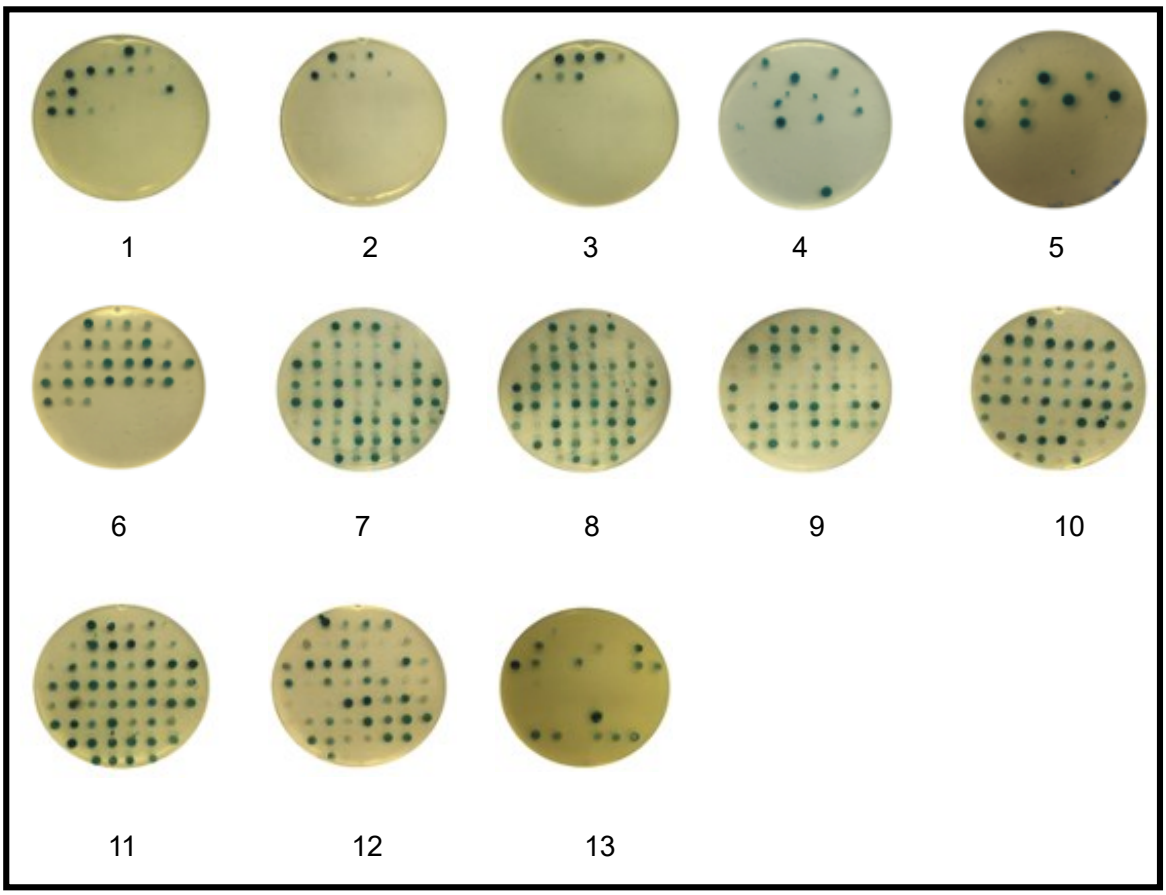

Figure 3.3: Second screening to detect potential interactors on interaction +X-Gal plates

The 385 colonies from the first screen were grown on interaction selection plate were picked and resuspended in 100 µl 0.9% (w/v) NaCl. Then 2.5 µl of the resuspended colony was spotted onto interaction selection plate (SD-Trp-Leu-Ade-His) containing X-Gal. Blue colonies indicate colonies where bait and prey proteins may have interacted.

Table 3.1: Shades of colonies growing as protein interactors at second screen for SLC4A11 in MYTH screening

Color Of Colony	Number of Colonies
Very Dark	11
Dark	61
Light	120
Faint	84
No growth	109
Total Number	**385**

smaller the colony, the more intense blue appearing on the colony. Overall, there were 276 blue colonies, and the intensity of blue color of colonies were categorized into five shades to indicate the strength of interaction (Table 3.1 and Figure 3.3).

3.2.4 Analysis of screened hits

Colonies that were blue (276 colonies) in the second screen on the X-Gal interaction plates were subjected to additional analysis. First, plasmids were isolated from yeast and transformed into *E. coli.* The plasmids were then amplified, purified from *E. coli* cultures, and each plasmid was subjected to DNA sequencing. The resulting sequence, in-frame with the tags in the prey vector until the stop codon, were translated into amino acids using an online translation bioinformatics tool (Expasy translate, https://web.expasy.org/translate/). Amino acid sequences underwent BLAST analysis (https://blast.ncbi.nlm.nih.gov) to determine the identified protein. The list of interactors was further analysed by checking the amino acid sequence from each sequenced hit. A summarized list of all possible hits is shown in (Table 3.2).

Exclusion criteria for the identified interactors included: i) Amino acid sequences for membrane proteins missing their first transmembrane segments, which would misfold. ii) Proteins that in the mature state do not have a cytoplasmic N-terminus (secreted proteins and membrane proteins with extracellular N-terminus). iii) Proteins with fewer than 10 amino acids, are very small proteins that are interacting as false positive interactors. iv) Un-identified proteins or proteins similar to species other than bovine, likely arise from cDNAs cloned out of frame. v) Biosynthetic apparatus proteins, that SLC4A11 would normally interact with. Biosynthetic apparatus proteins are those involved in the cellular synthesis and trafficking of proteins and are summarized in Table 3.3. vi) highly truncated proteins (in this study four hits corresponded to only 1-24% of the full-

length cDNA). These proteins sizes ranged 22-74 amino acids. Such short proteins representing such a small fraction of the full protein led to concerns about appropriate folding of the identified interactor.

3.2.5 Possible SLC4A11-protein interactors

In total, twenty-five unique hits were detected from the MYTH screening, with six of them being full-length proteins with an identifiable cytoplasmic N-termini. The possible interacting hits are summarized (Table 3.4 and Figure 3.4) and a summary of each potential interactor can be found in the following section 3.3.1.

3.2.6 Expression of SLC4A11-protein interactors in HEK293 cells

To assess the validity of the interactions identified in the MYTH screen, HEK293 cells were used to study the expression of selected potential SLC4A11 interactors. cDNAs for the potential bovine protein interactors: Ociad1, Tmem 254, Ormdl2, and Tmem 128 from the detected colonies were cloned into the vector pcDNA 3.1 that also encoded an N-terminal Myc epitope tag to facilitate protein detection. The interactors were cloned into pcDNA empty vector. Then the plasmids cloned with SLC4A11-potential interactors were transiently transfected into HEK293 cells and lysates from these cells were processed on immunoblots. These samples were probed with an anti- Myc antibody. The bands detected for each interactor were at the following molecular weights: Ociad1, 28 kDa, Tmem 254, 14 kDa, Ormdl2, 17 kDa, and Tmem 128, 19 kDa (Figure 3.5). All interactors were detected on the blot at the correct size of bands.

Table 3.2: List of all hits from MYTH screening

Abbreviations: *: Sequence ID from BLAST NCBI, i) Amino acid sequences for membrane proteins missing their first transmembrane segments, ii) Proteins that in the mature state do not have a cytoplasmic N-terminus, iii) Proteins with fewer than 10 amino acids, iv) Un-identified proteins or proteins similar to species other than bovine, v) Biosynthetic apparatus proteins, vi) highly truncated proteins, and vii) possible hits.

Name of protein	NCBI reference sequence *	Intensity of blue color	Number of times detected	Data Analysis
Frame-shifted proteins			168	iv
Transmembrane protein 254	NP_001068696.1	Light, faint, dark	18	vii
ATP6	ABC84252.1	Light, faint, dark	11	i
10 amino acids or fewer			10	iii
P53 apoptosis effector related to PMP-22	NP_001029522.1	Light, dark	6	i
Signal peptidase complex catalytic subunit SEC11C	NP_776890.1	Very dark, dark, light	5	vii, v
Translocation protein SEC62	NP_001192533.1	Dark, faint	5	vii, v
NEDD4 family-interacting protein 1 isoform X4, partial	XP_024850999.1	Light	4	ii
Homocysteine-responsive endoplasmic reticulum-resident ubiquitin-like domain member 2 protein	XP_010802560.1	Light, dark	3	i
Transmembrane 9 superfamily member 2-like	DAA23751.1	Light, dark	3	i
CD9 antigen	NP_776325.1	Dark	2	i
Estradiol 17-beta-dehydrogenase 2	NP_001069194.1	Faint, dark	2	i
Fibronectin type-III domain-containing protein 3A	XP_005213644.3	Light	2	ii
Leptin receptor overlapping transcript-like 1	NP_001032539.1	Light	2	vii

Major facilitator superfamily domain-containing protein 1	NP_001068819.1	Faint	2	i
Major facilitator superfamily domain-containing protein 1 isoform X1	NP_001068819.1	Dark, light	2	i
Protein kish-A precursor	NP_001107983.1	Light, faint	2	ii
Protein odr-4 homolog	NP_001074371.2	Light, faint	2	i
Transmembrane protein 128	NP_001029626.1	Faint	2	vii
Alpha-2-macroglobulin isoform X1	XP_005207113.1	Faint	1	ii
Androgen-induced gene 1 protein isoform d	NP_001273517.1	Dark	1	ii
ATP-binding cassette sub-family A member 9	XP_024835488.1	Dark	1	i
Brain-specific angiogenesis inhibitor 3-like		Light	1	vi
Calcium-transporting ATPase type 2C member 1	XP_010799921.1	Faint	1	i
CMP-SAT	NP_001029809.1	Light	1	vii
Growth hormone-inducible transmembrane protein	NP_001029224.1	Faint	1	i
Hemicentin-2 isoform X4	XP_011516770.1	Dark	1	vi
Hippocampus abundant transcript 1 protein	XP_010801468.1	Very dark	1	i
Hippocampus abundant transcript 1 protein isoform X1	XP_010801468.1	Light	1	i
Inositol 1,4,5-trisphosphate receptor type 2	DAA29438.1	Light	1	i
Major facilitator superfamily domain-containing protein 8	NP_001192752.1	Dark	1	i
Mitochondrial import receptor subunit TOM6 homolog	NP_001107190.1	Light	1	vii, v
OCIA domain-containing protein 1	NP_001015648.1	Very dark	1	vii
Olfactory receptor 4A47	XP_010847186.1	Light	1	vi
ORM1-like protein 2	NP_001014931.1	Faint	1	vii
Renin receptor precursor	NP_001091491.1	Faint	1	ii
Reverse transcriptase-like	CAA10770.1	Light	1	vi

Signal peptidase complex subunit 2	XP_002693515.2	Faint	1	vii, v
Translocon-associated protein subunit gamma	NP_001070512.1	Faint	1	vii, v
Transmembrane protein 165 precursor	ELR54048.1	Dark	1	i
UBX domain protein 4	AAI03097.1	Light	1	ii
Zinc finger protein 266	DAA28012.1	Light	1	ii
Zinc transporter 5	NP_001179103.1	Dark	1	i
Zinc transporter ZIP6	NP_001137564.1	Light	1	i

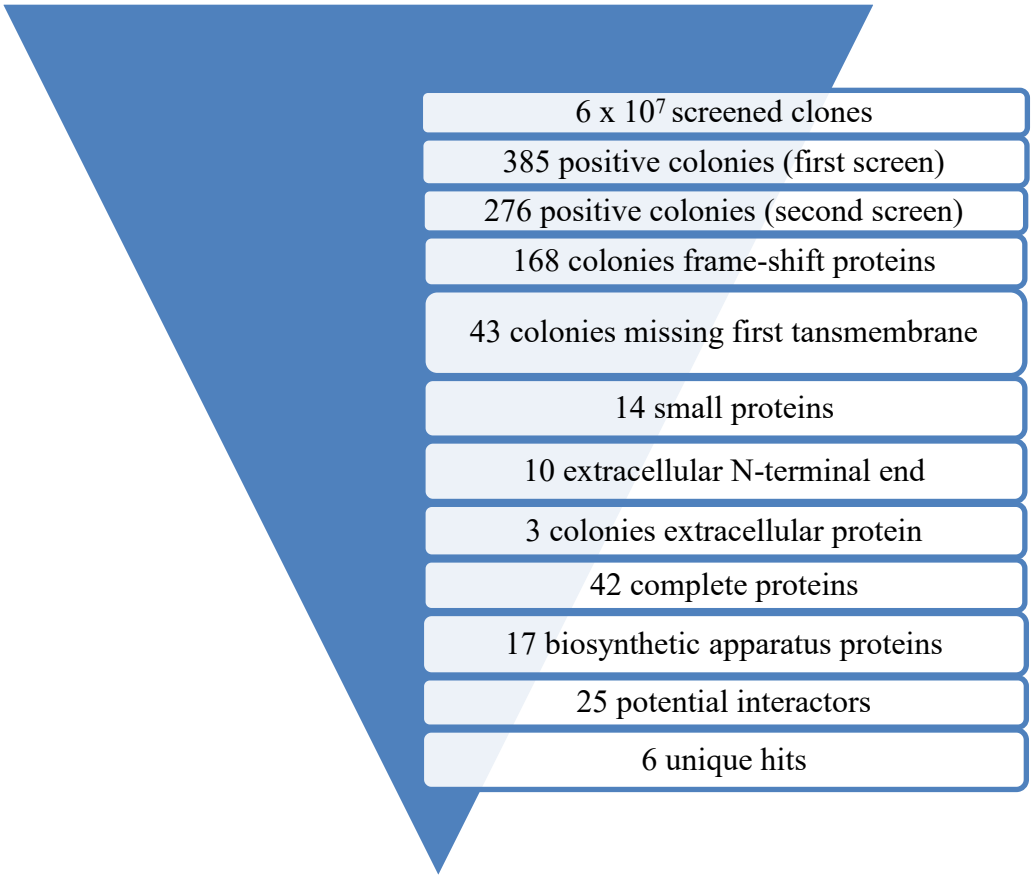

Figure 3.4: Summary of MYTH screened colonies

A summary of the number of screened clones for SLC4A11-MYTH screening. The number of screened colonies was 6 x 10^7 colonies. After analysis of each hit, the number of unique interactors was six potential interactors.

Table 3.3: Detected biosynthetic apparatus proteins as interactors from SLC4A11-MYTH screen

Biosynthetic Apparatus Proteins	No. of Times Detected	Residues aligning with the hit	Length of protein (amino acids)	NCBI Reference Sequence
P53 apoptosis effector related to PMP-22	6	79-147	184	NP_001029522.1
Translocation protein SEC62	5	1-302	399	NP_001192533.1
Signal peptidase complex catalytic subunit SEC11C	3	156-192	192	NP_776890.1
Mitochondrial import receptor subunit TOM6 homolog	1	1-74	74	NP_001107190.1
Signal peptidase complex subunit 2	1	27-256	256	XP_002693515.2
Translocon-associated protein subunit gamma	1	1-185	185	NP_001070512.1

Table 3.4: Identified SLC4A11-protein interactors

Number of times detected refers to the number of clones identified encoding that possible interactor. Residues aligning with the hit represents the amino acids of the protein that were in the identified cDNA. Sequences of proteins were based on the information from NCBI (https://www.ncbi.nlm.nih.gov) and UniProt (https://www.uniprot.org).

Potential SLC4A11 Interactors	No. of Times Detected	Residues aligning with the hit	Length of protein (amino acids)	NCBI Reference Sequence (UniProt database)
Transmembrane protein 254 (TMEM 254)	18	1-124	124	NP_001068696.1 (Q0D2G3)
Leptin receptor overlapping transcript-like 1 (LEPROTL1)	2	2-131	131	NP_001032539.1 (Q32PD8)
ORM1-like protein 2 (ORMDL2)	1	1-153	153	NP_001014931.1 (Q5E972)
CMP-SAT (CMP-SAT)	1	1-337	337	NP_001029809.1 (Q3SZP1)
Transmembrane protein 128 (TMEM 128)	2	1-165	165	NP_001029626.1 (Q3T0S0)
OCIA domain-containing protein 1 (OCIAD1)	1	1-247	247	NP_001015648.1 (Q5E948)

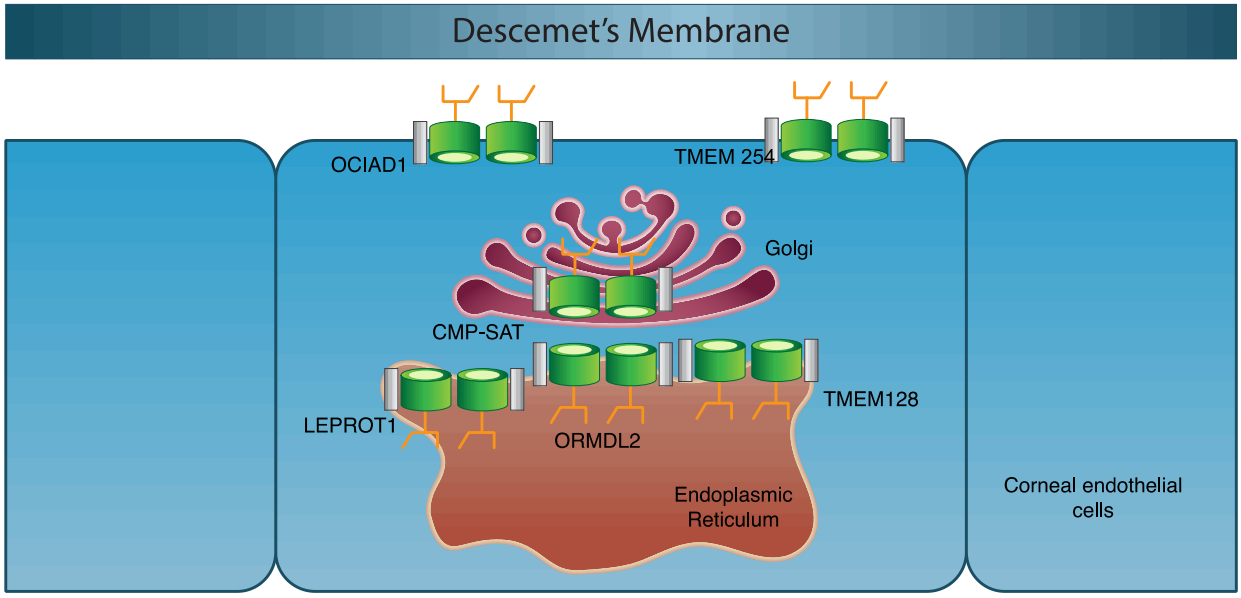

Figure 3.5: Summary of SLC4A11-protein interactors detected from MYTH screening

An illustration of the possible interactions of SLC4A11 detected from MYTH screening. The figure illustrates SLC4A11 as a dimer in green, interacting with OCIAD1 and TMEM 254 at the PM, while the SLC4A11 and CMP-SAT interaction occurs at Golgi apparatus. Additionally, SLC4A11 possibly interacts with LEPROT1, ORMDL2, and TMEM 128 at the ER.

Table 3.5: TMEM 254 hits detected from MYTH screening

Amino acid sequences for the TMEM 254 eighteen hits detected. #: Number of colonies.

#	Amino acid sequence
1	ILSFGYYTWMIFWPESIPYQSLGPLGPFTQYLLKHHHTLVHAWYWLAWMIHVGESLYAIVLCKSKGITNTWT QLLWFLQTFLFGLASLYYLIAFRPKHQKQT
2	WMIFWPESIPYQSLGPLGPFTQYLLKHHHTLVHAWYWLAWMIHVGESLYAIVLCKSKGITNTWTQLLWFLQ TFLFGLASLYYLIAFRPKHQKQT
3	ILSFGYYTWMIFWPESIPYQSLGPLGPFTQYLLKHHHTLVHAWYWLAWMIHVGESLYAIVLCKSKGITNTW TQLLWFLQTFLFGLASLYYLIAFRPKHQKQT
4	FQRSSLFWVTIIILSFGYYTWMIFWPESIPYQSLGPLGPFTQYLLKHHHTLVHAWYWLAWMIHVGESLYAIV LCKSKGITNTWTQLLWFLQTFLFGLASLYYLI
5	IIILSFGYYTWMIFWPESIPYQSLGPLGPFTQYLLKHHHTLVHAWYWLAWMIHVGESLYAIVLCKSKGITNT WTQLLWFLQTFLFGLASLYYLIAFRPKHQKQT
6	MRKARGDEAYFQRSSLFWVTIIILSFGYYTWMIFWPESIPYQSLGPLGPFTQYLLKHHHTLVHAWYWLAW MIHVGESLYAIVLCKSKGITNTWTQLLWFLQTFLFGLASLYYLIAFRPKHQKQT
7	GDFQRSSLFWVTIIILSFGYYTWMIFWPESIPYQSLGPLGPFTQYLLKHHHTLVHAWYWLAWMIHVGESLYA IVLCKSKGITNTWTQLLWFLQTFLFGLASLYYLIAFRPKHQKQT
8	MRKARGDEAYFQRSSLFWVTIIILSFGYYTWMIFWPESIPYQSLGPLGPFTQYLLKHHHTLVHAWYWLAWM IHVGESLYAIVLCKSKGITNTWTQLLWFLQTFLFGLASLYYLIAFRPEHQKQT
9	GRGDEAYFQRSSLFWVTIIILSFGYYTWMIFWPESIPYQSLGPLGPFTQYLLKHHHTLVHAWYWLAWMIHV GESLYAIVLCKSKGITNTWTQLLWFLQTFLFGLASLYYLIAFGPKHQKQT
10	MRKARGDEAYFQRSSLFWVTIIILSFGYYTWMIFWPESIPYQSLGPLGPFTQYLLKHHHTLVHAWYWLAWM IHVGESLYAIVLCKSKGITNTWTQLLWFLQTFLFGLASLYYLIAFRPEHQKQT
11	MRKARGDEAYFQRSSLFWVTIIILSFGYYTWMIFWPESIPYQSLGPLGPFTQYLLKHHHTLVHAWYWLAWM IHVGESLYAIVLCKSKGITNTWTQLLWFLQTFLFGLASLYYLIAFRPEHQKQT
12	LQTFLFGLASLYYLIAFRPKHQKQT
13	GEARGDEAYFQRSSLFWVTIIILSFGYYTWMIFWPESIPYQSLGPLGPFTQYLLKHHHTLVHAWYWLAWMI HVGESLYAIVLCKSKGITNTWTQLLWFLQTFLFGLASLYYLIAFRPKHQKQT
14	GRGDEAYFQRSSLFWVTIIILSFGYYTWMIFWPESIPYQSLGPLGPFTQYLLKHHHTLVHAWYWLARMIHVG

	ESLYAIVLCKSKGITNTWTQLLWFLQTFLFGLASLYYLIAFGPKHQKQT
15	MRKARGDEAYFQRSSLFWVTIIILSFGYYTWMIFWPESIPYQSLGPLGPFTQYLLKHHHTLVHAWYWLAWM IHVGESLYAIVLCKSKGITNTWTQLLWFLQTFLFGLASLYYLIAFRPEHQKQT
16	MRKARGDEAYFQRSSLFWVTIIILSFGYYTWMIFWPESIPYQSLGPLGPFTQYLLKHHHTLVHAWYWLAWM IHVGESLYAIVLCKSKGITNTWTQLLWFLQTFLFGLASLYYLIAFRPEHQKQT
17	MRKARGDEAYFQRSSLFWVTIIILSFGYYTWMIFWPESIPYQSPGPLGPFTQYLLKHHHTLVHAWYWLAWM IHVGESLYAIVLCKSKGITNTWTQLLWFLQTFLFGLASLYYLIAFRPKHQKQT
18	VLSFGYYTWMIFWPESIPYQSLGPLGPFTQYLLKHHHTLVHAWYWLAWMIHVGESLYAIVLCKSKGITNT WTQLLWFLQTFLFGLASLYYLIAFRPKHQKQT

3.2.7 Expression of SLC4A11-protein interactors in HEK293 cells

For future identification and confirmation of the interactions in bovine corneas, we first needed to develop antibodies recognizing the identified interactors. Custom antibodies were ordered for the interactors, Ociad1, Tmem 254 and Ormdl2. To test the ability of these custom antibodies to detect their target proteins, lysates from transfected HEK293 cells with Ociad1, Tmem 254 or Ormdl2 were processed on immunoblots and detected with the custom antibodies. The presence of bands of expected size in each case indicated that the antibodies were able to detect their antigen and that the potential interactors were expressed in transfected HEK293 cells. Absence of a band of appropriate size in empty vector-transfected cells revealed specificity of the antibodies (Figure 3.6).

3.2.8 Expression of human isoforms of identified SLC4A11 interactors

To assess the validity of the possible interactors identified in the MYTH screen, we used HEK293 cells as a model to study the expression of identified SLC4A11 interactors. The cDNA for human orthologs of each protein interactor, OCIAD1, TMEM 254, ORMDL2, or CMP-SAT, were cloned into the vector pcDNA 3.1 with an N-terminal Myc tag. These plasmids were transiently transfected into HEK293 cells and cell lysates were processed on immunoblots. These samples were probed with an anti- Myc antibody. Specificity of detection was demonstrated the lack of bands in the lane from cells transfected with empty vector, pcDNA 3.1 (Figure 3.7). The presence of a band of expected size for each antigen indicates that all interactors could be expressed in HEK293 cells and detected with the Myc antibody.

Detection of an SLC4A11 interaction with other proteins in human corneas requires the use of custom antibodies as well. Custom antibodies were used for the interactors human OCIAD1

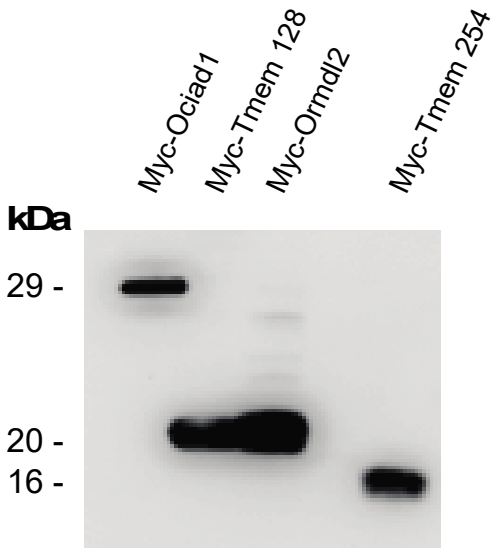

Figure 3.6: Expression of tagged bovine potential interactors in HEK293 cells

Lysates of HEK293 cells transiently transfected with bovine Myc-Ociad1 cDNA (pNDA8), bovine Myc-Tmem 128 cDNA (pNDA15), bovine Myc-Ormdl2 cDNA (pNDA20), or bovine Myc-Tmem 254 cDNA (pNDA12). Transfected cells were lysed, resolved on SDS-PAGE, and probed with rabbit anti-Myc antibody. Migration and molecular weight of sizing standards are indicated on the left.

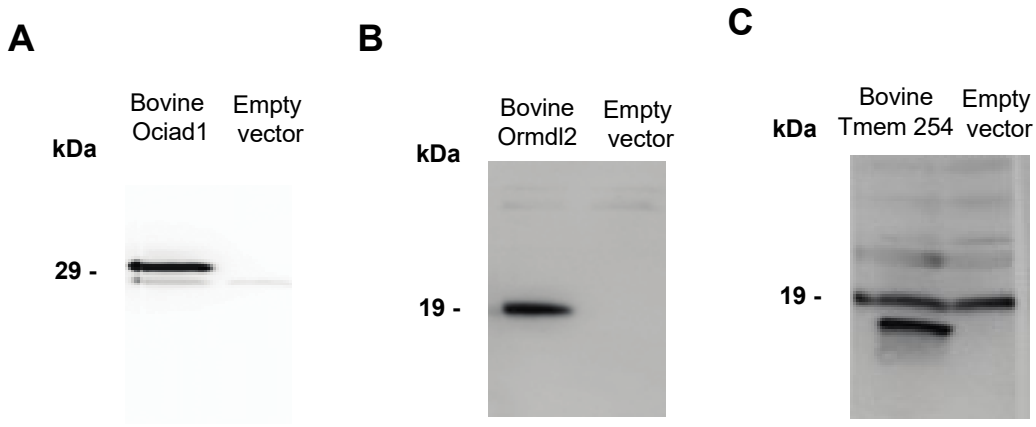

Figure 3.7: Expression of interactors in HEK293 cells (custom antibodies detection)

Lysates of HEK293 cells transiently transfected with **A.** Bovine Myc-Ociad1 cDNA (pNDA8) or empty vector (pcDNA). **B.** Bovine Myc-Ormdl2 cDNA (pNDA20) or empty vector (pcDNA). **C.** Bovine Myc-Tmem 254 cDNA (pNDA12) or empty vector (pcDNA). Transfected cells were lysed and probed on immunoblots using the antibodies mouse anti-Ociad1, mouse anti-Ormdl2, and mouse anti-Tmem 254. Migration and molecular weight of sizing standards are indicated on the left.

and ORMDL2. Transfected cells were processed on immunoblots and detected with custom antibodies. Specificity of the custom antibodies was determined by detection of a clear signal for the empty vector-transfected cells (Figure 3.8).

3.2.9 Interaction of SLC4A11 and ORMDL2

Since we detected ORMDL2 as a potential interacting protein with full-length protein from the MYTH screen, we tested its possible interaction with SLC4A11. First, we used a bioinformatics approach to obtain a predicted secondary structure of ORMDL2 from the online tool TMHMM (http://www.cbs.dtu.dk/services/TMHMM/), which predicted two transmembrane segments and an N-terminal cytoplasmic end. This indicated that the reporter tags can reach the nucleus for activation of selective genes in MYTH (Figure 3.9). Then, we examined the amino acid sequence of both human and bovine ORMDL2 (Figure 3.10). The high identity between human and bovine SLC4A11 amino acid sequences (84% identity) led us to consider the two proteins as interchangeable. That is, interactors with human SLC4A11 will also interact with bovine Slc4a11.

We thus assessed a possible interaction between human SLC4A11 and human ORMDL2 in HEK293 cells by co-immunoprecipitation. HEK293 cells were transiently co-transfected with human Myc-ORMDL2 cDNA and either HA-SLC4A11, or non- tagged SLC4A11. Lysates were immunoprecipitated (IP) with mouse anti-HA antibody, resolved by SDS-PAGE, blotted, and probed with a rabbit anti-Myc antibody (Figure 3.11). SLC4A11/ORMDL2 association is indicated by co-immunoprecipitation of HA-SLC4A11 with Myc-ORMDL2. Absence of immunoprecipitation with untagged SLC4A11 indicates specificity.

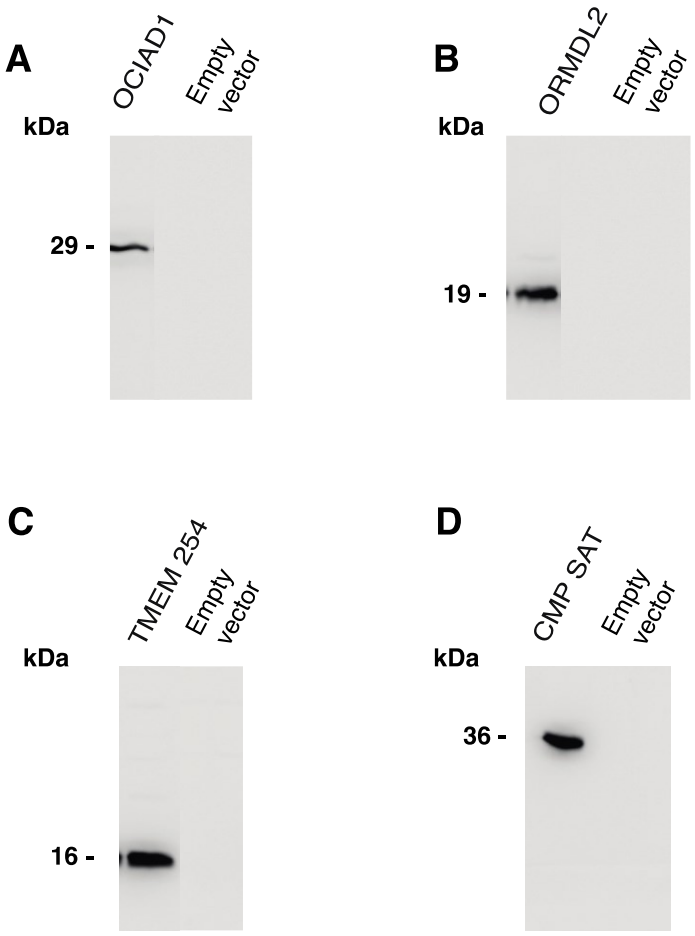

Figure 3.8: Detection of Myc tag on human sequences of Myc-epitope tagged identified interactors expressed in HEK293 cells

Lysates of HEK293 cells transiently transfected with **A.** Human Myc-OCIAD1 cDNA (pNDA22) or empty vector (pcDNA). **B.** Human Myc-ORMDL2 cDNA (pNDA24) or empty vector (pcDNA). **C.** Human Myc-TMEM 254 cDNA (pNDA23) or empty vector (pcDNA). **D.** Human Myc-CMP sialic acid transporter cDNA (pNDA25) or empty vector (pcDNA). Transfected cells were lysed, resolved on SDS-PAGE gels blotted onto PVDF membranes, and probed on immunoblots with mouse anti-Myc antibody. Migration position and molecular weight of sizing standards are indicated on the left.

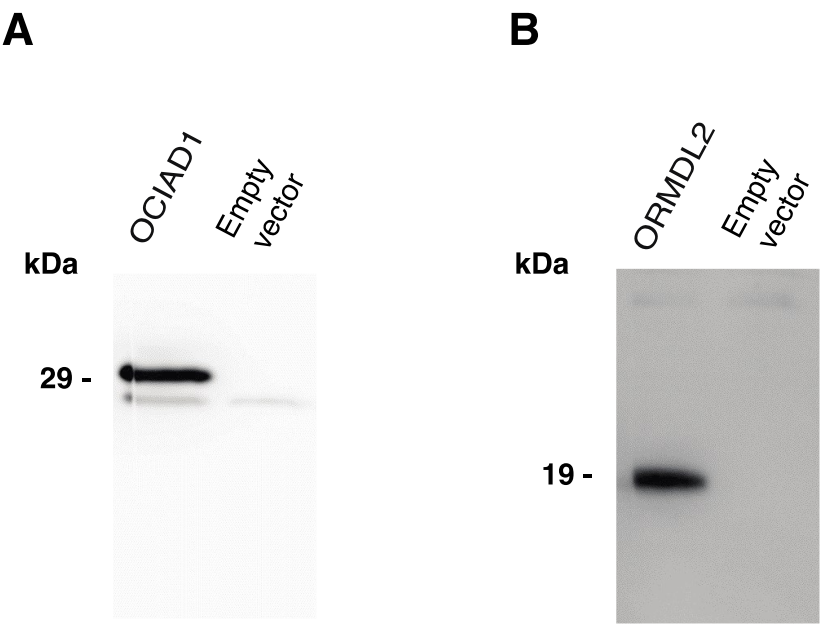

Figure 3.9: Detection of the expression of human cDNAs of identified interactors expressed in HEK293 cells using custom antibodies

Lysates of HEK293 cells transiently transfected with **A.** Human Myc-OCIAD1 cDNA (pNDA22) or empty vector (pcDNA). **B.** Human Myc-ORMDL2 cDNA (pNDA24) or empty vector (pcDNA). Transfected cells were lysed, resolved on SDS-PAGE, and corresponding immunoblots were probed with mouse anti-OCIAD1 antibody or mouse anti-ORMDL2 antibody. Migration position and molecular weight of sizing standards are indicated on the left.

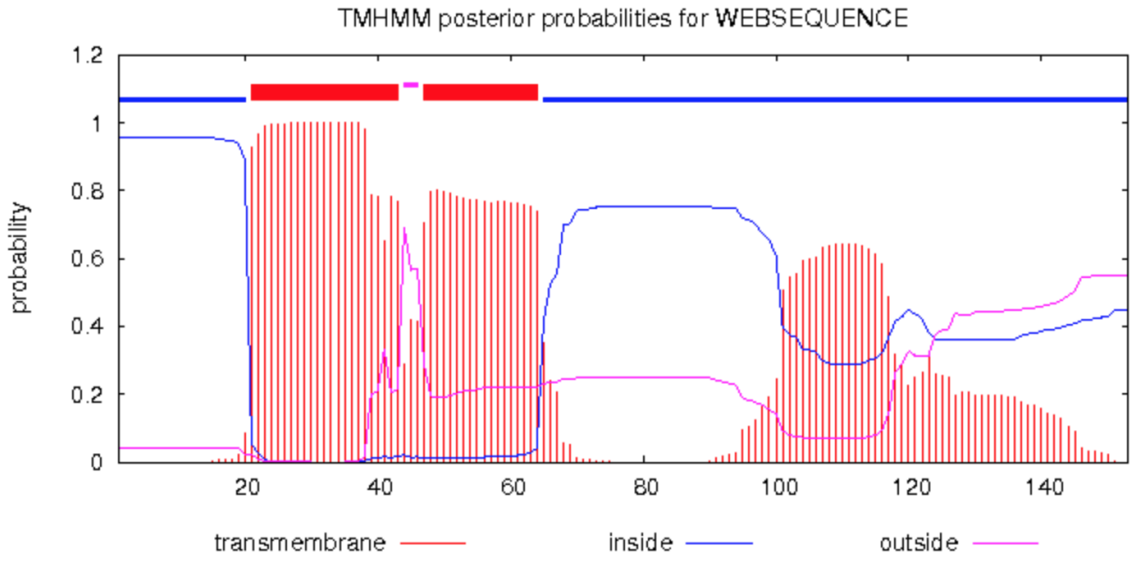

Figure 3.10: Predicted transmembrane segments in ORMDL2

Prediction of transmembrane segments in ORMDL2 protein using the graphical output predicted by the TMHMM software http://www.cbs.dtu.dk/services/TMHMM/. Probabilities for transmembrane (red), inside (i.e., cytoplasmic, blue), and outside (i.e., luminal, or exterior; purple) regions are displayed.

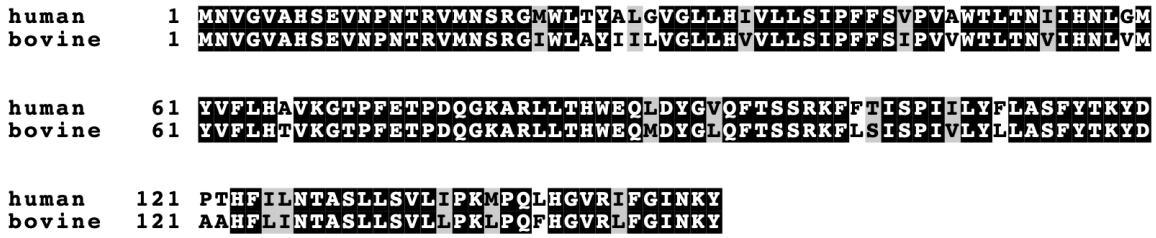

Figure 3.11: Alignment of human and bovine ORMDL2 amino acid sequences.

Human and bovine ORMDL2 amino acid sequences were obtained from the NCBI database and aligned using the Clustal Omega multiple sequence alignment tool https://www.ebi.ac.uk/Tools/msa/clustalo/. Amino acids were colored using the tool https://embnet.vital-it.ch/software/BOX_form.html. Black shaded amino acids represent identical residues, whereas the grey shade represents conserved amino acids. The sequence identity is 84%.

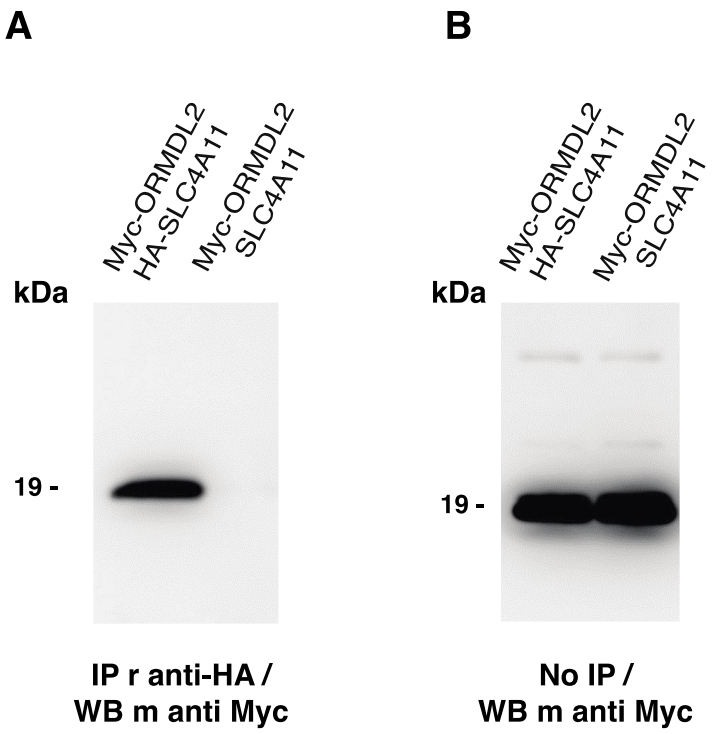

Figure 3.12: SLC4A11/ORMDL2 Interaction in transfected HEK293 cells

Co-immunoprecipitation of human SLC4A11 and human ORMDL2. **A.** Lysates of HEK293 cells transiently co-transfected with human Myc-ORMDL2 cDNA (pNDA24) and HA-SLC4A11, or HEK293 cells transiently co-transfected with human Myc-ORMDL2 cDNA (pNDA24) and non-tagged SLC4A11, were prepared. Lysates were immunoprecipitated (IP) with rabbit anti-HA antibody, resolved by SDS-PAGE, blotted, and probed with or without mouse anti-Myc antibody. **B.** The same samples did not undergo immunoprecipitation and were resolved by SDS-PAGE and probed with a mouse anti-Myc antibody as an indicator of total protein and expression in HEK293 cells. Migration positions and molecular weight of sizing standards are indicated on the left.

3.3 Discussion

The primary aim of this project was to better understand the role and involvement of SLC4A11 in the context of ECD by identifying SLC4A11 protein interactors. Using human SLC4A11 as the bait protein and a cDNA library from bovine cornea as the prey protein, a yeast two-hybrid (MYTH) screen was conducted to identify these proteins. After screening of the 38 uniquely identified hits based on the previously mentioned exclusion criteria, we discovered six full length protein interactors with SLC4A11: TMEM 254, ORMDL2, OCIAD1, LEPROTL1, CMP-SAT, and TMEM 128.

3.3.1 What is known about identified SLC4A11 interactors?

3.3.1.1 TMEM 254

Transmembrane 254 (TMEM 254) is a transmembrane protein and has no known function. The detected isoform from MYTH screening has three transmembrane segments at positions 16 to 36, 62 to 82, and 96 to 116. Only the N-terminus of the protein is oriented towards the cytoplasm (121). The TMEM 254 was detected in eighteen separate colonies as an interactor with SLC4A11 from the MYTH screen, suggesting high level of interaction or that the interactor is highly expressed in the cDNA library (Table 3.5).

Interestingly, TMEM 254 was detected to interact with alpha A-crystallin (CRYAA) using a human proteome microarray (122). Crystallin heat shock proteins function as chaperones and are highly expressed in the lens. Crystallin proteins are involved in several functions including chaperone capabilities, cell apoptosis inhibitors, in protein phosphorylation, cell survival, autophagy, and cell growth. Alpha crystallin proteins have multiple substrate binding sites that tend to bind to destabilized and unstructured proteins and function as chaperones in the prevention

of protein aggregation (123). It is possible that CRYAA functions as a chaperone along with TMEM 254 in corneal endothelial cells, however, the expression of CRYAA in corneal endothelial cells has not been determined. Gene expression of CRYAA has been reported in corneas from mice, and CRYAA protein expression has been identified in fetal corneal epithelial and limbal stem cell cultures from adult human tissue, indicating its presence in corneal cells and its importance in corneal transparency (124). Interestingly, when cultured corneal epithelial cells were exposed to lipopolysaccharide or hydrogen peroxide, CRYAA expression was significantly increased, suggesting expression of the protein responds to exogenous stimuli (124). Despite these data, no further characterization of the proteins involvement in corneal cells has been conducted, nor has its association with TMEM254.

3.3.1.2 LEPROTL1

One of the identified interactors by the MYTH screen was Leptin receptor overlapping transcript like 1 (LEPROTL1), also known as endospanin-2, a membrane protein with a diverse expression profile that regulates leptin receptor trafficking to the cell surface. The detected form from MYTH screening has four transmembrane segments at the positions, 7-27, 32-52, 69-89, 100-120 and was detected two times as a potential interactor. The N-terminus and C-terminus of the protein are located on the same side and are oriented towards the cytoplasm (125).

To date, no studies have specifically investigated LEPROTL1 expression or function in the cornea or its relationship with certain transporter proteins such as SLC4A11. Recent reports in mice have shown overexpression of LEPROTL1 decreases muscle mitochondrial ROS production, induces a muscle fiber-type switch from oxidative to glycolytic, and increases glucose homeostasis to improve running capacity (126). Likewise, knockout of the protein in animals increases lipid peroxidation and reduces overall endurance capacity in animals, suggesting LEPROTL1 has a

significant role in substrate utilization and glucose homeostasis during exercise (126). Aside from its role in skeletal muscle, additional studies have found that LEPROTL1 expression is low in many cancer types, suggesting that low expression of the protein may be involved in tumorigenesis (127). To accompany this theory, loss-of-function mutations have been identified in the *LEPROTL1* gene in various tumors in humans, especially breast cancer, indicating that promoter mutations of the gene may play a role in the development of cancer (127).

LEPROTL1 is highly expressed in the heart, testis, adrenal glands, thymus, and spleen. Lower expression levels of LEPROTL1 are detected in the lungs and skeletal muscle (128). The protein has several splicing variants. In transgenic mice, elevated expression of LEPROTL1 causes growth retardation, low sensitivity to growth hormone in the kidney, and decreased plasma insulin-like growth factor 1 (IGF1) levels. In addition, LEPROTL1 knockdown in rat hepatocyte cell lines elevates growth hormone sensitivity. It has been established that LEPROTL1 regulates growth hormone signalling, nutritional signalling, and metabolism (129). In bovine models, the binding of Janus kinase 3 (JAK3) to LEPROTL1 was previously reported to reduce the potential negative feedback of LEPROTL1 on growth hormone (GH) signaling and increase the growth promoting polypeptide IGF-1 availability in the growing follicle (130). Lastly, LEPROTL1 was also associated with the regulation of growth hormone sensitivity, and elevated expression increases skeletal muscle activity, decreases leptin signalling in muscles, and increases insulin signalling (126, 131).

Due to the lack of research regarding this protein, we can only speculate on why we discovered it as a protein interactor. Evidence suggests that SLC4A11 can localize to the inner mitochondrial matrix of the corneal endothelium, and, like LEPROTL1, reduced expression of it significantly increases ROS production (79). Thus, the SLC4A11-LEPROTL1 interaction may be

important to mitigate ROS within the corneal endothelium; however, further investigation is necessary to better understand this association.

3.3.1.3 ORMDL2

The *ORM1* like (*ORMDL)* gene is conserved in mammals and encodes the three proteins (ORMDL1, ORMDL2, and ORMDL3) (132). *ORM1* gene is the human homolog in *Saccharomyces cerevisiae* (132). The detected hit from MYTH screening has two transmembrane domains at the positions 22-42, and 43-63. both N-terminus and C-terminus ends of the protein are cytoplasmic (133). ORMDL2 is involved in biosynthetic pathways, such as the regulation of the synthesis of sphingolipids (134). Indeed, previous studies suggest that like transmembrane protein identification, proteins involved in basic biosynthesis pathways that are identified by the two-hybrid screening method tend to have higher false-discovery rates as well, suggesting ORMDL2 may be a false-positive hit (135). However, ORMDL2 negatively regulates sphingolipid synthesis (136), and this lipid class has previously been implicated in corneal diseases including FECD (137). More specifically, recent studies indicate eight sphingomyelin species are elevated in the aqueous humor of CHED eyes compared to healthy control patients (138). These data suggest that the identification of ORMDL2 as a protein interactor with SLC4A11 may not be a false-positive as it is involved in the negative regulation of a lipid class previously implicated in CHED. ORMDL2 may negatively regulate sphingolipid synthesis to combat elevations of sphingomyelin in the aqueous humor, although further work in this area is required. Moreover, sphingolipids are components of the PM that are important for cell signalling and cell surface organization (139, 140). ORMDL2 the sphingolipid regulator may have a role in the trafficking of

SLC4A11 to the PM. Further investigations are required to discover the role of ORMDL2 in the expression of SLC4A11 at the cell surface.

ORMDL 2 deficiency also potentiates ORMDL3-dependent changes in mast cell signaling (141), and deficiencies in ORMDL2 and ORMDL3 promote increased IκB-α phosphorylation, degranulation, and production of interleukin-4, interleukin-6, and TNF-α cytokines in activated mast cells (142). In mouse studies, ORMDL2 is also associated with the inhibition of serine palmitoyl transferase which, in turn, mediates the synthesis of sphingolipids (143). ORMDL2 expression is also upregulated by nitric oxide *in vitro* (144) and is expressed, along with ORMDL1 and ORMDL3, in atopic asthmatic patients (145).

3.3.1.4 CMP-SAT

In eukaryotes, cytidine-5'-monophosphate sialic acid transporter (CMP-SAT) is a Golgi-localized transporter protein originally cloned as an isoform of the human UDP-galactose transporter and belongs to the nucleotide sugar transporter gene class (146-148). This protein is located in the Golgi apparatus and exhibits several topological domains (cytoplasmic and luminal), and eight transmembrane helical domains (positions 12 to 30, position 42 to 64, position 143 to 160, position 175 to 195, position 207 to 227, position 239 to 262, position 274 to 291, and position 297 to 315. Both N-terminus and C-terminus are found on the same side, and oriented towards the cytoplasm (149). CMP-SAT regulates protein glycosylation via polysaccharide translocation into the Golgi apparatus (148).

Interestingly, *SLC4A11* mutations found in CHED and FECD patients cause the recognition of SLC4A11 as misfolded protein that are targeted for degradation which can be detected on immunoblots as immature partially glycosylated protein (48). Specifically, when

HEK293 cell lysates were transfected to express tagged wild-type SLC4A11 or mutant SLC4A11 and treated with endoglycosidase H or PNGase F, two compounds commonly used to distinguish post-translational modifications of proteins, the mutated SLC4A11 cells displayed significantly altered molecular weight shifts in response to treatment (48). N-glycosylation occurs in the ER and all Asparagines that are glycosylated receive the same core carbohydrate structure, which is refined in the Golgi (48). The two different carbohydrate structures are associated with the ER and post ER (i.e. Golgi and PM) (48). These data indicate that SLC4A11 mutations observed in some CHED patients result in alterations to glycosylation status. Glycosylation is a known mediator of proper protein folding, transport, and surface expression (150), and perturbations in sialic acid biosynthesis (particularly, Uridine diphosphate N-acetylglucosamine 2-epimerase/*N*-acetylmannosamine) the key enzyme sialic acid biosynthesis can cause serious complications, including proteinuria, renal failure, severe hemorrhaging of the eye during infancy to toddlerhood and more (147, 151). Concerning CMP-SAT's involvement in CHED, no studies have investigated the expression or interaction of CMP-SAT with mutated SLC4A11. This relationship may be an interesting follow-up study to better understand the interaction between SLC4A11 with CMP-SAT.

Some of the main limitations of the MYTH screening method used in this study have already been outlined (primarily concerning high rates of false discovery), other constraints of the method exist which are worth discussion. First, the technique requires the use of *Saccharomyces cerevisiae* as the host cell, which means the protein of interest (in this case SLC4A11) must be able to fold correctly in the yeast cell, otherwise any meaningful protein-protein interactions which occur in other organisms can essentially be rendered false. Another significant drawback to the MYTH technique is that certain protein-protein interactions depend on post-translational

modifications that may not occur in yeast. This disadvantage is particularly concerning considering one of the hits of this study was CMP-SAT, a protein involved in the transport of a monosaccharide chain involved in glycosylation status; however, previous studies have reported yeast proteins undergo glycosylation (8). Besides these clear disadvantages, the MYTH screening method allows for high throughput, large-scale protein-protein interactions, as well as protein purification, at a low cost and in much less time compared to other biochemical or proteomic methods. Moreover, the host yeast cells used in the MYTH screen are a higher eukaryotic especially when compared to other *in vitro* or bacterial approaches, making them a good organism to correlate data with human data.

3.3.1.5 TMEM 128

Transmembrane 128 (TMEM 128) is composed of 165 amino acids and located in the cell membrane. It has four helical domains at positions 49 to 69, 81 to 101, 119 to 139, and 144 to 164 (152). The C-terminus and N-terminus are facing the same side and are oriented towards the cytoplasm. TMEM 128 has no known function but was previously reported to interact with the ceroid-lipofuscinosis neuronal 8 (CLN8) protein in a MYTH screen (153). As an endoplasmic reticulum transmembrane protein, CLN8 performs functions related to lipid transport, synthesis, or sensing. Patients with *CLN8* mutations have altered levels of sphingolipid and phospholipids in the brain, causing the autosomal recessive neurodegenerative disorder known as neuronal ceroid-lipofuscinosis (NLC), a type of lysosomal storage disease (LSD) (154). Additional studies have identified TMEM 128 from a MYTH screen using a human Jurkat T-cell cDNA library to interact with the cluster of differentiation 3 delta (CD3δ) protein. CD3δ is a subunit of the T-cell receptor (TCR) that is required for TCR surface expression and signalling (155). The TCR is a complex of

transmembrane proteins that activates T-cells in response to an antigen. Likewise, activation of TCR initiates positive and negative cascades leading to cellular differentiation, proliferation, and the activation of cell death responses (155).

Furthermore, while the yeast two-hybrid system provides large-scale analysis on protein-protein interactions, high false-discovery and false-negative rates of detected hits have been well documented (135). Importantly, these false-discovery rates may be particularly specific to membrane or membrane-bound signaling proteins because membrane proteins contain hydrophobic residues. This may make them vulnerable to non-specific interactions (135, 156). However, statistical analyses on the relationship between hydrophobicity and membrane protein interaction false-discovery rates using the yeast two-hybrid screen have not yet been confirmed (135). Taken together, the potential limitations of this screening method concerning false positives suggests that, at the very least, the interaction between SLC4A11 with TMEM128 should be met with a degree of hesitation, and further investigation is required to not only confirm the association between these proteins, but also to characterize the function of these transmembrane proteins as well.

3.3.1.6 OCIAD1

Ovarian carcinoma immunoreactive antigen domain 1 (OCIAD1) is a protein composed of 245 amino acids and is located in the inner mitochondrial membrane (157). OCIAD1 contains an ovarian carcinoma antigen (OCIA) region with unknown function (158), At the positions 23 to 109. Also contains two disordered regions in positions 111 to 141 and 169 to 245 (159). In addition, it has predicted phosphorylation sites at the positions, 108, 116, 123, 193 for a phosphoserine modification (159). The C-terminus and N-terminus are both oriented towards the intermembrane

space of the mitochondria (159). OCIAD1 was discovered as a highly expressed protein in the ovarian carcinoma cDNA expression library. It is associated with ovarian cell carcinoma adhesion (87) and promotes chemotherapeutic resistance against cell detachment in the presence of lysophosphatidic acid (160). Two different forms of OCIAD1 have been identified, including the long form (245 amino acids) and a short form (208 amino acids) (87). The long form of OCIAD1 was detected by our MYTH screen as an SLC4A11-protein interactor.

Overexpression of OCIAD1 increases LPA-induced cell adhesion of HEY ovarian cancer cells to collagen type I and laminin 10/11 at the extracellular matrix, even in the presence of paclitaxel, a cell adhesion inhibitor (160). Lysophosphatidic acid (LPA) is a biologically active signalling molecule elevated in ovarian cancer. In humans, LPA triggers the adhesion of ovarian cancer cells to the extracellular matrix, cellular invasion, cell migration, and cell survival (160). Inhibition of OCIAD expression decreases LPA-induced cell adhesion of ovarian cancer cells to collagen I and laminin 10/11, along with collagen IV (88). Moreover, OCIAD1 is involved in cell–matrix interactions by interacting with α actinin 4, which regulates the architecture of β actin and the function of integrins (88). In cell matrix interactions, OCIAD1 interacts with α actinin 4 to regulate β actin architecture and modulate the function of integrins (88). OCIAD1/SLC4A11 interaction may play a major role in role cell adhesion cells or may be involved in the regulation of ROS to prevent the loss of cells in ECD. The investigation of OCIAD1 and SLC4A11 interaction will be discussed in Chapter 4.

3.3.1.7 TOM6

One of the most interesting, detected interactors that was characterized as a biosynthetic apparatus protein, is the translocase of the outer mitochondrial membrane six (TOM6) which is a

mitochondrial import receptor (161). TOM6 is part of the TOM complex and important for its stabilization (161). SLC4A11 is expressed in the inner mitochondrial membrane and regulates oxidative stress (79). However, SLC4A11 does not have the mitochondrial targeting signal sequence which means it is suggested that it is targeted through a chaperone attachment pathway (162). This supports the idea that OCIAD1/SLC4A11 interaction is involved in targeting SLC4A11 expression in mitochondria. However, *Neurospora crassa* strain lacking TOM6 has a clear defect in mitochondrial import of preproteins (161). Could be that the interaction of TOM6 and SLC4A11 be involved in the targeting of SLC4A11 into mitochondrial sub compartments. Further investigations are required to understand the nature of this interaction.

Altogether, while the MYTH screen has clear advantages and disadvantages regarding identification of protein-protein interactions, the results identified in this study provide insight on the potential interactions between SLC4A11 and other proteins. However, further work is required to better characterize these findings and what exactly the interaction between these proteins represents.

In conclusion, six full-length protein interactors with SLC4A11 were identified after screening and applying exclusion criteria: TMEM254, ORMDL2, OCIAD1, LEPROTL1, CMP-SAT, and TMEM128. Some of these proteins are currently poorly characterized with no specified function as TMEM254 and TMEM128, although research on their homologues or association with other proteins provide some indication of their functionality. Protein interactors involved in biosynthetic pathways were a common theme, including ORMDL2, which mediates sphingolipid synthesis, and CMP-SAT, a protein that regulates protein glycosylation; and previous studies have identified both of these processes to be involved in CHED and FECD patients (32). OCIAD1 was also identified by the MYTH screen and recent work has illustrated its involvement in cell adhesion

and the mitochondrial electron transport chain (79). Due to these functions (particularly cell adhesion), Chapter 4 aims to further characterize the interaction between SLC4A11 and OCIAD1.

Chapter 4: SLC4A11/OCIAD1 Interaction

All experiments were performed by Dr. Bernardo Alvarez (Figures 4.1-4.11). Cloning of bovine (pNDA8) Ociad1 and Slc4a11 (pNDA35) was done by Nada Alshumaimeri.

4.1 Introduction

The innermost region of the cornea is the DM, a highly structured extracellular matrix composed of COL8A1 and COL8A2, fibronectin and laminins to which CEC adhere (114). Recently, SLC4A11 was identified as a cell adhesion molecule (CAM) that contributes to CEC adhesion (62). The MYTH screen in Chapter 3 described our identification of a novel protein interactor with SLC4A11, OCIAD1, which may function as a cell adhesion molecular (CAM) and may contribute to cell adhesion of the CECs (160). A homology model of SLC4A11 displays EL3 at the dimeric interface, where each monomer of the EL3 will dimerize (Figure 1.6) (63, 114). Moreover, a recent study revealed that some mutations of the SLC4A11 gene may result in CHED or FECD due to perturbations in cell adhesion function (63). Specifically, the study demonstrated that SLC4A11 promotes adhesion to the DM via the EL3 region. Interestingly, when HEK293 cells was incubated with an antibody against the SLC4A11-EL3 region, the cells showed dramatically reduced adhesion (114). Overall, these studies highlight the reasoning behind why CECs may be lost in some ECD patients: certain mutations result in diminished CAM-like properties of SLC4A11, reducing cell adhesion and, ultimately, binding of the EL3 region to the DM. Thus, for the MYTH screen we hypothesized that proteins interacting with SLC4A11 may be involved in cell adhesion, which led us to further investigate and characterize its relationship with OCIAD1.

Previous research on OCIAD1 has focused solely on its role in ovarian cancer, which is where the protein was originally found. The protein was found to be highly expressed in metastatic ovarian cancers and this over-expression induced cell adhesion, representing a possible mechanism involved in tumor metastasis (88). This adhesion function of OCIAD1 is significant considering our current understanding of SLC4A11 mutations and how they reduce cell adhesion, resulting in CEC loss and/or eventually endothelial corneal dystrophies.

OCIAD1 at the plasma membrane has a role in cell adhesion. In addition, genome wide CRISPRi evidence also suggests that OCIAD1 is expressed in the inner mitochondrial membrane and is necessary for the assembly of Complex III of the mammalian ETC (157). Specifically, OCIAD1 depletion in the mitochondria disrupted the ETC (157). Interestingly, OCIAD1's mitochondrial role further highlights the potential importance of its interaction with SLC4A11. Recent work suggested that SLC4A11 regulates glutamine catabolism in mammalian CECs to prevent oxidative stress, and loss of this regulatory ability potentiates oxidative stress and CEC death, resulting in ECD, corneal edema, and vision loss (79). These data suggest that SLC4A11's regulatory function on glutamine metabolism is highly important for corneal endothelial pathologies. Additional studies have shown that glutamine specifically effects Complex 1 and III of the ETC to cause mitochondrial dysregulation (115). Considering the functional similarities (both mitochondrial and their involvement in cell adhesion) between OCIAD1 and SLC4A11, we hypothesized that their interaction was particularly significant in corneal endothelial dystrophy, and that loss of this interaction results in dysregulation of typical cell adhesion. Thus, Chapter 4 investigates this hypothesis and the interaction between OCIAD1 with SLC4A11 using a variety of *in vitro* techniques and bovine cornea tissues.

4.2 Results

4.2.1 Bioinformatic analysis of OCIAD1

We first performed bioinformatic analysis of OCIAD1. We compared the amino acid sequence from human and bovine (Figure 4.1), revealing high identity between human and bovine SLC4A11 (92% amino acid sequence identity). This sequence conservation strongly suggests that human and bovine SLC4A11 will function interchangably and thus SLC4A11/ OCIAD1 interaction can be

tested with human or bovine proteins. Moreover, these data led us to test the interaction between human SLC4A11 and human OCIAD1 in the next step. Since OCIAD1 has been subject to little previous study and no structural characterization, we analyzed the predicted secondary structure of human OCIAD1 using the online tool for the prediction of transmembrane helices based on a hidden Markov model (TMHMM) (http://www.cbs.dtu.dk/services/TMHMM/). The prediction displays two transmembrane segments with N- and C-terminal cytoplasmic ends (Figure 4.2). We further predicted the three-dimensional structure of human OCIAD1, using the online Phyre2 software (Figure 4.3). The amino acid sequence for human OCIAD1 was from NCBI website ((NP_001073308.1). The model suggests that OCIAD1 contains two hydrophobic helices, which could act as transmembrane segments, and a cytoplasmic N-terminal end. Finally, this analysis confirms OCIAD1 could activate the selective genes in the MYTH screen, which requires N and C-terminal cytoplasmic locations.

4.2.2 Interaction of SLC4A11 and OCIAD1

4.2.2.1 Heterologous expression system

Next, we assessed the possible interaction between human or bovine SLC4A11 and bovine Ociad1, expressed in transfected HEK293 cells. HEK293 cells were co-transfected with Myc-tagged bovine Ociad1 (Ociad1-Myc) cDNA (pNDA8) and human SLC4A11 cDNA (pAMC1) or bovine Slc4a11 cDNA (pNDA35). Bovine Ociad1 was immunoprecipitated from the transfected HEK293 cells with the anti-Myc antibody. Immunoprecipitation of SLC4A11 and Ociad1 indicates that they physically associate

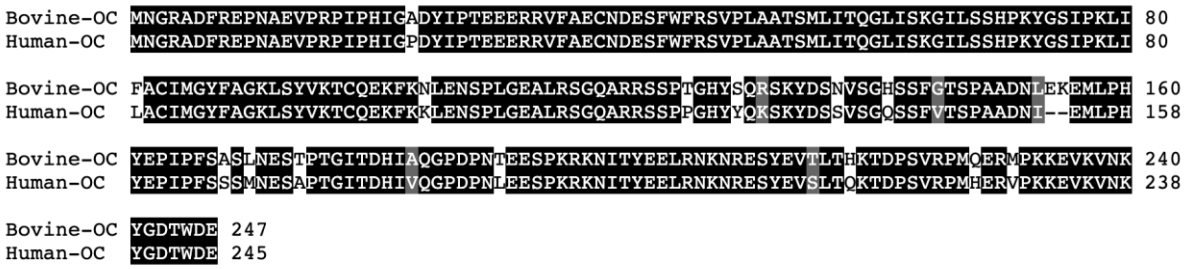

Figure. 4.1: Alignment of Human and Bovine OCIAD1 proteins

Human (NP_001073308.1) and bovine OCIAD1 (OC) (AAI03461.1) amino acid sequences were obtained from the NCBI database and aligned using Clustal Omega Multiple Sequence Alignment tool (CLUSTALW) https://www.ebi.ac.uk/Tools/msa/clustalo/. Amino acids were colored using the tool https://embnet.vital-it.ch/software/BOX_form.html. Black shaded amino acids represent conserved residues, whereas unshaded amino acids represent divergent amino acids. The overall sequence identity is 92%.

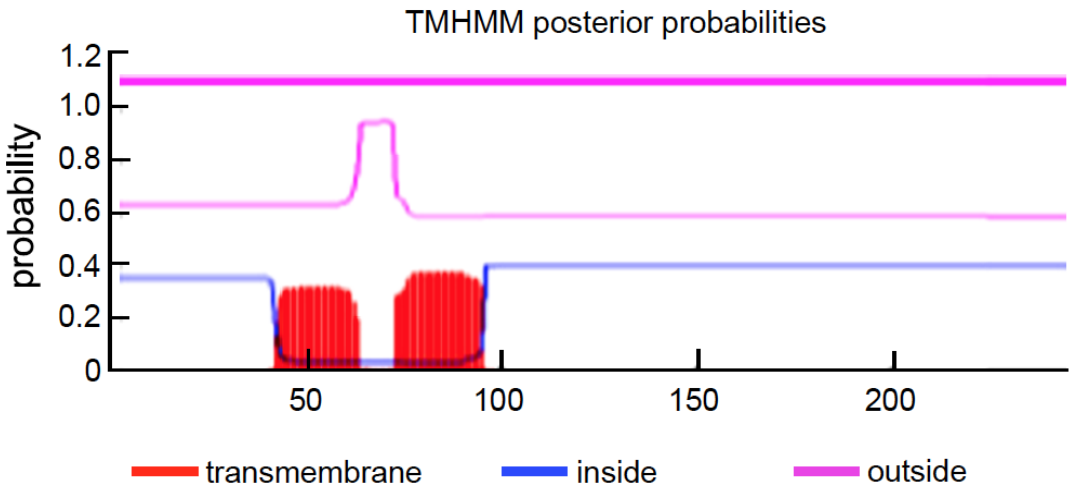

Figure 4.2: Prediction of transmembrane helices in OCIAD1

Prediction of transmembrane helices in the human OCIAD1 (NP_001073308.1) from NCBI was analysed using the graphical output predicted by the TMHMM software http://www.cbs.dtu.dk/services/TMHMM/. Probabilities for transmembrane (red), inside (i.e., cytoplasmic, blue), and outside (i.e., luminal, or extracellular; purple) regions are displayed. Two transmembrane regions are predicted for the OCIAD1 protein.

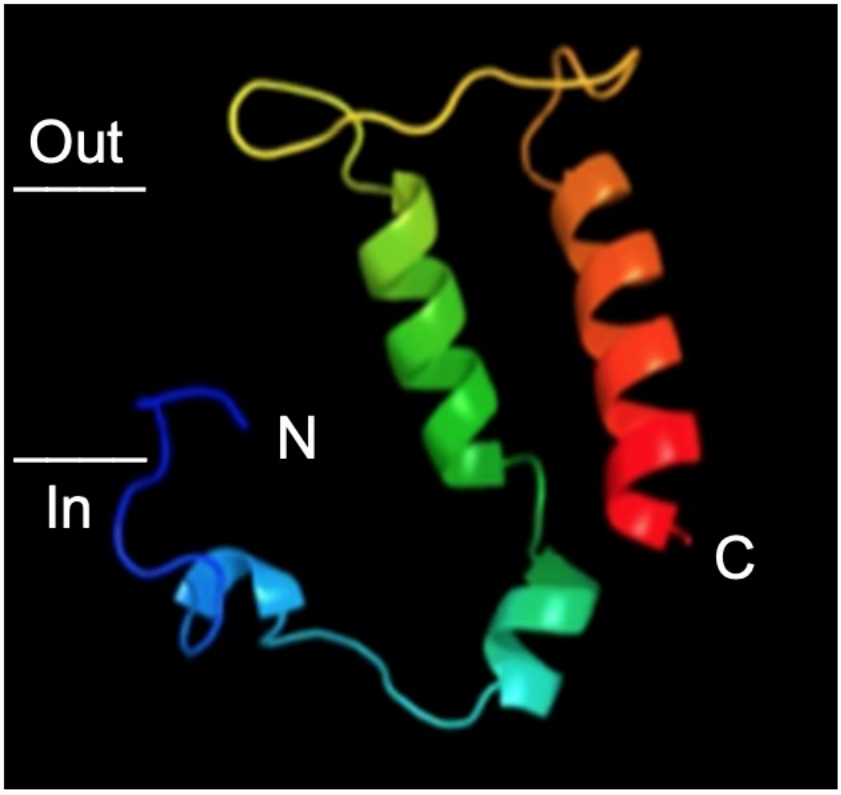

Figure 4.3: Predicted structure of OCIAD1

Cartoon diagram illustrating the 3D structure of human OCIAD1 (NP_001073308.1) was predicted with the online protein homology/analogy recognition engine v2 (Phyre2) server http://www.sbg.bio.ic.ac.uk/phyre2/html/page.cgi?id=index, with amino-(N) and carboxyl-terminal (C) ends of OCIAD1 marked. The predicted structure displays OCIAD1 contains two helical transmembrane segments and one N-terminal cytoplasmic loop.

(Figure 4.4), which is consistent with the MYTH results. The association of the Myc-tagged bovine Ociad1 is consistent when co- immunoprecipitated with human SLC4A11 and bovine Slc4a11, respectively. Expression of human SLC4A11 and bovine Slc4a11 protein is also detected in the lysates of total protein as expected. Moreover, expression of the Myc-tagged bovine Ociad1 protein was detected in the lysates of total protein. Specificity of the interaction was indicated by the absence of signal for the pcDNA empty vector transfected cells, indicating no co-immunoprecipitation of ociad1 with the negative control.

4.2.2.2 Interaction in Human Ovarian Cancer Cells

We next tested the protein expression and interaction in human ovarian cancer cell line, SKOV3. SKOV3 cells are a metastatic cancer cell line expressing high levels of OCIAD1 protein (160), a marker of metastatic cancer, which promotes cell migration and invasion (poor prognosis and advanced ovarian cancer) (88). OCIAD1 promotes adhesion to collagen I, fibronectin, laminin, and other extracellular matrix components (88). Moreover, OCIAD1 associates with β-actin and alpha-actinin 4 and links cytoskeletal proteins to integrins in metastatic cancer cell lines (88). Here, SKOV3 cells were transfected with human SLC4A11-HA cDNA (pAMC1) or an empty vector (pCDNA). Transfected and untransfected cells were immunoprecipitated with an anti-HA antibody, resolved by SDS-PAGE, and then probed with an anti-OCIAD1 antibody. The results demonstrated that OCIAD1 binds human HA-SLC4A11 and do not immunoprecipitate with pCDNA and non-transfected cells (Figure 4.5A).

SKOV3 cells were transfected with human HA-SLC4A11 cDNA (pAMC1), and cell lysates were immunoprecipitated with an anti-OCIAD1 antibody, resolved by SDS-PAGE and

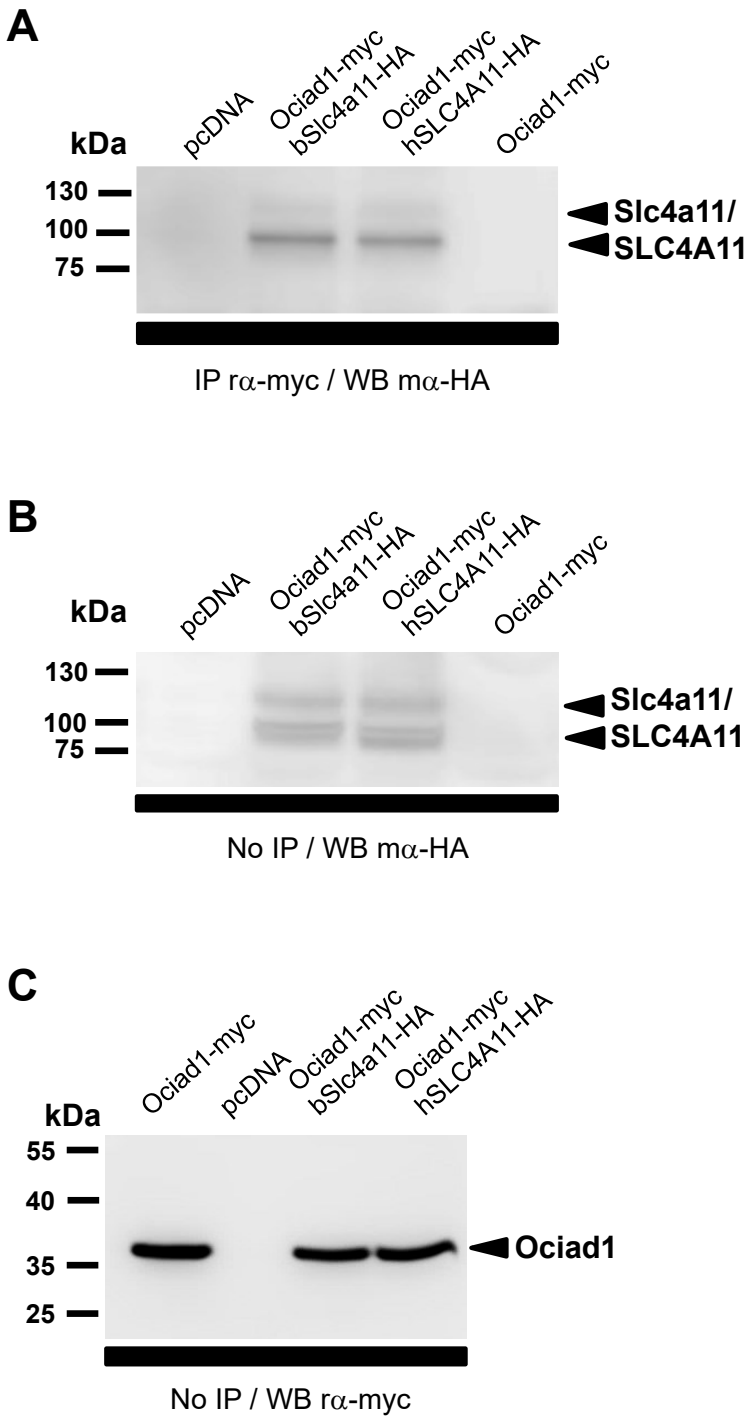

Figure 4.4: SLC4A11/Ociad1 Interaction in transfected HEK293 cells

Co-immunoprecipitation of SLC4A11 and bovine Ociad1. **A.** Lysates of HEK293 cells were transiently transfected with empty vector (pcDNA), Myc-tagged bovine Ociad1 (Ociad1-myc) cDNA (pNDA8), were transiently co-transfected with Ociad1-Myc and a HA tag bovine Slc4a11 (bSlc4a11-HA), the plasmid (pNDA35), or co-transfected with Ociad1-Myc and a HA tag human SLC4A11 (hSLC4A11-HA). Lysates were immunoprecipitated (IP) with a rabbit anti-Myc antibody, resolved by SDS-PAGE, blotted, and probed with a mouse anti-HA antibody. Lysate samples were probed to indicate the total amount of bSlc4a11-HA/hSLC4A11-HA. **B.** The samples were not IP, resolved by SDS-PAGE and probed with a mouse anti-HA antibody. **C.** The samples were not IP, resolved by SDS-PAGE and probed with a mouse anti-Myc antibody. Black arrows indicate protein the detected bands at the expected molecular weights. Migration position and molecular weight of sizing standards are indicated on the left.

probed with an anti-SLC4A11 antibody (Figure 4.5B). SLC4A11 migrates as two separate bands when resolved by SDS-PAGE. The upper band (mature form) of SLC4A11 is at the plasma membrane and is characterized by complex glycosylation, while the lower (immature) band is intracellularly retained at the endoplasmic reticulum and is partially glycosylated (118). The detected bands from (Figure 4.5 B) show a higher intensity for the immature form of SLC4A11. These data indicate the association of OCIAD1 with SLC4A11 is higher with the immature form of SLC4A11 in SKOV3 cells.

Next, we examined specificity of the interactions in SKOV3 cells. SKOV3 cells were transfected with human HA-SLC4A11 cDNA (pAMC1) or pcDNA (empty vector). Transfected and untransfected cells were immunoprecipitated with an anti-OCIAD1 antibody, resolved by SDS-PAGE, and probed with an anti-Na^+/K^+ ATPase antibody. The Na^+/K^+ ATPase is endogenously expressed and was used as a negative control. Transfected and untransfected cells showed no background interaction of Na^+/K^+ ATPase with SLC4A11, pCDNA, and OCIAD1 (Figure 4.5C). Samples of the lysate were probed to indicate the total amount and expression of SLC4A11 in the sample.

4.2.2.3 SLC4A11/OCIAD1 Interaction in bovine cornea

The interaction of SLC4A11 and OCIAD1 was detected in HEK293 and SKOV3 cells, which led us next to test their interaction in bovine corneas. As a negative control, lysates of bovine corneas were immunoprecipitated with an anti-Na^+/K^+ ATPase antibody, resolved using SDS-PAGE, and blotted with an anti-bovine Slc4a11 antibody (Figure 4.6A left blot). Bovine cornea lysates showed no association of endogenous bovine Slc4a11 with the Na^+/K^+ ATPase. Lysates of bovine cornea were immunoprecipitated with anti-human OCIAD1, resolved using SDS-PAGE,

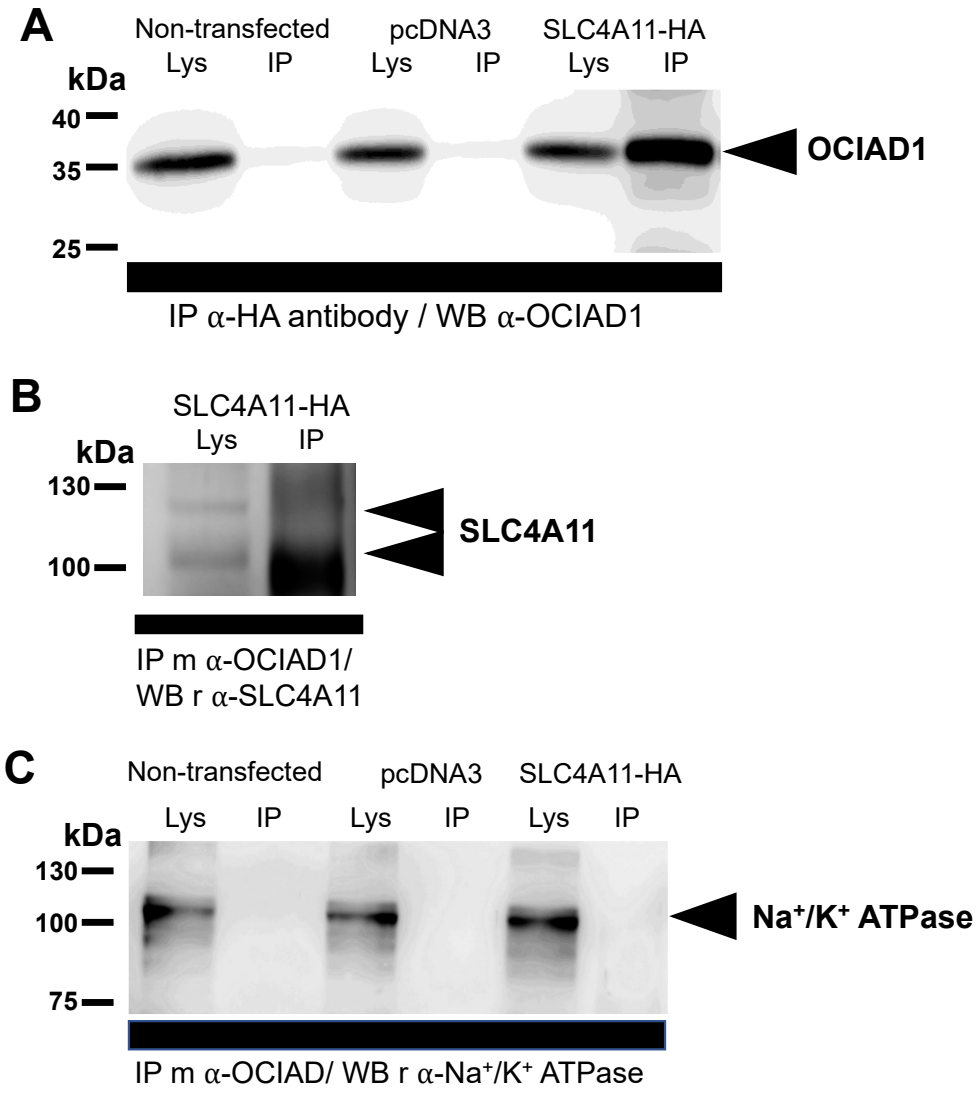

Figure 4.5: SLC4A11 and OCIAD1 Interaction in Human Ovarian Cancer Cells

A. Co-immunoprecipitation of SLC4A11 and human OCIAD1. Lysates of untransfected SKOV3 ovarian cancer cells, SKOV3 cells transiently transfected with pcDNA (empty vector) cDNA or transfected with SLC4A11-HA cDNA (pAMC1), were prepared. Lysates were immunoprecipitated (IP) with a rabbit anti-HA antibody, resolved by SDS-PAGE, blotted, and probed with a mouse anti-OCIAD1 antibody. Lysate samples were probed to indicate the total

amount of OCIAD1 in each sample. **B.** Reciprocal co-immunoprecipitation of SLC4A11 and OCIAD1 was conducted in SKOV3 cells transfected with SLC4A11-HA cDNA. Cell lysates were IP with a mouse anti-OCIAD1 antibody, resolved by SDS-PAGE, blotted, and probed with a rabbit anti-HA antibody to detect SLC4A11. Lysate samples were probed to indicate the total amount of SLC4A11 in the sample. **C.** Lysates of untransfected SKOV3 cells, SKOV3 cells transiently transfected with pcDNA (empty vector) cDNA, or SKOV3 cells transiently transfected with SLC4A11-HA cDNA, were IP with a mouse anti-OCIAD1 antibody, resolved by SDS-PAGE, blotted, and probed with a rabbit anti-Na^+/K^+ ATPase antibody. Lysate samples were probed to indicate the total amount of Na^+/K^+ ATPase in each sample. Black arrows indicate the detected bands at the expected molecular weights of the proteins. Migration position and molecular weight of sizing standards are indicated on the left.

and blotted with anti-bovine Slc4a11 (Figure 4.6A right blot,). The antibody used against human OCIAD1 can detect OCIAD1 expression from both human and bovine evidence as detected in Figures 5.5 and 4.6A. Lysates of bovine corneas showed an association of Slc4a11 with Ociad1 (Figure 4.6A right blot).

Using bovine corneas to detect the interaction between SLC4A11 and OCIAD1, we compared the expression of Ociad1 in SKOV3 cells and bovine cornea. Bovine cornea and SKOV3 cells were lysed, resolved using SDS- PAGE, and blotted with an anti-OCIAD1 antibody. OCIAD1 is highly expressed in SKOV3 cells compared to its expression in bovine corneas. This approach confirmed that OCIAD1 is expressed in bovine cornea (Figure 4.6B). Lysate samples were probed to indicate the total amount and expression of SLC4A11 in the sample.

4.2.3 Localization of SLC4A11 and OCIAD1

4.2.3.1 localization in heterologous expression system

Since the interaction between SLC4A11 and OCIAD1 was confirmed by immunoprecipitation in HEK293 cells, SKOV3 cells, and bovine corneas, we next investigated the colocalization of SLC4A11 and OCIAD1 by confocal immunofluorescence. SKOV3 cells transiently transfected with SLC4A11-HA cDNA and untransfected cells were plated on poly-L-lysine coated glass coverslips. Cells were stained with an anti-SLC4A11 or anti-HA antibody, followed by Alexa Fluor 488-conjugated chicken anti-rabbit IgG secondary antibody. We also ran further analysis on cells stained with an anti-OCIAD1 antibody, followed by Alexa Fluor 594-conjugated chicken anti-goat IgG. Then, nuclei were stained with DAPI. Immunocytochemical analysis showed that SLC4A11 is expressed endogenously in SKOV3 cells (Figure 4.7). In addition, results revealed that transiently transfected SLC4A11-HA and endogenous SLC4A11 colocalizes with OCIAD1 at

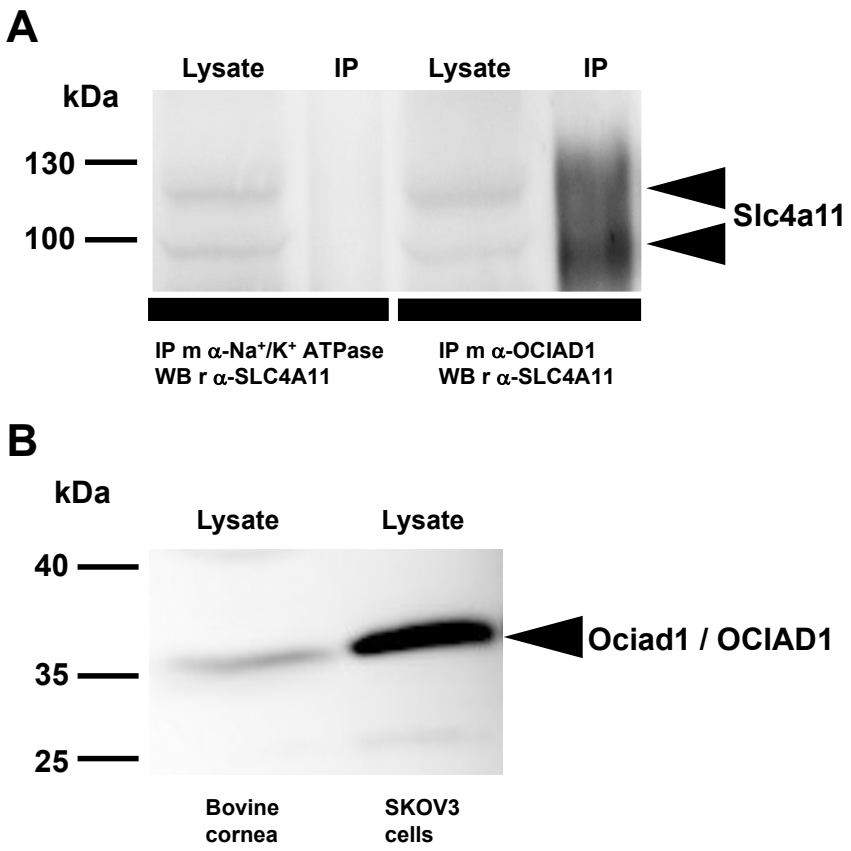

Figure 4.6: Interaction of Slc4a11 and Ociad1 proteins in the bovine cornea

A. Cornea lysates was prepared and 220 μg of total protein was immunoprecipitated with 2 μg of IgG mouse polyclonal anti-OCIAD1 antibody, or immunoprecipitated with 2 μg of IgG mouse monoclonal anti-Na^+/K^+ ATPase antibody. Lysates were resolved on 7.5% acrylamide SDS-PAGE, blotted, and probed with a rabbit anti-SLC4A11 antibody. Samples of the lysate were probed to indicate the total amount of bovine Slc4a11. **B.** Samples of the cornea lysate were also resolved on 10% acrylamide SDS-PAGE, blotted, and probed to indicate the total amount of OCIAD1 in the sample. Lysates of SKOV3 cells which endogenously expressed OCIAD1 were used as expression control for the Ociad1 protein. Black arrows indicate position of the proteins. Migration position and molecular weight of sizing standards are indicated on the left.

the same compartments of SKOV3 cells because there is pericellular staining consistent with PM and also intracellular staining, which would be consistent with ER and possibly mitochondria.

4.2.3.2 localization in bovine cornea

To identify the colocalization of SLC4A11 and OCIAD1, first we examined the histology of bovine corneas. Cross sections of bovine corneas were stained via Hematoxylin and Eosin staining (Figure 4.8A). The stained cross sections showed the multiple layers of the cornea with the epithelium at the top, Bowman's membrane, stroma, Descemet's membrane, and the endothelium at the bottom.

We assessed the colocalization of SLC4A11 and OCIAD1 by confocal immunofluorescence in bovine corneas. Cross sections of the bovine corneas were fixed and labeled with rabbit anti-SLC4a11 and anti-OCIAD1 primary antibodies. Immunofluorescence signals were visualized by Alexa fluor 488-conjugated antibody (green) for SLC4A11 and Alexa fluor 594-conjugated anti-mouse IgG antibody (red) for OCIAD1. Sections were mounted in a DAPI media, and images were collected. Images of bovine cross sections revealed the position of nuclei in nucleated cells of the cornea (endothelium, keratocytes in the stroma and endothelial cells). The staining pattern indicates that SLC4A11 and OCIAD1 colocalize in endothelial cells at the bottom most cell layer, below the stroma (Figure 4.8B).

4.2.4 Role of OCAID1 in the abundance of SLC4A11 at the cell surface

We next assessed whether OIAD1 affects SLC4A11 cell surface trafficking. HEK293 cells were transiently transfected with SLC4A11 cDNA and co-transfected with or without OCIAD1 cDNA.

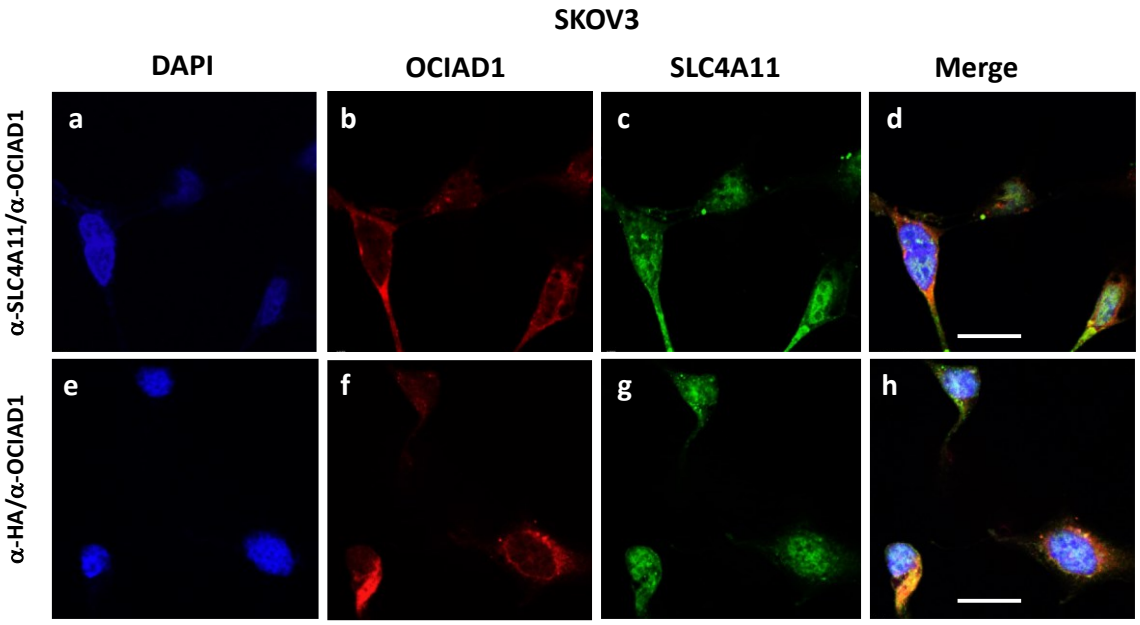

Figure 4.7: Localization of SLC4A11 and OCIAD1 Proteins in SKOV3 Cells

a-d. Immunocytochemical analysis of SKOV3 cells expressing endogenous SLC4A11 and endogenous OCIAD1 proteins. **e-h.** SKOV3 cells transiently transfected with SLC4A11-HA cDNA (pAMC1) and expressing endogenous OCIAD1. Transfected and untransfected cells were plated on poly-L-lysine coated glass coverslips. Cells were stained as indicated on the left side, with rabbit anti-SLC4A11 antibody or rabbit anti-HA antibody, followed by Alexa Fluor 488-conjugated chicken anti-rabbit IgG secondary antibody (c, g; green) or with mouse anti-OCIAD1 antibody, followed by Alexa Fluor 594-conjugated chicken anti-goat IgG (b, f; red). **a, e; (blue)** Nuclei were stained with DAPI. **d, h; (yellow).** Merged images display SLC4A11 and OCIAD1 labeling overlapped. Scale bar = 20 μm.

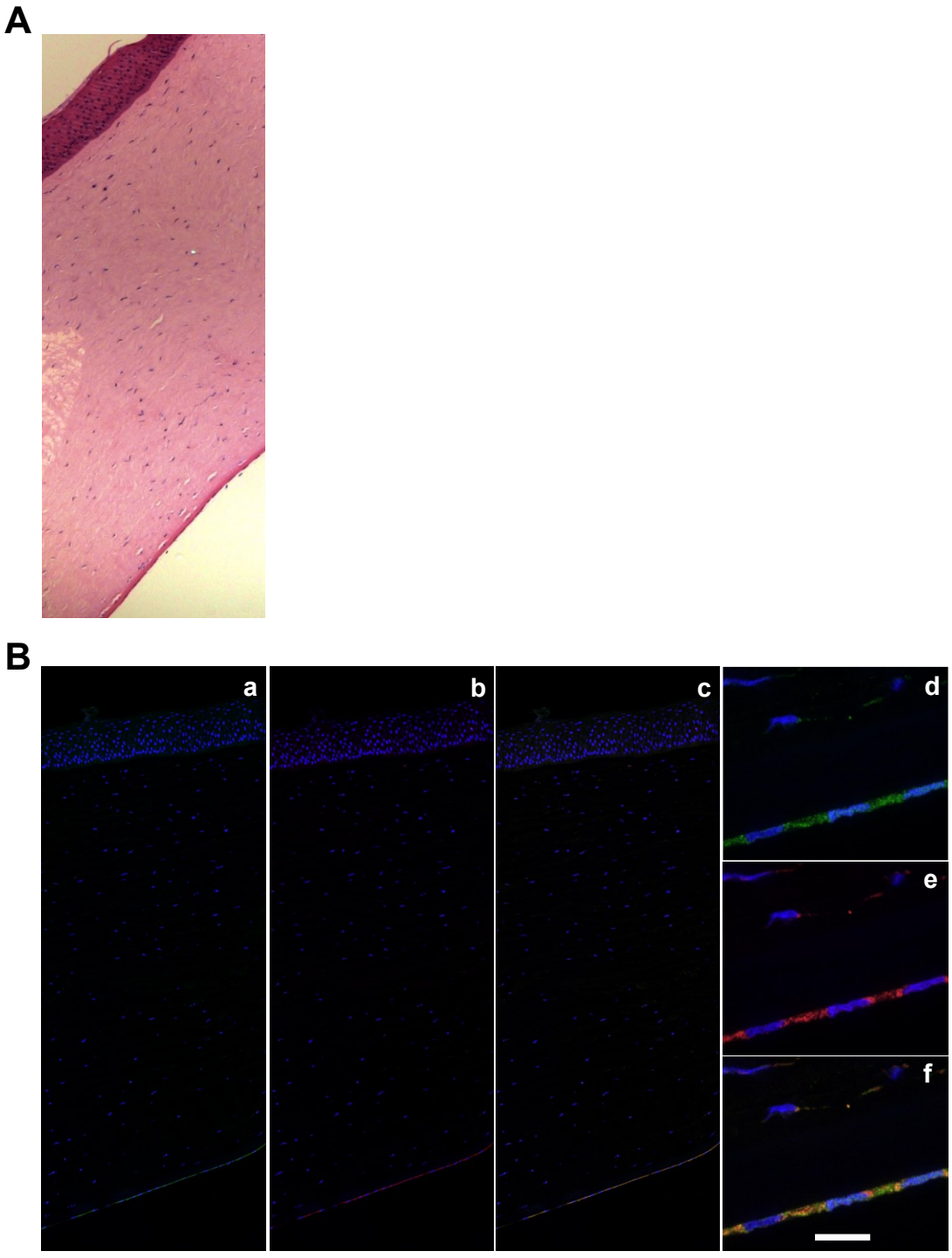

Figure 4.8: Localization of Slc4a11 and Ociad1 Proteins in Bovine Cornea

A. Bovine cornea stained with Hematoxylin and Eosin. **B.** (a-f) Confocal images of bovine cornea cross sections. Whole corneas were fixed and stained with rabbit anti-SLC4A11 antibody (**a, c, d, f;** green) and mouse anti-OCIAD1 antibody (**b, c, e, f;** red). Corneas were labeled with rabbit anti-SLC4a11 (1∶100 dilution) and mouse anti-OCIAD1 (1∶250 dilution) antibodies. Immunofluorescence signals were visualized by Alexa fluor 488-conjugated antibody (green, 1:100 dilution; **a, c, d, f**), and Alexa fluor 594-conjugated anti-mouse IgG antibody (red, 1∶100 dilution; **b, c, e, f**). Sections were mounted in a DAPI media to identify nuclei, and images collected with a Zeiss LSM 510 laser-scanning confocal microscope with a x20 oil immersion objective (**a-c**) or visualized with a x40 oil immersion objective (**d-f**). Merged images (c, f; yellow) display SLC4A11 and OCIAD1 labeling overlapping. Scale bar=20 μm.

Transfected cells were labeled with membrane-impermeant Sulpho-NHS-SS-biotin (SNSB) that binds cell surface proteins. Samples were lysed and half of the lysate was incubated with streptavidin-agarose resin to remove biotinylated proteins. Equal volumes of total lysate (T) and unbound supernatant fraction (U) were processed for immunoblotting. Membranes were probed with anti-SLC4A11 or an anti-OCIAD1 antibody. When SLC4A11 was co-expressed with OCIAD1, SLC4A11 displayed no significant alteration in the fraction of protein present at the cell surface (Figure 4.9A, C). Interestingly, OCIAD1 cell surface localization increased when co-expressed with SLC4A11 (Figure 4.9B, D). This reveals that the expression of OCIAD1 did not change the trafficking of SLC4A11 to the surface of the cells. Conversely, SLC4A11 increased the amount of OCIAD1 present at the cell surface.

4.2.5 Role of OCIAD1 in cell adhesion

4.2.5.1 Cell adhesion in heterologous expression system

OCIAD1 is over-expressed in metastatic ovarian cancer tissues, and the effect of OCIAD1 on cell adhesion may give rise to its adaptive function in ovarian cancer (88). We examined the role of OCIAD1 in cell adhesion and the effect of SLC4A11 expression on OCIAD1 cell adhesion, using a previously established assay (62). In these experiments, we tested the ability of HEK293 cells co-transfected with enhanced green fluorescent protein (eGFP) and SLC4A11, OCIAD1, SLC4A11/OCIAD1, or pcDNA3.1 (empty vector), to bind to DM extracts coated on 96-well dishes. Cells were quantified by measuring GFP fluorescence before and after removal of loosely adhered cells by inverted centrifugation. Fractional cell adhesion was quantified by measuring the ratio of cell associated GFP fluorescence before and after centrifugation. Cells expressing

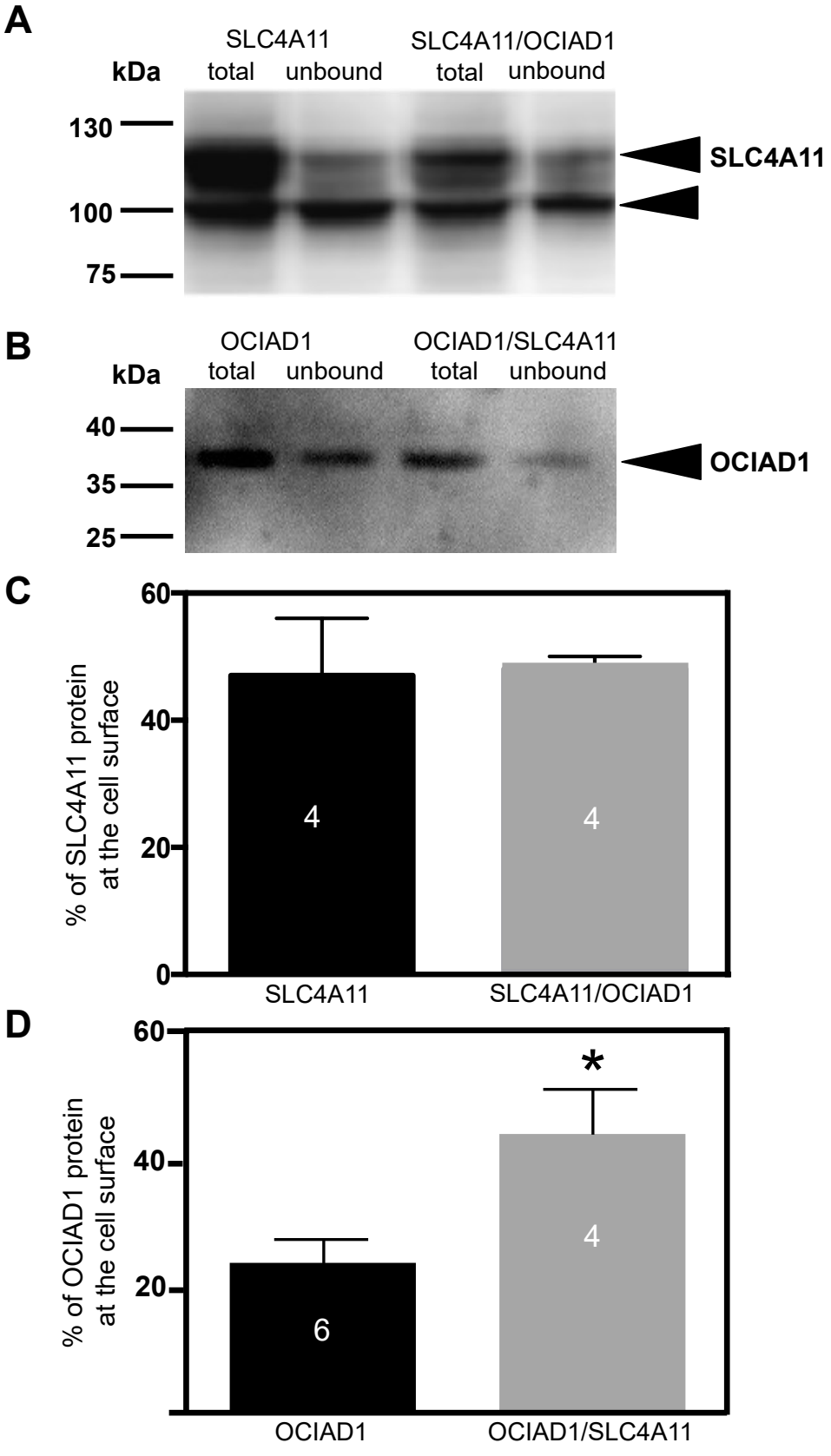
A
SLC4A11
SLC4A11/OCIAD1
kDa
total
unbound
total
unbound
130
100
75
SLC4A11
B
OCIAD1
OCIAD1/SLC4A11
kDa
total
unbound
total
unbound
40
35
25
OCIAD1
C
% of SLC4A11 protein at the cell surface
60
40
20
0
4
4
SLC4A11
SLC4A11/OCIAD1
D
% of OCIAD1 protein at the cell surface
60
40
20
*
4
6
OCIAD1
OCIAD1/SLC4A11

Figure 4.9: Cell surface Abundance of SLC4A11 and OCIAD1 in HEK293 cells

HEK293 cells were transfected with cDNAs coding for SLC4A11 (pAMC1), or transfected with OCIAD1 cDNA(pNDA35), or co-transfected with SLC4A11 and OCIAD1 cDNAs. **A.** Forty-hour post-transfection cells were labeled with membrane-impermeant Sulpho-NHS-SS-biotin (SNSB). Samples were lysed and half of the lysate was incubated with streptavidin-agarose resin to remove biotinylated proteins. Equal volumes of total lysate (T) and unbound supernatant fraction (U) were processed for immunoblotting. Membranes were probed with anti-SLC4A11. Migration position and molecular weight of sizing standards are indicated on the left. **B.** The same samples were processed similarly and probed with anti-OCIAD1 antibodies. Black arrow indicates position of the proteins. **C.** The fraction of SLC4A11 present at the cell surface was calculated relative to the level found for SLC4A11 protein, by normalizing the expression levels of protein to their cell surface processing efficiency. **D.** Same analysis was performed to measure fraction of OCIAD1 at the cell surface. Error bars represent standard error. Number of experiments is displayed inside bars. *Standard error ($P<0.05$).

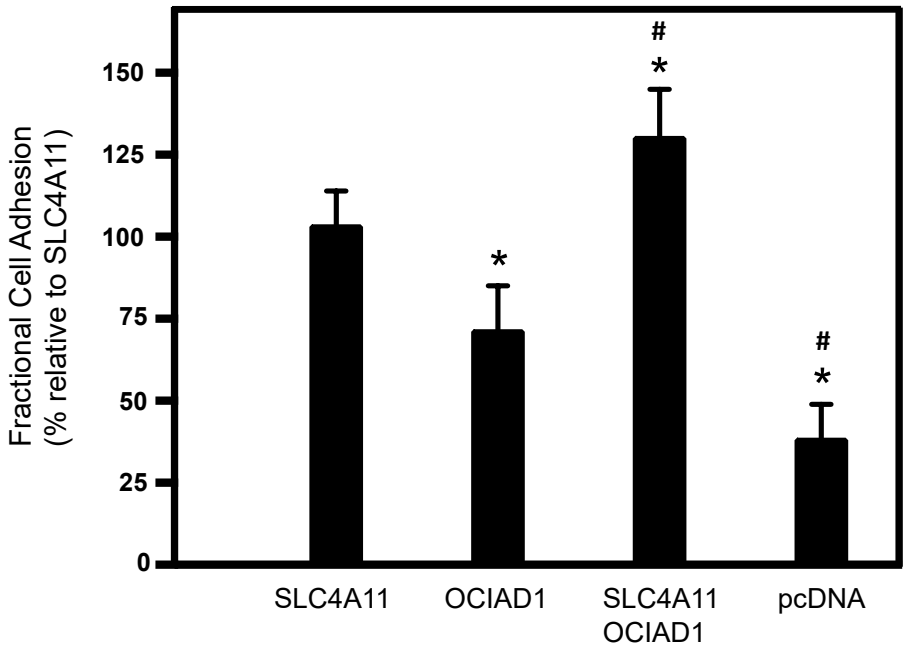

Figure 4.10: Role of SLC4A11 and OCIAD1 in Cell Adhesion to Cornea Descemet's Membrane

HEK293 cells, co-transfected with cDNA encoding eGFP and SLC4A11 or OCIAD1, or SLC4A11/OCIAD1, or empty vector, were grown on DM-coated. Cell adhesion was determined from the number of cells remaining on the dish after washing off and centrifugation of loosely adhered cells. Fractional cell adhesion was calculated as: (eGFP fluorescence post-disruption/ eGFP fluorescence pre-disruption) × 100%. Cell adhesion assays were performed, and fractional cell adhesion was plotted relative to SLC4A11-transfected cells on DM-coated dish. (n = 10-12 from three independent replicates). *$P<0.05$ relative to SLC4A11, and $^{\#}P<0.05$ relative to OCIAD1 (two-way ANOVA).

SLC4A11 have higher adherence to DM-coated wells compared to cells transfected with empty vector (Figure 4.10). Interestingly, OCIAD1, which firmly adheres to Collagen I and other extracellular matrix components (88), also adhered strongly to the DM-coated dishes. In addition, we compared the degree of cell adhesion in cells expressing OCIAD1 or SLC4A11, or co-expressing SLC4A11 and OCIAD1. The results show that co-expression of SLC4A11/OCIAD1 promoted cell adhesion to DM-coated dishes that was significantly different from SLC4A11 and OCIAD1. The increase of cell adhesion of cells co-expressing SLC4A11 and OCIAD1 have an additive effect of the adhesions from cells expressing SLC4A11 and OCIAD1 alone.

4.2.5.2 Cell adhesion in SKOV3 cells

OCIAD1/SLC4A11 expression has a role in increasing cellular adhesion. Therefore, we investigated the effect of OCIAD1 inhibition on cell adhesion SKOV3 ovarian cancer cells were transiently transfected with scrambled (SC-RNAi) and OCIAD1 specific siRNA (OCIAD1-RNAi), or co-transfected with OCIAD1-RNAi and SLC4a11 cDNA. Transfected or untransfected cells were probed with anti-OCIAD1 and anti-GAPDH antibodies. Cell adhesion assays on SKOV3 cells were conducted on collagen I-coated dishes. Cells were quantified by fluorescence measurements before and after loosely/non-adhering cells were removed by several wash steps. Overall, these tests revealed that transfection of an OCIAD1-specific siRNA, but not the scrambled siRNA, down-regulated endogenous OCIAD1 expression in SKOV3 cells. Reduced expression of OCIAD1 in SKOV3 cells decreased cell adhesion on Collagen I matrices. Interestingly, expression of SLC4A11 rescued the adhesion of SKOV3 cells expressing low levels of OCIAD1 protein when compared to control cells (Figure 4.11).

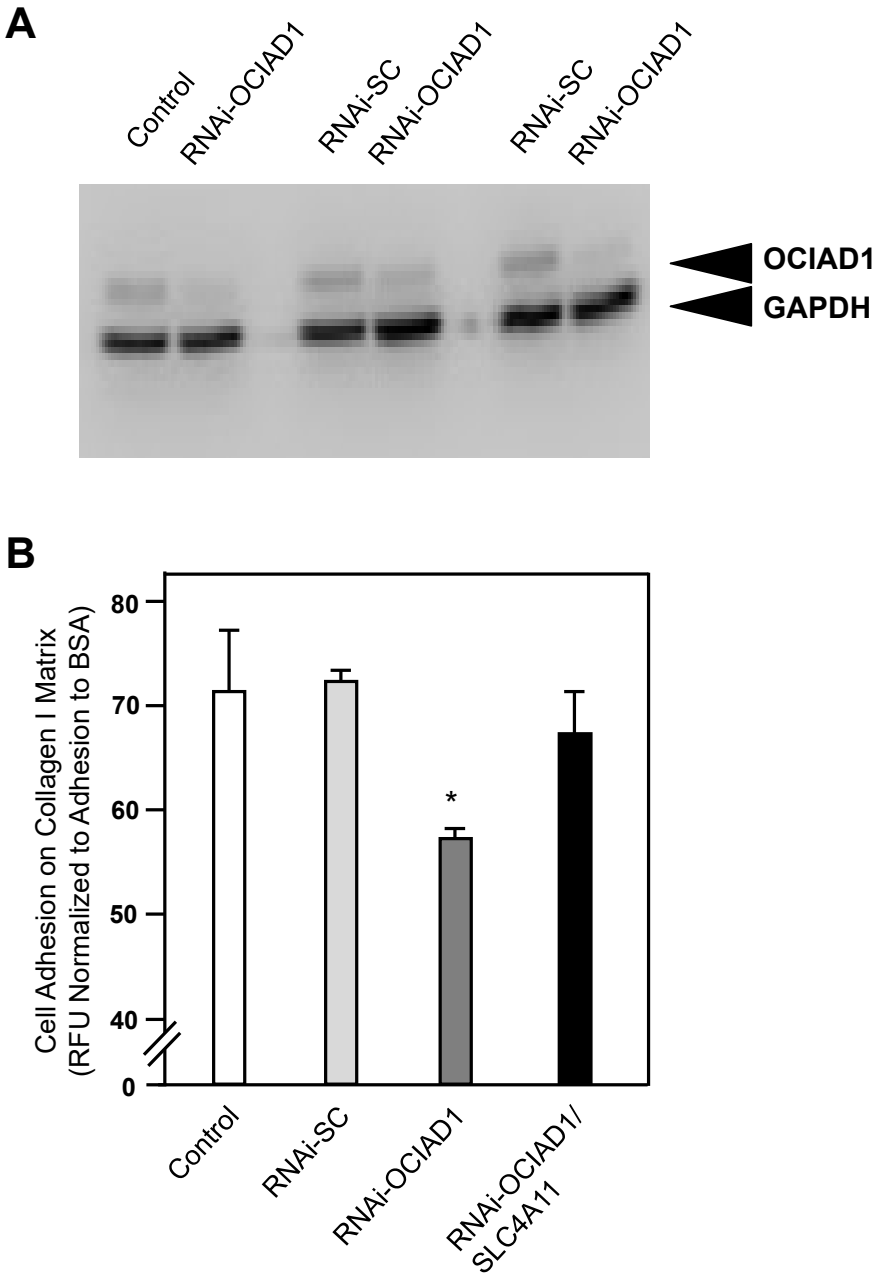

Figure 4.11: Role of SLC4A11 and OCIAD1 in Ovarian Cancer Cell Adhesion

SKOV3 ovarian cancer cells were transfected with scrambled (SC-RNAi) and OCIAD1 specific siRNA (OCIAD1-RNAi), using Lipofectamine 3000 reagent, or co-transfected with OCIAD1-

RNAi and SLC4A11 cDNA. **A.** Immunoblots of whole cell lysates in SKOV3 control cells, or cells transfected with SC-RNAi, or cells transfected with OCIAD1-RNAi were probed with mouse anti-OCIAD1 and mouse anti-GAPDH antibodies. Black arrows indicate position of the proteins. Migration position and molecular weight of sizing standards are indicated on the left. **B.** Cell adhesion assays of SKOV3 cells were done on Collagen I matrix, and adhesion of cells normalized to BSA adhesion. Data are presented as mean ± SD for four independent replicates. *Standard Error ($P<0.05$).

4.3 Discussion

The MYTH screen identified an interaction between SLC4A11 and OCIAD1, which was further supported by coimmunoprecipitation of the two proteins two cell lines and in bovine corneas. This interaction was further established via immunofluorescence, which revealed a clear colocalization of SLC4A11 with OCIAD1 in SKOV3 cells and in bovine corneas. We also found that expression of SLC4A11 protein significantly increased OCIAD1 abundance at the cell surface. Concerning cell adhesion, we also found that suppression of OCIAD1 via RNAi significantly reduced SKOV3 cell adhesion to DM. Further, co-transfection of SLC4A11/OCIAD1 increased cell adhesion in SKOV3 and HEK293 cells. Together, these results elucidate a key interaction between SLC4A11 and OCIAD1 that mediates cell adhesion.

OCIAD1 is involved in cellular adhesion. Previous work on tumors demonstrated that OCIAD1 enhances cellular adhesion to extracellular matrix proteins, specifically collagen I and laminin 10/11 (88). OCIAD1's involvement in these processes may be due to its regulation of the JAK/STAT signaling pathway, as additional studies found that OCIAD1 induces STAT3, a protein highly involved in intercellular adhesion and cytoskeletal modulation through phosphorylation of focal-adhesion kinase (93, 94). Cell adhesion assays using HEK293 cells transfected with SLC4A11 found that SLC4A11 increases adhesion to Descemet's membrane (DM) (114). Interestingly, when these cells were treated with an antibody against the extracellular loop 3 of SLC4A11, the cells displayed significantly less adhesion, indicating this loop is the DM-binding site (114). Taken together, these results indicate that SLC4A11 regulates cell adhesion and loss of this regulation is associated with FECD. Likewise, our confirmation of the interaction between SLC4A11 with OCIAD1 indicates that OCIAD1 and SLC4A11 may work together to regulate CEC adhesion, which is critical in ECDs.

OCIAD1 and SLC4A11 interaction may have significance beyond cell adhesion. Recently a role of OCIAD1 in the mitochondrial electron transport chain (ETC) was revealed. A genome wide CRISPRi study discovered that OCIAD1 is an inner mitochondrial membrane protein involved in the assembly of Complex III of the ETC in mammals (157). The study also found OCIAD1 was required for maintenance of Complex III, and that when mitochondria were depleted of OCIAD1, unprocessed cytochrome c_1 were incorporated into Complex III, resulting dysfunction of the ETC which may potentiate reducing reactive oxygen species (ROS) production (157).

This mitochondrial role of OCIAD1 is significant as SLC4A11 is an NH_3 sensitive membrane transporter with H^+ channel-like properties that facilitates glutamine catabolism in both the human and mouse corneal endothelium, resulting in the prevention of oxidative stress (79). Specifically, this work suggested that SLC4A11 localizes to the inner mitochondrial membrane of the corneal endothelium and acts as a H^+ gradient uncoupler to enhance glutamine-dependent oxygen consumption, electron transport chain activity, and ATP levels by reducing ROS production. The *Slc4a11*$^{-/-}$ mouse model demonstrated that loss of SLC4A11 causes ECD, characterized by a significant increase in oxidative stress and cell death as well as corneal edema and vision loss (79). This oxidative stress appears to be glutamine-related, as results from oxygen consumption measurement experiments demonstrate SLC4A11 knockout cells exposed to glutamine have significantly greater oxygen consumption and oxidative stress compared to wild-type cells exposed to the same treatment (79). Clearly, glutamine induces free radical production in corneal endothelial cells, and previous research indicates this effect arises from glutamine-induced respiratory oxidation, resulting in a leakage of electrons and mitochondrial dysregulation (87).

Considering the function of OCIAD1, the association between glutamine and mitochondrial Complex III suggests that OCIAD1 may be involved in the regulation of oxidative stress in corneal endothelial cells. SLC4A11 may bind OCIAD1, targeting OCIAD1 to the plasma membrane, thus reducing its abundance in mitochondria. In the absence of SLC4A11, mitochondrial OCIAD1 can form a complex with supramolecular prohibitin to stabilize cytochrome c_1, a pivotal component of the ETC (157). Alternatively, SLC4A11 may interact with OCIAD1 during protein biosynthesis in the ER, pulling it to the plasma membrane, whereas in the absence of SLC4A11, OCIAD1 is localized elsewhere to impact mitochondrial processes. However, this is merely a postulated function of OCIAD1, and further research specifically on the role of OCIAD1 in ECD or other diseases related to corneal endothelial cells is required to better understand its role. In the context of corneal endothelial cells, SLC4A11 may function by pulling OCIAD1 to the plasma membrane to enable its effects on cell adhesion as well (Figures 4.9, 4.10, 4.11).

OCIAD1 was initially discovered due to its role in cell adhesion as part of tumor formation, particularly in ovarian cancer. Interestingly, several studies have linked SLC4A11 to various cancer pathways, and recently *in silico* analyses have indicated induction of *SLC4A11* gene may be a biomarker for ovarian cancer (84). Further investigations revealed that elevated SLC4A11 is associated with both high and low-grade serous carcinomas, mucinous adenocarcinoma, and metastatic serous carcinoma, and that high expression of SLC4A11 is an independent predictor of poor overall survival of these cancer patients as well (85, 86). Clearly, both OCIAD1 and SLC4A11 are implicated in ovarian cancer (85, 88), but the relationship between the two is not well understood. In addition, localization of SLC4A11 in the mitochondria, as detected in human and mouse corneal endothelial cells, has been proposed to be required for the formation of free

radicals and ROS (162). Interestingly, enhanced ROS formation is a property typical of almost all cancer cell lines which can initiate cancer angiogenesis, metastasis, and survival (163). Moreover, OCIAD1 is a regulator of ROS production (157). This function indicates SLC4A11 and OCIAD1 may cooperate to regulate ROS production in the mitochondria, and this process may be potentiated in various cancer. Overall, the association of SLC4A11 and OCIAD1 might indicate their role in cell adhesion and localization at the plasma membrane in the eye. However, in cancer cells their association suggests their involvement in the regulation of ROS production. This role in ROS may also prove to be important in CEC physiology. Finally, the association detected for co-immunoprecipitation in Chapter 4, of OCIAD1 with core glycosylated SLC4A11 might suggest a significant role in the cell intracellularly. Further studies are required to investigate the significance of the interaction of core glycosylated SLC4A11 with OCIAD1.

Chapter 5: Summary and Future Directions

5.1 Summary

The overall objectives of this thesis were to 1) identify any significant SLC4A11 protein interactions using the MYTH screening method, and 2) to further test and characterize SLC4A11's interaction with OCIAD1, a protein previously identified in ovarian cancer that may play a major role in ECDs as well. In summary, the data presented in this thesis identifies novel SLC4A11 protein interactors and describes one significant protein interactor to be OCIAD1, a protein highly involved in the regulation of cell adhesion that, when not interacting with SLC4A11, results in diminished cell adhesion to the DM. These data provide novel insight into the function of SLC4A11 and OCIAD1 and, although further investigations are needed regarding their role in ECD, their interaction represent one potential mechanism/strategy to treat ECDs.

5.1.1 Identification of SLC4A11-protein interactors

Despite being a member of the bicarbonate transporter family, SLC4A11 does not display any bicarbonate transporter capabilities (36). Instead, research over the last two decades has revealed that the protein is primarily involved in the regulation of water movement, direct NH_3 transport, or indirect NH_3 transport when coupled with H^+ (36, 117). As discussed in Section 3.1, both the MD and CD are highly important for the normal function of SLC4A11, and disruption of these regions results in protein misfolding that eventually leads to degradation of the protein in the ER. The MD of SLC4A11 regulates water transport, and defects in the MD (possibly due to SLC4A11 mutations) provide a connection between SLC4A11 and ECD-related corneal edema. Furthermore, the whole SLC4A11 protein must be expressed in experiments as neither the CD nor the MD expressed alone (67). Thus, the MYTH screening method was utilized to identify SLC4A11 protein interactors and better understand the regulatory pathways it is involved in.

Once the bait construct was validated as not giving false positives on its own, and the cDNA library from bovine corneas was synthesized, we were able to successfully conduct the MYTH screen. The analysis revealed six full-length SLC4A11 protein interactors: TMEM254, LEPROTL1, ORMDL2, CMP-SAT, TMEM128, and OCIAD1. Section 3.2.5 of this thesis details the function of these proteins.

Importantly, while the MYTH screening method is a high-throughput and cost-effective assay to detect protein-protein interactions, high false-discovery detection rates are somewhat prominent. This is particularly the case for membrane or membrane-bound signaling proteins due to non-specific binding of their hydrophobic residues, and their high likelihood of undergoing structural modifications in the ER that can lead to non-specific interactions (135, 156). Thus, some of the MYTH screening results should be met with a degree of hesitation until further biochemical and molecular assays are done to confirm their interaction with SLC4A11. Based on many of the currently known functions of these proteins (or their homologues in other mammalian species), though, we believe these six proteins do interact with SLC4A11 and that their association is significant to the structure, function, or protein stability of SLC4A11 as a whole.

5.1.2 SLC4A11/OCIAD1 Interaction

OCIAD1 is involved in the regulation of cell adhesion in ovarian cancer cell lines (88), while additional studies demonstrated the protein's expression in the inner mitochondrial membrane is required for normal assembly and function of the mammalian electron transport chain (ETC) (157). Interestingly, recent work suggests SLC4A11 has similar functions to OCIAD1. Specifically, studies have shown SLC4A11 acts as a cell adhesion molecular (CAM) to assist in CEC adhesion; and SLC4A11 prevents mitochondrial over polarization that could lead to free radical induced

damage by acting as a H^+ channel in the mitochondrial inner membrane (79, 162, 164). Thus, we hypothesized the SLC4A11-OCIAD1 interaction was important for cell adhesion specifically in the context of CECs and ECD.

Since our MYTH screen was performed using a cDNA library from bovine corneas, we first aligned human and bovine OCIAD1 amino acid sequences and found they shared 92% sequence identity. After bioinformatic analysis to identify the predicted structure and transmembrane domains of OCIAD1, we began our analysis specifically on the interaction between SLC4A11 and OCIAD1. Endogenous and heterologous expression systems (transfected HEK293 and SKOV3 human ovarian cancer cell line) along with bovine cornea tissues and revealed expression of OCIAD1 protein and a clear interaction between SLC4A11 and OCIAD1, consistent with the MYTH result. We discovered that both endogenous and transfected SLC4A11 proteins colocalize with OCIAD1 in SKOV3 ovarian cancer cell line, most likely at the plasma membrane or ER. This colocalization was also observed in bovine cornea tissue, where SLC4A11 and OCIAD1 associated together in the endothelial layer (Figure 4.8). Moreover, we found the interaction between SLC4A11 and OCIAD1 increased localization of OCIAD1 at the cell surface. Finally, the SLC4A11-OCIAD1 interaction appears to play an integral role in cell adhesion to the DM; specifically, cell adhesion to the DM was significantly improved with co-expression of SLC4A11 and OCIAD1 when compared to transfection of SLC4A11 or OCIAD1 alone, or with empty vector. Altogether, these results not only confirm the validity of the SLC4A11-OCIAD1 interaction identified from the MYTH screen, but also indicate that their interaction is necessary for full cell adhesion to the DM.

5.2 Future Directions

Endothelial corneal dystrophies negatively affect vision quality. SLC4A11 is highly expressed in corneal endothelial cells, and its mutations lead to ECDs. The overall thesis goal was to gain understanding of SLC4A11's physiological role in ECDs by studying SLC4A11-protein interactions. We identified six unique candidate proteins that interact with SLC4A11 in a MYTH screen.

In this section I will discuss some ideas to further investigate the interactions of SLC4A11 and the roles of its interactors in corneal endothelial cells. This will focus on investigations of SLC4A11 interactions with emphasis on OCIAD1 and TMEM 254. Because OCIAD1 is involved in cell-extracellular matrix interactions, it may play a major role in cell adhesion of endothelial cells to Descemet's membrane and TMEM 254 stand out because it was detected as an interactor in 18 different colonies in the MYTH screen.

5.2.1 Confirmation of SLC4A11 Interactions with the Detected potential interactors

Preliminary data from MYTH screening in Chapter 3 revealed six potential SLC4A11 interactors, TMEM 254, LEPROTL1, ORMDL2, CMP-SAT, TMEM 128 and OCIAD1. TMEM 254 was identified as a hit from the MYTH screening eighteen times. Despite the unknown function of TMEM 254, it interacts with the chaperone protein CRYAA (122) which points towards the idea that TMEM 254 may function as a chaperone for SLC4A11. The second interactor, LEPROTL1 regulates ROS production (165). SLC4A11 is similarly indirectly involved in ROS production (79). We speculate that LEPROTL1/complex is a regulator of oxidative stress in CEC leading to ECD when the interaction is disrupted. Moreover, ORMDL2 the negative regulator of sphingolipid synthesis (136), which may compensate for the increase of sphingomyelin in CHED defected CEC (138) or could facilitate the biosynthesis of SLC4A11. Furthermore, CMP-SAT the sialic acid

transporter which regulates post-translational modifications during protein synthesis (148). The interaction of CMP-SAT may regulate SLC4A11 biosynthesis. TMEM128 is anticipated to be a false positive interactor due its detection in two different MYTH screens (154, 166) and due to its unknown function (152). However, TMEM 128 might interact with SLC4A11 and play a major role in the function of SLC4A11.

Additional studies are needed to confirm the interactions of SLC4A11. Co-IP can be used as performed in Chapter 4. The interactions can be tested by transiently transfecting HA-tagged SLC4A11 cDNA in the presence or absence of Myc-tagged protein interactors cDNA. Immunoprecipitation of the transfected cells can be achieved by incubation with anti-HA and anti-Myc antibodies. Moreover, Myc-SLC4A11 and HA-SLC4A11 transfected cells can be used as a positive control as confirmation of interaction for co-IP because SLC4A11 physiologically forms a dimer (118). Similarly, interactions in bovine corneas can be tested with anti-SLC4A11 and anti-potential interactors antibodies. Also, appropriate negative controls will be non-immune serum, non-interacting protein such as Na^+/K^+-ATPase and/or a negative construct, such as the empty vector (pcDNA).

Other than co-IP experiments, proximity ligation assay (PLA) can be used to detect protein-protein interactions. The principle of PLA is detection of two interacting proteins by specific antibodies conjugated to complementary oligonucleotides. When the two oligonucleotides are in proximity due to protein interaction, the DNA strands can interact through the addition of other circle-forming DNA oligonucleotides to form circular DNA. The circular DNA is then ligated, amplified by circular motion, and detected by additional hybridization with complementary oligonucleotides that are conjugated to a fluorophore (167). HEK293 cells can be transiently cotransfected on poly-L-lysine coated glass coverslips with HA-SLC4A11 and its Myc-tagged

interactors. Transfected cells can be fixed, permeabilized, and incubated with primary antibodies against the HA tag and Myc tag. Fixed cells could be incubated with the secondary antibodies conjugated to complementary oligonucleotides to detect the interactions. The confirmation of SLC4A11 interactions will provide us a better understanding of the nature and significance of SLC4A11 role in causing ECD.

5.2.2 Immunofluorescence to Detect the Colocalization of SLC4A11 Interactors

The cDNA library that was used in the MYTH screen was constructed from a bovine cornea. Thus, the identified protein interactors could be expressed in the different layers of the cornea such as the epithelial layer or in endothelial cells. One way to investigate the expression of protein interactors, is to check RNA sequence of CEC. CEC extracted from FECD diseased eyes undergoing keratoplasty from three tissue samples (168) and primary and immortalized cells human endothelial corneal cells (169) were subjected to RNA sequence analysis to identify differentiation in expressed genes, lists of identified genes were generated. From these studies, I looked for the expression of the six SLC4A11-detected interactors from Chapter 3 in the published list to determine if they are expressed in CEC (168, 169). Not all SLC4A11-potential interactors were listed with the genes that had change in expression or maybe they just had not changed in expression. This indicates that the interactors could be expressed in the corneal epithelium, or these interactors are not detected due to low expression. This applies to bovine Ociad1 where its expression is detected in CEC (Figure 4.8), but not detected as an expressed gene in the studied CECs (168, 169). However, could be because of the use of cells from different species.

The colocalization of SLC4A11 and identified interactors can be detected by immunofluorescence using bovine corneas. This assay will only indicate the localization of

proteins, not that whether the interactors directly bind SLC4A11. As discussed, direct interaction can be assessed using the proximity ligation assay. Flat mounted bovine or human corneas can be sectioned and fixed to detect the interactors with the custom-designed antibody against the bovine and human potential interactors in immunofluorescence experiments (170). The nucleus can be stained with a DAPI fluorescent stain and primary antibodies can be bound to the secondary antibodies conjugated to Alexa 488 or Alexa 594. Markers for colocalization can be used for each cell compartment to define the cellular location of interactions. Calnexin a chaperone protein residing in ER can be used as marker for ER (170). In addition, the markers GM130 a peripheral cytoplasmic protein attached to cis-Golgi membrane and TGN46 can be used for trans-Golgi translocation (171). The predicted subcellular interaction of SLC4A11 and TMEM 254 is at the PM, while the SLC4A11 and CMP-SAT interaction could occur at Golgi apparatus. SLC4A11 possibly interacts with LEPROT1, ORMDL2, and TMEM 128 at the ER.

Moreover, OCIAD1 is expressed and has an important role in the mitochondria (98). In chapter 4, our results revealed that OCIAD1 is expressed at PM and the fraction of OCIAD1 increased at the cell surface when co-expressed with SLC4A11 (Figure 4.9). Also, SLC4A11 increased cell adhesion of SKOV3 cells when co-expressed with OCIAD1. This indicates that SLC4A11 influences the localization level and cell adhesion function of OCIAD1 at the plasma membrane. The predicted subcellular localization of OCIAD1 is at the mitochondria and when SLC4A11 is highly expressed, OCIAD1 travels to the PM. To test this hypothesis, we can use the marker Cytochrome C oxidase subunit 4 (COXIV) for mitochondria (170) and SLC4A11 as a marker at the PM where it is expressed at basolateral side or Na^+/K^+ ATPase for PM expression (36).

5.2.3 Test Suggested Functions of SLC4A11-Protein Interactors

5.2.3.1 OCIAD1 and SLC4A11 function in mitochondria

OCIAD1 is expressed in mitochondria and regulates the activity of respiratory complex I which contributes to the production of ROS (98). Over expression of OCIAD1 reduces the production of ROS two-fold in human pluripotent stem cells (98). From the data in Chapter 4, co-expression of SLC4A11 with OCAID1 could displace OCIAD1 from its mitochondrial localization and increase localization of OCIAD1 at the plasma membrane. Depending on the result, if OCIAD1 moves from mitochondria to plasma membrane when expressed with SLC4A11 we would hypothesize an effect on mitochondrial ROS levels. ROS levels can be measured in transfected cells HEK293. The proposed controls to test the trafficking of OCIAD1 is co-transfection of OCIAD1 and WT-SLC4A11, SLC4A11-R125H, SLC4A11-S213L, SLC4A11-G583D or SLC4A11-T584K mutants. The mutant SLC4A11-R125H is functionally inactive mutant with similar expression at the plasma membrane compared to WT (36, 76), while the mutant SLC4A11-S213L is immature as detected on immunoblots (73). Also, SLC4A11-G583D mutant is not detected on immunoblots as it is degraded in the ER (73). SLC4A11-T584K mutant is a misfolded protein not recognized in the ER (73). The predicted result is WT-SLC4A11 and the mutant SLC4A11-R125H should prevent OCIAD1-mediated ROS decrease equally to WT. Because the trafficking of the SLC4A11-R215H mutant is not affected and therefore this mutant should bring OCIAD1 to the plasma membrane, displacing OCIAD1 from the mitochondria. Co-expression of OCIAD1 with SLC4A11-S213L, SLC4A11-G583D or SLC4A11-T584K mutants should not affect the OCIAD1-mediated ROS decrease in HEK293 because these mutants do not process to the plasma membrane and therefore should not pull OCIAD1 to the plasma membrane. In addition, a proper control for

the baseline of ROS production in cells would be measuring the levels of ROS in pCDNA (empty vector) transfected cells.

ROS can be measured using 5-(and-6) chloromethyl-2',7' dichlorodihydrofluorescein diacetate acetyl ester (CM-H_2DCFDA) fluorescent probe with a microplate reader (172, 173). CM-H_2DCFDA is membrane permeant and passively diffuses into cells. CM-H_2DCFDA is retained in the cell due to its cleavage by esterases and reacts with ROS to produce a highly fluorescent product. Measurement of ROS-dependent CM-H_2DCF oxidation can be conducted with the use of a monochromator-based microplate reader. Excitation can be performed at 495 nm and fluorescence emission detection at 530 nm. Untransfected (control) HEK293 cells, or HEK293 cells could be transfected with OCIAD1, SLC4A11, or cotransfected with OCIAD1 and SLC4A11, or cotransfected with OCIAD1 and SLC4A11 mutants and seeded into 96-well plate after 40 h after transfection and incubated by further 24 h. After the addition of CM-H_2DCFDA to transfected cells, ROS levels could be determined from an H_2O_2 standard curve.

5.2.3.2 TMEM254 and SLC4A11 function

TMEM 254 is predicted to function as a molecular chaperone in regulating proper folding of SLC4A11 and trafficking to the plasma membrane, as argued earlier in this thesis. Membrane protein synthesis involves post-translational modifications in the ER and Golgi apparatus, including glycosylation. The glycosylation state of SLC4A11 is an indicator of its localization to the plasma membrane or the ER (48). SLC4A11 migrates on SDS-PAGE as two separate bands, 80 and 120 kDa, representing core glycosylated (immature) and complex glycosylated (mature) states, respectively (48). The immature band of SLC4A11 represents its ER-retained form, and the mature band is the fraction that is targeted to the plasma membrane and non-glycosylated proteins

are targeted for degradation. Most of the SLC4A11 point mutants are recognized as misfolded proteins and then eliminated by the ER-associated protein degradation (ERAD) pathway (48). Some of SLC4A11 misfolded mutants can be rescued either by incubation at lower temperature during expression or by the application of the NSAID drug, Glafenine (78). Interestingly, some of the rescued mutants were recognized as properly folded proteins and trafficked to the plasma membrane and can function as wild type SLC4A11 (78). After the confirmation of SLC4A11 and TMEM 254 interaction, the rescue of SLC4A11 mutants to the cell surface by TMEM 254 can be tested in HEK293 cells by quantifying rescued mutants using cell surface biotinylation assay as used in Chapter 4. Second, the rescued SLC4A11 mutants can be tested for function. The known functions of SLC4A11 that can be assessed by well-established methods are water flux (36), cell adhesion (62), transport of NH_3 (35) and H^+ or OH^- transport (61).

5.3 Significance of Research:

The significance of this research may be to enable further studies of identified SLC4A11-interactors and their role in the development of endothelial corneal dystrophies (32, 58). The proteins that were detected as interactors for SLC4A11 and predicted to be involved in trafficking of SLC4A11 to the PM are potential target for the rescue of SLC4A11 to the PM. In this work, for the first time, OCIAD1 was identified as an important interactor, and its presence was detected in bovine corneas, specifically localized at the plasma membrane (PM). OCIAD1, when co-expressed with SLC4A11, increases the trafficking of OCIAD1 at PM, improving cell adhesion. However, this increase of cell adhesion in cells co-expressing SLC4A11 and OCIAD1 is additive and not synergetic, suggesting that their functions are not dependent on each other. The increase of cell adhesion induced by OCIAD1 (88, 160) might compensate for the loss of endothelial cells in ECD.

However, more evidence has to be found to confirm this theory. On the other hand, SLC4A11/OCIAD1 interaction may have important roles in cancer progression: 1- increased cell adhesion may promote tumor metastasis (62, 160) or 2- altered ROS homeostasis may be expected upon movement of OCIAD1 to the cell surface (79, 98).

Bibliography

1. **Alshumaimeri, N.A. and Casey, J.R.** Identification of Protein-Protein Interactors of The Corneal Dystrophy-Causing Protein, SLC4A11. In: *Association for Research in Vision and Ophthalmology*, 2016.

2. **Berkovitz, B.K.B., Ellis, H., Gray, H. and Standring, S.** Gray's Anatomy: The Anatomical Basis of Clinical Practice (39th ed.). Edinburgh: Elsevier Churchill Livingstone, 2005.

3. **Willoughby, C.E., Ponzin, D., Ferrari, S., Lobo, A., Landau, K. and Omidi, Y.** Anatomy and Physiology of the Human Eye: Effects of Mucopolysaccharidoses Disease on Structure and Function – a Review. *Clinical & Experimental Ophthalmology* 38: 2-11, 2010.

4. **Nickla, D.L. and Wallman, J.** The Multifunctional Choroid. *Progress in Retinal and Eye Research* 29: 144-168, 2010.

5. **Keeling, E., Lotery, A.J., Tumbarello, D.A. and Ratnayaka, J.A.** Impaired Cargo Clearance in the Retinal Pigment Epithelium (RPE) Underlies Irreversible Blinding Diseases. *Cells* 7, 2018.

6. **Strauss, O.** The Retinal Pigment Epithelium in Visual Function. *Physiological Reviews* 85: 845-881, 2005.

7. **Manik Goel, R.G.P., Richard K. Lee and Sanjoy K. Bhattacharya.** Aqueous Humor Dynamics: A Review. *The Open Opthalmology Journal* 4: 52-59, 2010.

8. **Petrash, J.M.** Aging and Age-Related Diseases of the Ocular Lens and Vitreous Body. *Investigative Ophthalmology and Visual Science* 54: ORSF54-59, 2013.

9. **DelMonte, D.W. and Kim, T.** Anatomy and Physiology of the Cornea. *The Journal of Cataract and Refractive Surgery* 37: 588-598, 2011.

10. **Barar, J., Asadi, M., Mortazavi-Tabatabaei, S.A. and Omidi, Y.** Ocular Drug Delivery; Impact of in vitro Cell Culture Models. *Journal of Ophthalmic and Vision Research* 4: 238-252, 2009.

11. **Rüfer, F., Schröder, A. and Erb, C.** White-to-White Corneal Diameter: Normal Values in Healthy Humans Obtained with the Orbscan II Topography System. *Cornea* 24: 259-261, 2005.

12. **Feizi, S., Jafarinasab, M.R., Karimian, F., Hasanpour, H. and Masudi, A.** Central and Peripheral Corneal Thickness Measurement in Normal and Keratoconic Eyes Using Three Corneal Pachymeters. *Journal of Ophthalmic and Vision Research* 9: 296-304, 2014.

13. **Massoudi, D., Malecaze, F. and Galiacy, S.D.** Collagens and Proteoglycans of the Cornea: Importance in Transparency and Visual Disorders. *Cell and Tissue Research* 363: 337-349, 2016.

14. **Torricelli, A.A.M., Singh, V., Santhiago, M.R. and Wilson, S.E.** The Corneal Epithelial Basement Membrane: Structure, Function, and Disease. *Investigative Ophthalmology and Visual Science* 54: 6390-6400, 2013.

15. **Faralli, J.A., Filla, M.S. and Peters, D.M.** Role of Fibronectin in Primary Open Angle Glaucoma. *Cells* 8, 2019.

16. **Sridhar, M.S.** Anatomy of cornea and ocular surface. *Indian Journal of Ophthalmology* 66: 190-194, 2018.

17. **Al-Fahdawi, S., Qahwaji, R., Al-Waisy, A.S. and Ipsopn, S.** An Automatic Corneal Subbasal Nerve Registration System Using FFT and Phase Correlation Techniques for an Accurate DPN Diagnosis. *2015 IEEE International Conference on Computer and Information Technology; Ubiquitous Computing and Communications; Dependable, Autonomic and Secure Computing; Pervasive Intelligence and Computing*, 2015, p. 1035-1041.

18. **Merindano Ma.D., Costa J., Canals M., Potau J.M. and D., R.** A Comparative Study of Bowman's Layer in Some Mammals: Relationships with Other Constituent Corneal Structures. *European Journal of Anatomy* 6: 133-139, 2002.

19. **Wilson, S.E.** Bowman's Layer in the Cornea-Structure and Function and Regeneration. *Experimental Eye Research* 195: 108033, 2020.

20. **Ho, L.T.Y., Harris, A.M., Tanioka, H., Yagi, N., Kinoshita, S., Caterson, B., Quantock, A.J., Young, R.D. and Meek, K.M.** A Comparison of Glycosaminoglycan Distributions, Keratan Sulphate Sulphation Patterns and Collagen Fibril Architecture from Central to Peripheral Regions of the Bovine Cornea. *Matrix Biology* 38: 59-68, 2014.

21. **Zhang, Y., Yeh, L.K., Zhang, S., Call, M., Yuan, Y., Yasunaga, M., Kao, W.W. and Liu, C.Y.** Wnt/β-Catenin Signaling Modulates Corneal Epithelium Stratification Via Inhibition of Bmp4 During Mouse Development. *Development* 142: 3383-3393, 2015.

22. **Carrington, L.M. and Boulton, M.** Hepatocyte Growth Factor and Keratinocyte Growth Factor Regulation of Epithelial and Stromal Corneal Wound Healing. *The Journal of Cataract and Refractive Surgery* 31: 412-423, 2005.

23. **Kabosova, A., Azar, D.T., Bannikov, G.A., Campbell, K.P., Durbeej, M., Ghohestani, R.F., Jones, J.C., Kenney, M.C., Koch, M. and Ninomiya, Y.** Compositional Differences between Infant and Adult Human Corneal Basement Membranes. *Investigative Ophthalmology and Visual Science* 48: 4989-4999, 2007.

24. **de Oliveira, R.C. and Wilson, S.E.** Descemet's Membrane Development, Structure, Function and Regeneration. *Experimental Eye Research* 197: 108090, 2020.

25. **Bourne, W.M.** Biology of the Corneal Endothelium in Health and Disease. *Eye* 17: 912-918, 2003.

26. **Joyce, N.C., Harris, D.L. and Mello, D.M.** Mechanisms of Mitotic Inhibition in Corneal Endothelium: Contact Inhibition and TGF-β2. *Investigative Ophthalmology and Visual Science* 43: 2152-2159, 2002.

27. **Waring, G.O., 3rd.** Posterior Collagenous Layer of the Cornea. Ultrastructural Classification of Abnormal Collagenous Tissue Posterior to Descemet's Membrane in 30 Cases. *Archives of Ophthalmology* 100: 122-134, 1982.

28. **Bonanno, J.A.** Molecular Mechanisms Underlying the Corneal Endothelial Pump. *Experimental Eye Research* 95: 2-7, 2012.

29. **Petroll, W.M., Hsu, J.K., Bean, J., Cavanagh, H.D. and Jester, J.V.** The Spatial Organization of Apical Junctional Complex-Associated Proteins in Feline and Human Corneal Endothelium. *Current Eye Research* 18: 10-19, 1999.

30. **Riley, M.V., Winkler, B.S., Peters, M.I. and Czajkowski, C.A.** Relationship Between Fluid Transport and in Situ Inhibition of Na^+-K^+ Adenosine Triphosphatase in Corneal Endothelium. *Investigative Ophthalmology and Visual Science* 35: 560-567, 1994.

31. **Srinivas, S.P.** Dynamic regulation of barrier integrity of the corneal endothelium. *Optometry and Vision Science* 87: E239-254, 2010.

32. **Malhotra, D. and Casey, J.R.** Molecular Mechanisms of Fuchs and Congenital Hereditary Endothelial Corneal Dystrophies. *Reviews of Physiology, Biochemistry and Pharmacology* 178: 41-81, 2020.

33. **Bonanno, J.A.** Identity and Regulation of Ion Transport Mechanisms in the Corneal Endothelium. *Progress in Retinal and Eye Research* 22: 69-94, 2003.

34. **Edelhauser, H.F.** The Balance between Corneal Transparency and Edema the Proctor Lecture. *Investigative Ophthalmology and Visual Science* 47: 1755-1767, 2006.

35. **Loganathan, S.K., Schneider, H.-P., Morgan, P.E., Deitmer, J.W. and Casey, J.R.** Functional Assessment of SLC4A11, an Integral Membrane Protein Mutated in Corneal Dystrophies. *American Journal of Physiology-Cell Physiology* 311: C735-C748, 2016.

36. **Vilas, G.L., Loganathan, S.K., Liu, J., Riau, A.K., Young, J.D., Mehta, J.S., Vithana, E.N. and Casey, J.R.** Transmembrane Water-Flux through SLC4A11: A Route Defective in Genetic Corneal Diseases. *Human Molecular Genetics* 22: 4579-4590, 2013.

37. **Jalimarada, S.S., Ogando, D.G., Vithana, E.N. and Bonanno, J.A.** Ion Transport Function of SLC4A11 in Corneal Endothelium. *Investigative Ophthalmology and Visual Science*, 2013.

38. **Joyce, N.C.** Proliferative Capacity of Corneal Endothelial Cells. *Experimental Eye Research* 95: 16-23, 2012.

39. **Feizi, S.** Corneal Endothelial Cell Dysfunction: Etiologies and Management. *Therapeutic Advances in Ophthalmology* 10: 2515841418815802, 2018.

40. **Sumide, T., Nishida, K., Yamato, M., Ide, T., Hayashida, Y., Watanabe, K., Yang, J., Kohno, C., Kikuchi, A. and Maeda, N.** Functional Human Corneal Endothelial Cell Sheets Harvested from Temperature‐Responsive Culture Surfaces. *Federation of American Societies for Experimental Biology* 20: 392-394, 2006.

41. **Aldave, A.J., Han, J. and Frausto, R.F.** Genetics of the Corneal Endothelial Dystrophies: An Evidence‐Based Review. *Clinical Genetics* 84: 109-119, 2013.

42. **Darlington, J.K., Adrean, S.D. and Schwab, I.R.** Trends of Penetrating Keratoplasty in the United States from 1980 to 2004. *Ophthalmology* 113: 2171-2175, 2006.

43. **Keenan, T.D., Jones, M.N., Rushton, S. and Carley, F.M.** Trends in the Indications for Corneal Graft Surgery in the United Kingdom: 1999 through 2009. *Archives of Ophthalmology* 130: 621-628, 2012.

44. **Higa, A., Sakai, H., Sawaguchi, S., Iwase, A., Tomidokoro, A., Amano, S. and Araie, M.** Prevalence of and Risk factors for Cornea Guttata in a Population-Based Study in a Southwestern Island of Japan: the Kumejima Study. *Archives of Ophthalmology* 129: 332-336, 2011.

45. **Eghrari, A.O. and Gottsch, J.D.** Fuchs' Corneal Dystrophy. *Expert Review of Ophthalmology* 5: 147-159, 2010.

46. **Biswas, S., Munier, F.L., Yardley, J., Hart-Holden, N., Perveen, R., Cousin, P., Sutphin, J.E., Noble, B., Batterbury, M. and Kielty, C.** Missense Mutations in COL8A2, the Gene Encoding the α2 Chain of Type VIII Collagen, Cause Two Forms of Corneal Endothelial Dystrophy. *Human Molecular Genetics* 10: 2415-2423, 2001.

47. **Mok, J.W., Kim, H.S. and Joo, C.K.** Q455V Mutation in COL8A2 is Associated with Fuchs' Corneal Dystrophy in Korean Patients. *Eye* 23: 895-903, 2009.

48. **Vithana, E.N., Morgan, P.E., Ramprasad, V., Tan, D.T., Yong, V.H., Venkataraman, D., Venkatraman, A., Yam, G.H., Nagasamy, S., Law, R.W., Rajagopal, R., Pang, C.P., Kumaramanickevel, G., Casey, J.R. and Aung, T.** SLC4A11 Mutations in Fuchs Endothelial Corneal Dystrophy (FECD). *Human Molecular Genetics* 17: 656-666, 2008.

49. **Riazuddin, S.A., Vithana, E.N., Seet, L.F., Liu, Y., Al‐Saif, A., Koh, L.W., Heng, Y.M., Aung, T., Meadows, D.N. and Eghrari, A.O.** Missense Mutations in the Sodium Borate Cotransporter SLC4A11 Cause Late‐Onset Fuchs Corneal Dystrophy. *Human Mutation* 31: 1261-1268, 2010.

50. **Soumittra, N., Loganathan, S.K., Madhavan, D., Ramprasad, V.L., Arokiasamy, T., Sumathi, S., Karthiyayini, T., Rachapalli, S.R., Kumaramanickavel, G. and Casey, J.R.** Biosynthetic and Functional Defects in Newly Identified SLC4A11 Mutants and Absence of COL8A2 Mutations in Fuchs Endothelial Corneal Dystrophy. *Journal of Human Genetics* 59: 444-453, 2014.

51. **Weiss, J.S., Møller, H., Lisch, W., Kinoshita, S., Aldave, A.J., Belin, M.W., Kivelä, T., Busin, M., Munier, F.L. and Seitz, B.** The IC3D Classification of the Corneal Dystrophies. *Cornea* 27: S1, 2008.

52. **Davidson, A.E., Liskova, P., Evans, C.J., Dudakova, L., Noskova, L., Pontikos, N., Hartmannova, H., Hodaňová, K., Stránecký, V. and Kozmík, Z.** Autosomal-Dominant Corneal Endothelial Dystrophies CHED1 and PPCD1 Are Allelic Disorders Caused by Non-Coding Mutations in the Promoter of OVOL2. *The American Journal of Human Genetics* 98: 75-89, 2016.

53. **Weiss, J.S., Møller, H.U., Aldave, A.J., Seitz, B., Bredrup, C., Kivelä, T., Munier, F.L., Rapuano, C.J., Nischal, K.K. and Kim, E.K.** IC3D Classification of Corneal Dystrophies—Edition 2. *Cornea* 34: 117-159, 2015.

54. **Vithana, E.N., Morgan, P., Sundaresan, P., Ebenezer, N.D., Tan, D.T., Mohamed, M.D., Anand, S., Khine, K.O., Venkataraman, D. and Yong, V.H.** Mutations in Sodium-Borate

Cotransporter SLC4A11 Cause Recessive Congenital Hereditary Endothelial Dystrophy (CHED2). *Nature Genetics* 38: 755-757, 2006.

55. **Lopez, I.A., Rosenblatt, M.I., Kim, C., Galbraith, G.C., Jones, S.M., Kao, L., Newman, D., Liu, W., Yeh, S. and Pushkin, A.** *Slc4a11* Gene Disruption in Mice Cellular Targets of Sensorineuronal Abnormalities. *Journal of Biological Chemistry* 284: 26882-26896, 2009.

56. **Desir, J. and Abramowicz, M.** Congenital Hereditary Endothelial Dystrophy with Progressive Sensorineural Deafness (Harboyan Syndrome). *Orphanet Journal of Rare Diseases* 3: 28, 2008.

57. **Siddiqui, S., Zenteno, J.C., Rice, A., Chacón-Camacho, O., Naylor, S.G., Rivera-de la Parra, D., Spokes, D.M., James, N., Toomes, C., Inglehearn, C.F. and Ali, M.** Congenital Hereditary Endothelial Dystrophy Caused by Slc4a11 Mutations Progresses to Harboyan Syndrome. *Cornea* 33: 247-251, 2014.

58. **Kim, J.H., Ko, J.M. and Tchah, H.** Fuchs Endothelial Corneal Dystrophy in a Heterozygous Carrier of Congenital Hereditary Endothelial Dystrophy Type 2 with a Novel Mutation in SLC4A11. *Ophthalmic Genetics* 36: 284-286, 2015.

59. **Chaurasia, S., Ramappa, M., Annapurna, M. and Kannabiran, C.** Coexistence of Congenital Hereditary Endothelial Dystrophy and Fuchs Endothelial Corneal Dystrophy Associated With SLC4A11 Mutations in Affected Families. *Cornea* 39: 354-357, 2020.

60. **Zhang, W., Ogando, D.G., Bonanno, J.A. and Obukhov, A.G.** Human SLC4A11 Is a Novel NH_3/H^+ Co-transporter. *Journal of Biological Chemistry* 290: 16894-16905, 2015.

61. **Kao, L., Azimov, R., Abuladze, N., Newman, D. and Kurtz, I.** Human SLC4A11-C Functions as a DIDS-Stimulatable H^+ (OH^-) Permeation Pathway: Partial Correction of R109H Mutant Transport. *American Journal of Physiology-Cell Physiology* 308: C176-C188, 2015.

62. **Malhotra, D., Jung, M., Fecher-Trost, C., Lovatt, M., Peh, G.S.L., Noskov, S., Mehta, J.S., Zimmermann, R. and Casey, J.R.** Defective Cell Adhesion Function of Solute Transporter, SLC4A11, in Endothelial Corneal Dystrophies. *Human Molecular Genetics* 29: 97-116, 2019.

63. **Badior, K.E., Alka, K. and Casey, J.R.** SLC4A11 Three‐Dimensional Homology Model Rationalizes Corneal Dystrophy‐Causing Mutations. *Human Mutation* 38: 279-288, 2017.

64. **Arakawa, T., Kobayashi-Yurugi, T., Alguel, Y., Iwanari, H., Hatae, H., Iwata, M., Abe, Y., Hino, T., Ikeda-Suno, C., Kuma, H., Kang, D., Murata, T., Hamakubo, T., Cameron,**

A.D., Kobayashi, T., Hamasaki, N. and Iwata, S. Crystal Structure of the Anion Exchanger Domain of Human Erythrocyte Band 3. *Science* 350: 680-684, 2015.

65. **Vilas, G.L., Morgan, P.E., Loganathan, S.K., Quon, A. and Casey, J.R.** A Biochemical Framework for SLC4A11, the Plasma Membrane Protein Defective in Corneal Dystrophies. *Biochemistry* 50: 2157-2169, 2011.

66. **Malhotra, D., Loganathan, S.K., Chiu, A.M., Lukowski, C.M. and Casey, J.R.** Human Corneal Expression of SLC4A11, a Gene Mutated in Endothelial Corneal Dystrophies. *Scientific Reports* 9: 9681, 2019.

67. **Loganathan, S.K., Lukowski, C.M. and Casey, J.R.** The Cytoplasmic Domain Is Essential for Transport Function of the Integral Membrane Transport Protein SLC4A11. *American Journal of Physiology-Cell Physiology* 310: C161-C174, 2016.

68. **Chng, Z., Peh, G.S., Herath, W.B., Cheng, T.Y., Ang, H.-P., Toh, K.-P., Robson, P., Mehta, J.S. and Colman, A.** High Throughput Gene Expression Analysis Identifies Reliable Expression Markers of Human Corneal Endothelial Cells. *PLoS One* 8: e67546, 2013.

69. **Damkier, H.H., Nielsen, S. and Praetorius, J.** Molecular Expression of SLC4-Derived Na+-Dependent Anion Transporters in Selected Human Tissues. *American Journal of Physiology-Regulatory, Integrative and Comparative Physiology* 293: R2136-R2146, 2007.

70. **Gröger, N., Fröhlich, H., Maier, H., Olbrich, A., Kostin, S., Braun, T. and Boettger, T.** SLC4A11 Prevents Osmotic Imbalance Leading to Corneal Endothelial Dystrophy, Deafness, and Polyuria. *Journal of Biological Chemistry* 285: 14467-14474, 2010.

71. **Han, S.B., Ang, H.-P., Poh, R., Chaurasia, S.S., Peh, G., Liu, J., Tan, D.T., Vithana, E.N. and Mehta, J.S.** Mice with a Targeted Disruption of *Slc4a11* Model the Progressive Corneal Changes of Congenital Hereditary Endothelial Dystrophy. *Investigative Ophthalmology and Visual Science* 54: 6179-6189, 2013.

72. **Ogando, D.G., Shyam, R., Kim, E.T., Wang, Y.C., Liu, C.Y. and Bonanno, J.A.** Inducible *Slc4a11* Knockout Triggers Corneal Edema Through Perturbation of Corneal Endothelial Pump. *Investigative Ophthalmology and Visual Science* 62: 28, 2021.

73. **Alka, K. and Casey, J.R.** Molecular Phenotype of SLC4A11 Missense Mutants: Setting the Stage for Personalized Medicine in Corneal Dystrophies. *Human Mutation* 39: 676-690, 2018.

74. **Malhotra, D., Loganathan, S.K., Chiu, A.M., Lukowski, C.M. and Casey, J.R.** Human Corneal Expression of SLC4A11, a Gene Mutated in Endothelial Corneal Dystrophies. *Scientific Reports* 9: 9681-9681, 2019.

75. **Alka, K. and Casey, J.R.** Ophthalmic Nonsteroidal Anti-Inflammatory Drugs as a Therapy for Corneal Dystrophies Caused by SLC4A11 Mutation. *Investigative Ophthalmology and Visual Science* 59: 4258-4267, 2018.

76. **Li, S., Hundal, K.S., Chen, X., Choi, M., Ogando, D.G., Obukhov, A.G. and Bonanno, J.A.** R125H, W240S, C386R, and V507I SLC4A11 Mutations associated with Corneal Endothelial Dystrophy Affect the Transporter Function but not Trafficking in PS120 Cells. *Experimental Eye Research* 180: 86-91, 2019.

77. **Loganathan, S.K. and Casey, J.R.** Corneal Dystrophy‐Causing SLC4A11 Mutants: Suitability for Folding‐Correction Therapy. *Human Mutation* 35: 1082-1091, 2014.

78. **Chiu, A.M., Mandziuk, J.J., Loganathan, S.K., Alka, K. and Casey, J.R.** High Throughput Assay Identifies Glafenine as a Corrector for the Folding Defect in Corneal Dystrophy–Causing Mutants of SLC4A11. *Investigative Ophthalmology and Visual Science* 56: 7739-7753, 2015.

79. **Ogando, D.G., Choi, M., Shyam, R., Li, S. and Bonanno, J.A.** Ammonia Sensitive SLC4A11 Mitochondrial Uncoupling Reduces Glutamine Induced Oxidative Stress. *Redox Biology* 26: 101260, 2019.

80. **Guha, S., Chaurasia, S., Ramachandran, C. and Roy, S.** SLC4A11 Depletion Impairs NRF2 Mediated Antioxidant Signaling and Increases Reactive Oxygen Species in Human Corneal Endothelial Cells During Oxidative Stress. *Scientific Reports* 7: 4074, 2017.

81. **Schlötzer-Schrehardt, U., Bachmann, B.O., Laaser, K., Cursiefen, C. and Kruse, F.E.** Characterization of the Cleavage Plane in Descemet's Membrane Endothelial Keratoplasty. *Ophthalmology* 118: 1950-1957, 2011.

82. **Stepp, M.A.** Corneal Integrins and Their Functions. *Experimental Eye Research* 83: 3-15, 2006.

83. **Frausto, R.F., Wang, C. and Aldave, A.J.** Transcriptome Analysis of the Human Corneal Endothelium. *Investigative Ophthalmology and Visual Science* 55: 7821-7830, 2014.

84. **Zahra, A., Dong, Q., Hall, M., Jeyaneethi, J., Silva, E., Karteris, E. and Sisu, C.** Identification of Potential Bisphenol A (BPA) Exposure Biomarkers in Ovarian Cancer. *Journal of Clinical Medicine* 10: 1979, 2021.

85. **Qin, L., Li, T. and Liu, Y.** High SLC4A11 Expression Is an Independent Predictor for Poor Overall Survival in Grade 3/4 Serous Ovarian Cancer. *PLoS One* 12: e0187385, 2017.

86. **Kwon, M.J. and Shin, Y.K.** Epigenetic regulation of cancer-associated genes in ovarian cancer. *International Journal of Molecular Sciences* 12: 983-1008, 2011.

87. **Luo, L.Y., Soosaipillai, A. and Diamandis, E.P.** Molecular Cloning of a Novel Human Gene on Chromosome 4p11 by Immunoscreening of an Ovarian Carcinoma cDNA Library. *Biochemical and Biophysical Research Communications* 280: 401-406, 2001.

88. **Wang, C., Michener, C.M., Belinson, J.L., Vaziri, S., Ganapathi, R. and Sengupta, S.** Role of the 18:1 Lysophosphatidic Acid–Ovarian Cancer Immunoreactive Antigen Domain Containing 1 (OCIAD1)–Integrin Axis in Generating Late-Stage Ovarian Cancer. *Molecular Cancer Therapeutics* 9: 1709-1718, 2010.

89. **Sengupta, S., Michener, C.M., Escobar, P., Belinson, J. and Ganapathi, R.** Ovarian cancer immuno-reactive antigen domain containing 1 (OCIAD1), a key player in ovarian cancer cell adhesion. *Gynecologic Oncology* 109: 226-233, 2008.

90. **Sengupta, S., Xiao, Y.J. and Xu, Y.** Novel Laminin-Induced LPA Autocrine Loop in the Migration of Ovarian Cancer Cells. *Federation of American Societies for Experimental Biology* 17: 1570-1572, 2003.

91. **Xu, Y., Shen, Z., Wiper, D.W., Wu, M., Morton, R.E., Elson, P., Kennedy, A.W., Belinson, J., Markman, M. and Casey, G.** Lysophosphatidic Acid as a Potential Biomarker for Ovarian and Other Gynecologic Cancers. *The Journal of the American Medical Association* 280: 719-723, 1998.

92. **Sutphen, R., Xu, Y., Wilbanks, G.D., Fiorica, J., Grendys, E.C., Jr., LaPolla, J.P., Arango, H., Hoffman, M.S., Martino, M., Wakeley, K., Griffin, D., Blanco, R.W., Cantor, A.B., Xiao, Y.J. and Krischer, J.P.** Lysophospholipids Are Potential Biomarkers of Ovarian Cancer. *Cancer Epidemiology, Biomarkers & Prevention* 13: 1185-1191, 2004.

93. **Wei, Z., Jiang, W., Wang, H., Li, H., Tang, B., Liu, B., Jiang, H. and Sun, X.** The IL-6/STAT3 Pathway Regulates Adhesion Molecules and Cytoskeleton of Endothelial Cells in Thromboangiitis Obliterans. *Cellular Signalling* 44: 118-126, 2018.

94. **Onishi, A., Chen, Q., Humtsoe, J.O. and Kramer, R.H.** STAT3 Signaling Is Induced by Intercellular Adhesion in Squamous Cell Carcinoma Cells. *Experimental Cell Research* 314: 377-386, 2008.

95. **Sinha, S., Bheemsetty, V.A. and Inamdar, M.S.** A Double Helical Motif in OCIAD2 Is Essential for Its Localization, Interactions and STAT3 Activation. *Scientific Reports* 8: 7362, 2018.

96. **Nagata, C., Kobayashi, H., Sakata, A., Satomi, K., Minami, Y., Morishita, Y., Ohara, R., Yoshikawa, H., Arai, Y., Nishida, M. and Noguchi, M.** Increased Expression of OCIA Domain Containing 2 During Stepwise Progression of Ovarian Mucinous Tumor. *Pathology International* 62: 471-476, 2012.

97. **Mizejewski, G.J.** Role of Integrins in Cancer: Survey of Expression Patterns. *Experimental Biology and Medicine* 222: 124-138, 1999.

98. **Shetty, D.K., Kalamkar, K.P. and Inamdar, M.S.** OCIAD1 Controls Electron Transport Chain Complex I Activity to Regulate Energy Metabolism in Human Pluripotent Stem Cells. *Stem cell reports* 11: 128-141, 2018.

99. **Calvo, S.E., Clauser, K.R. and Mootha, V.K.** Mitocarta2.0: An Updated Inventory of Mammalian Mitochondrial Proteins. *Nucleic Acids Research* 44: D1251-1257, 2016.

100. **Kulkarni, V., Khadilkar, R.J., Magadi, S.S. and Inamdar, M.S.** Asrij Maintains the Stem Cell Niche and Controls Differentiation During Drosophila Lymph Gland Hematopoiesis. *PLoS One* 6: e27667, 2011.

101. **Tran, H.T.L., Morikawa, K., Anggakusuma, Zibi, R., Thi, V.L.D., Penin, F., Heim, M.H., Quadroni, M., Pietschmann, T., Gouttenoire, J. and Moradpour, D.** OCIAD1 is a Host Mitochondrial Substrate of the Hepatitis C Virus NS3-4A Protease. *PLoS One* 15: e0236447, 2020.

102. **Snider, J., Kittanakom, S., Damjanovic, D., Curak, J., Wong, V. and Stagljar, I.** Detecting Interactions with Membrane Proteins Using a Membrane Two-Hybrid Assay in Yeast. *Nature Protocols* 5: 1281-1293, 2010.

103. **Inoue, H., Nojima, H. and Okayama, H.** High Efficiency Transformation of *Escherichia Coli* with Plasmids. *Gene* 96: 23-28, 1990.

104. **Green, R. and Rogers, E.J.** Transformation of Chemically Competent *E. Coli*. *Methods in Enzymology* 529: 329-336, 2013.

105. **Gonzales, M.F., Brooks, T., Pukatzki, S.U. and Provenzano, D.** Rapid Protocol for Preparation of Electrocompetent *Escherichia coli* and *Vibrio Cholerae*. *The Journal of Visualized Experiments*, 2013.

106. **Gietz, R.D. and Schiestl, R.H.** High-Efficiency Yeast Transformation Using the Liac/SS Carrier DNA/PEG Method. *Nature Protocols* 2: 31-34, 2007.

107. **Boratyn, G.M., Schaffer, A.A., Agarwala, R., Altschul, S.F., Lipman, D.J. and Madden, T.L.** Domain Enhanced Lookup Time Accelerated BLAST. *Biology Direct* 7: 12, 2012.

108. **Ruetz, S., Lindsey, A.E., Ward, C.L. and Kopito, R.R.** Functional Activation of Plasma Membrane Anion Exchangers Occurs in a Pre-Golgi Compartment. *Journal of Cell Biology* 121: 37-48, 1993.

109. **Laemmli, U.K.** Cleavage of Structural Proteins During the Assembly of the Head of Bacteriophage T4. *Nature* 227: 680-685, 1970.

110. **Basu, A., Mazor, S. and Casey, J.R.** Distance Measurements within a Concatamer of the Plasma Membrane Cl^-/HCO_3^- Exchanger, AE1. *Biochemistry* 49: 9226-9240, 2010.

111. **Willoughby, C.E., Ponzin, D., Ferrari, S., Lobo, A., Landau, K. and Omidi, Y.** Anatomy and physiology of the human eye: effects of mucopolysaccharidoses disease on structure and function – a review. *Clinical & Experimental Ophthalmology* 38 Suppl 1: 2-11, 2010.

112. **Parker, M.D., Ourmozdi, E.P. and Tanner, M.J.** Human BTR1, a New Bicarbonate Transporter Superfamily Member and Human AE4 from Kidney. *Biochemical and Biophysical Research Communications* 282: 1103-1109, 2001.

113. **Takano, J., Noguchi, K., Yasumori, M., Kobayashi, M., Gajdos, Z., Miwa, K., Hayashi, H., Yoneyama, T. and Fujiwara, T.** Arabidopsis Boron Transporter for Xylem Loading. *Nature* 420: 337-340, 2002.

114. **Malhotra, D., Jung, M., Fecher-Trost, C., Lovatt, M., Peh, G.S.L., Noskov, S., Mehta, J.S., Zimmermann, R. and Casey, J.R.** Defective cell adhesion function of solute transporter, SLC4A11, in endothelial corneal dystrophies. *Hum Mol Genet* 29: 97-116, 2020.

115. **Shei, W., Liu, J., Htoon, H.M., Aung, T. and Vithana, E.N.** Differential Expression of the Slc4 Bicarbonate Transporter Family in Murine Corneal Endothelium and Cell Culture. *Molecular Vision* 19: 1096-1106, 2013.

116. **Myers, E.J., Marshall, A., Jennings, M.L. and Parker, M.D.** Mouse Slc4a11 Expressed in Xenopus Oocytes Is an Ideally Selective H^+/OH^- Conductance Pathway That Is Stimulated by

Rises in Intracellular and Extracellular pH. *American Journal of Physiology-Cell Physiology* 311: C945-c959, 2016.

117. **Kao, L., Azimov, R., Shao, X.M., Abuladze, N., Newman, D., Zhekova, H., Noskov, S., Pushkin, A. and Kurtz, I.** SLC4A11 Function: Evidence for $H^+(OH^-)$ and $NH3^-H^+$ Transport. *American Journal of Physiology-Cell Physiology* 318: C392-C405, 2020.

118. **Vilas, G.L., Loganathan, S.K., Quon, A., Sundaresan, P., Vithana, E.N. and Casey, J.** Oligomerization of SLC4A11 Protein and the Severity of FECD and CHED2 Corneal Dystrophies Caused by SLC4A11 Mutations. *Human Mutation* 33: 419-428, 2012.

119. **Aldave, A.J., Yellore, V.S., Bourla, N., Momi, R.S., Khan, M.A., Salem, A.K., Rayner, S.A., Glasgow, B.J. and Kurtz, I.** Autosomal Recessive CHED Associated with Novel Compound Heterozygous Mutations in SLC4A11. *Cornea* 26: 896-900, 2007.

120. **Kiernan, J.A.** Indigogenic Substrates for Detection and Localization of Enzymes. *Biotechnic & Histochemistry* 82: 73-103, 2007.

121. https://www.uniprot.org/uniprot/Q0D2G3.

122. **Fan, Q., Huang, L.Z., Zhu, X.J., Zhang, K.K., Ye, H.F., Luo, Y., Sun, X.H., Zhou, P. and Lu, Y.** Identification of Proteins That Interact with Alpha A-Crystallin Using a Human Proteome Microarray. *Molecular Vision* 20: 117-124, 2014.

123. **Kannan, R., Sreekumar, P.G. and Hinton, D.R.** Novel Roles for α-Crystallins in Retinal Function and Disease. *Progress in Retinal Eye Research* 31: 576-604, 2012.

124. **Ren, S., Liu, T., Jia, C., Qi, X. and Wang, Y.** Physiological Expression of Lens Alpha-, Beta-, and Gamma-Crystallins in Murine and Human Corneas. *Molecular Vision* 16: 2745-2752, 2010.

125. https://www.uniprot.org/uniprot/Q32PD8.

126. **Lancel, S., Hesselink, M.K., Woldt, E., Rouille, Y., Dorchies, E., Delhaye, S., Duhem, C., Thorel, Q., Mayeuf-Louchart, A., Pourcet, B., Montel, V., Schaart, G., Beton, N., Picquet, F., Briand, O., Salles, J.P., Duez, H., Schrauwen, P., Bastide, B., Bailleul, B., Staels, B. and Sebti, Y.** Endospanin-2 Enhances Skeletal Muscle Energy Metabolism and Running Endurance Capacity. *Journal of Clinical Investigation Insight* 3, 2018.

127. **Mo, H.Y., Kim, M.S., Chung, N.G., Yoo, N.J. and Lee, S.H.** Promoter Mutation Analysis of LEPROTL1 Gene in Acute Leukemias and Solid Tumors. *Acta Haematol* 141: 214-215, 2019.

128. **Séron, K., Couturier, C., Belouzard, S., Bacart, J., Monté, D., Corset, L., Bocquet, O., Dam, J., Vauthier, V., Lecœur, C., Bailleul, B., Hoflack, B., Froguel, P., Jockers, R. and Rouillé, Y.** Endospanins Regulate a Postinternalization Step of the Leptin Receptor Endocytic Pathway. *Journal of Biological Chemistry* 286: 17968-17981, 2011.

129. **Touvier, T., Conte-Auriol, F., Briand, O., Cudejko, C., Paumelle, R., Caron, S., Baugé, E., Rouillé, Y., Salles, J.-P., Staels, B. and Bailleul, B.** LEPROT and LEPROTL1 Cooperatively Decrease Hepatic Growth Hormone Action in Mice. *The Journal of clinical investigation* 119: 3830-3838, 2009.

130. **Ndiaye, K., Castonguay, A., Benoit, G., Silversides, D.W. and Lussier, J.G.** Differential Regulation of Janus Kinase 3 (Jak3) in Bovine Preovulatory Follicles and Identification of Jak3 Interacting Proteins in Granulosa Cells. *Journal of Ovarian Research* 9: 71, 2016.

131. **Sommer, C., Lee, S., Gulseth, H.L., Jensen, J., Drevon, C.A. and Birkeland, K.I.** Soluble Leptin Receptor Predicts Insulin Sensitivity and Correlates With Upregulation of Metabolic Pathways in Men. *The Journal of Clinical Endocrinology and Metabolism* 103: 1024-1032, 2018.

132. **Hjelmqvist, L., Tuson, M., Marfany, G., Herrero, E., Balcells, S. and Gonzàlez-Duarte, R.** ORMDL Proteins are a Conserved New Family of Endoplasmic Reticulum Membrane Proteins. *Genome Biology* 3: Research0027, 2002.

133. https://www.uniprot.org/uniprot/Q5E972.

134. **Siow, D.L. and Wattenberg, B.W.** Mammalian ORMDL Proteins Mediate the Feedback Response in Ceramide Biosynthesis. *Journal of Biological Chemistry* 287: 40198-40204, 2012.

135. **Huang, H., Jedynak, B.M. and Bader, J.S.** Where Have All the Interactions Gone? Estimating the Coverage of Two-Hybrid Protein Interaction Maps. *PLOS Computational Biology* 3: e214, 2007.

136. **Breslow, D.K., Collins, S.R., Bodenmiller, B., Aebersold, R., Simons, K., Shevchenko, A., Ejsing, C.S. and Weissman, J.S.** Orm Family Proteins Mediate Sphingolipid Homeostasis. *Nature* 463: 1048-1053, 2010.

137. **Rowsey, T.G. and Karamichos, D.** The Role of Lipids in Corneal Diseases and Dystrophies: A Systematic Review. *Clinical and Translational Medicine* 6: 30, 2017.

138. **Cabrerizo, J., Urcola, J.A., Vecino, E. and Melles, G.** Changes in Lipidomic Profile of Aqueous Humour in Fuchs Endothelial Dystrophy. *Acta Ophthalmol* 95: 727-732, 2017.

139. **Eich, C., Manzo, C., Keijzer, S.d., Bakker, G.-J., Reinieren-Beeren, I., García-Parajo, M.F. and Cambi, A.** Changes in Membrane Sphingolipid Composition Modulate Dynamics and Adhesion of Integrin Nanoclusters. *Scientific Reports* 6: 20693, 2016.

140. **van Meer, G. and Lisman, Q.** Sphingolipid Transport: Rafts and Translocators. *Journal of Biological Chemistry* 277: 25855-25858, 2002.

141. **Bugajev, V., Halova, I., Demkova, L., Cernohouzova, S., Vavrova, P., Mrkacek, M., Utekal, P., Draberova, L., Kuchar, L., Schuster, B. and Draber, P.** ORMDL2 Deficiency Potentiates the ORMDL3-Dependent Changes in Mast Cell Signaling. *Frontiers in Immunology* 11: 591975, 2020.

142. **Zhu, W.K., Xu, W.H., Wang, J., Huang, Y.Q., Abudurexiti, M., Qu, Y.Y., Zhu, Y.P., Zhang, H.L. and Ye, D.W.** Decreased SPTLC1 Expression Predicts Worse Outcomes in ccRCC Patients. *Journal of Cellular Biochemistry* 121: 1552-1562, 2020.

143. **Clarke, B.A., Majumder, S., Zhu, H., Lee, Y.T., Kono, M., Li, C., Khanna, C., Blain, H., Schwartz, R., Huso, V.L., Byrnes, C., Tuymetova, G., Dunn, T.M., Allende, M.L. and Proia, R.L.** The *ORMDL* Genes Regulate the Sphingolipid Synthesis Pathway to Ensure Proper Myelination and Neurologic Function in Mice. *Elife* 8, 2019.

144. **Maiuthed, A., Prakhongcheep, O. and Chanvorachote, P.** Microarray-based Analysis of Genes, Transcription Factors, and Epigenetic Modifications in Lung Cancer Exposed to Nitric Oxide. *Cancer Genomics Proteomics* 17: 401-415, 2020.

145. **Toncheva, A.A., Potaczek, D.P., Schedel, M., Gersting, S.W., Michel, S., Krajnov, N., Gaertner, V.D., Klingbeil, J.M., Illig, T., Franke, A., Winkler, C., Hohlfeld, J.M., Vogelberg, C., von Berg, A., Bufe, A., Heinzmann, A., Laub, O., Rietschel, E., Simma, B., Genuneit, J., Muntau, A.C. and Kabesch, M.** Childhood Asthma Is Associated with Mutations and Gene Expression Differences of *ORMDL1* Genes That Can Interact. *Allergy* 70: 1288-1299, 2015.

146. **Ishida, N., Miura, N., Yoshioka, S. and Kawakita, M.** Molecular Cloning and Characterization of a Novel Isoform of the Human UDP-Galactose Transporter, and of Related Complementary Dnas Belonging to the Nucleotide-Sugar Transporter Gene Family. *Journal of Biochemistry* 120: 1074-1078, 1996.

147. **Martinez-Duncker, I., Dupré, T., Piller, V., Piller, F., Candelier, J.J., Trichet, C., Tchernia, G., Oriol, R. and Mollicone, R.** Genetic Complementation Reveals a Novel Human

Congenital Disorder of Glycosylation of Type II, Due to Inactivation of the Golgi CMP-Sialic Acid Transporter. *Blood* 105: 2671-2676, 2005.

148. **Ishida, N., Ito, M., Yoshioka, S., Sun-Wada, G.H. and Kawakita, M.** Functional Expression of Human Golgi CMP-Sialic Acid Transporter in the Golgi Complex of a Transporter-Deficient Chinese Hamster Ovary Cell Mutant. *Journal of Biochemistry* 124: 171-178, 1998.

149. https://www.uniprot.org/uniprot/Q3SZP1.

150. **Reily, C., Stewart, T.J., Renfrow, M.B. and Novak, J.** Glycosylation in Health and Disease. *Nature Reviews Nephrology* 15: 346-366, 2019.

151. **McLean, A.M., Cefali, E.A., Roden, J.S., Gonzalez, M.A. and Bialer, M.** Stability of Diltiazem in Different Biological Fluids. *Biopharmaceutics & drug disposition* 12: 327-334, 1991.

152. https://www.uniprot.org/uniprot/Q3T0S0.

153. **Winter, E. and Ponting, C.P.** TRAM, LAG1 and CLN8: Members of a Novel Family of Lipid-Sensing Domains? . *Trends in Biochemical Sciences* 27: 381-383, 2002.

154. **Cevik, S.I., Keskin, N., Belkaya, S., Ozlu, M.I., Deniz, E., Tazebay, U.H. and Erman, B.** CD81 Interacts with the T Cell Receptor to Suppress Signaling. *PLoS One* 7: e50396, 2012.

155. **Weiss, J.L.a.A.** T cell receptor signalling. *Cell science* 114: 243-244, 2001.

156. **Deeds, E.J., Ashenberg, O. and Shakhnovich, E.I.** A Simple Physical Model for Scaling in Protein-Protein Interaction Networks. *Proceedings of the National Academy of Sciences of the United States of America* 103: 311-316, 2006.

157. **Le Vasseur, M., Friedman, J., Jost, M., Xu, J., Yamada, J., Kampmann, M., Horlbeck, M.A., Salemi, M.R., Phinney, B.S., Weissman, J.S. and Nunnari, J.** Genome-Wide CRISPRi Screening Identifies OCIAD1 as a Prohibitin Client and Regulatory Determinant of Mitochondrial Complex III Assembly in Human Cells. *Elife* 10, 2021.

158. **Shen, C., Hui, Z., Wang, D., Jiang, G., Wang, J. and Zhang, G.** Molecular Cloning, Identification and Analysis of Lung Squamous Cell Carcinoma-Related Genes. *Lung Cancer* 38: 235-241, 2002.

159. https://www.uniprot.org/uniprot/Q5E948.

160. **Sengupta, S., Michener, C.M., Escobar, P., Belinson, J. and Ganapathi, R.** Ovarian Cancer Immuno-Reactive Antigen Domain Containing 1 (OCIAD1), a Key Player in Ovarian Cancer Cell Adhesion. *Gynecologic Oncology* 109: 226-233, 2008.

161. **Sherman, E.L., Go, N.E. and Nargang, F.E.** Functions of the Small Proteins in the TOM Complex of *Neurospora Crasssa*. *Molecular biology of the cell* 16: 4172-4182, 2005.

162. **Choi, M. and Bonanno, J.A.** Mitochondrial Targeting of the Ammonia-Sensitive Uncoupler SLC4A11 by the Chaperone-Mediated Carrier Pathway in Corneal Endothelium. *Investigative Ophthalmology and Visual Science* 62: 4, 2021.

163. **Aggarwal, V., Tuli, H.S., Varol, A., Thakral, F., Yerer, M.B., Sak, K., Varol, M., Jain, A., Khan, M.A. and Sethi, G.** Role of Reactive Oxygen Species in Cancer Progression: Molecular Mechanisms and Recent Advancements. *Biomolecules* 9, 2019.

164. **Luo, L.-Y., Soosaipillai, A. and Diamandis, E.P.** Molecular Cloning of a Novel Human Gene on Chromosome 4p11 by Immunoscreening of an Ovarian Carcinoma cDNA Library. *Biochemical and Biophysical Research Communications* 280: 401-406, 2001.

165. **Caputo, L., Granados, A., Lenzi, J., Rosa, A., Ait-Si-Ali, S., Puri, P.L. and Albini, S.** Acute Conversion of Patient-Derived Duchenne Muscular Dystrophy iPSC into Myotubes Reveals Constitutive and Inducible over-Activation of TGF Beta-Dependent Pro-Fibrotic Signaling. *Skeletal Muscle* 10: 13, 2020.

166. **Passantino, R., Cascio, C., Deidda, I., Galizzi, G., Russo, D., Spedale, G. and Guarneri, P.** Identifying Protein Partners of CLN8, an ER-Resident Protein Involved in Neuronal Ceroid Lipofuscinosis. *Biochimica et Biophysica Acta* 1833: 529-540, 2013.

167. **Bobrich, M.A., Schwabe, S.A., Brobeil, A., Viard, M., Kamm, M., Mooren, F.C., Krüger, K., Tag, C. and Wimmer, M.** PTPIP51: A New Interaction Partner of the Insulin Receptor and PKA in Adipose Tissue. *Journal of Obesity* 2013: 476240, 2013.

168. **Wieben, E.D., Baratz, K.H., Aleff, R.A., Kalari, K.R., Tang, X., Maguire, L.J., Patel, S.V. and Fautsch, M.P.** Gene Expression and Missplicing in the Corneal Endothelium of Patients With a TCF4 Trinucleotide Repeat Expansion Without Fuchs' Endothelial Corneal Dystrophy. *Investigative Ophthalmology and Visual Science* 60: 3636-3643, 2019.

169. **Frausto, R.F., Le, D.J. and Aldave, A.J.** Transcriptomic Analysis of Cultured Corneal Endothelial Cells as a Validation for Their Use in Cell Replacement Therapy. *Cell Transplant* 25: 1159-1176, 2016.

170. **He, Z., Forest, F., Gain, P., Rageade, D., Bernard, A., Acquart, S., Peoc'h, M., Defoe, D.M. and Thuret, G.** 3D Map of the Human Corneal Endothelial Cell. *Scientific Reports* 6: 29047, 2016.

171. **Krokowski, D., Guan, B.-J., Wu, J., Zheng, Y., Pattabiraman, P.P., Jobava, R., Gao, X.-H., Di, X.-J., Snider, M.D., Mu, T.-W., Liu, S., Storrie, B., Pearlman, E., Blumental-Perry, A. and Hatzoglou, M.** GADD34 Function in Protein Trafficking Promotes Adaptation to Hyperosmotic Stress in Human Corneal Cells. *Cell Reports* 21: 2895-2910, 2017.

172. **Oparka, M., Walczak, J., Malinska, D., van Oppen, L., Szczepanowska, J., Koopman, W.J.H. and Wieckowski, M.R.** Quantifying ROS levels using CM-H_2DCFDA and HyPer. *Methods* 109: 3-11, 2016.

173. **Wang, H. and Joseph, J.A.** Quantifying Cellular Oxidative Stress by Dichlorofluorescein Assay Using Microplate Reader. *Free Radical Biology and Medicine* 27: 612-616, 1999.